

1998

Thermal stress prediction for direct-chill casting of a high strength aluminum alloy.

Jian Wan

Follow this and additional works at: <https://researchrepository.wvu.edu/etd>

Recommended Citation

Wan, Jian, "Thermal stress prediction for direct-chill casting of a high strength aluminum alloy." (1998). *Graduate Theses, Dissertations, and Problem Reports*. 9965.
<https://researchrepository.wvu.edu/etd/9965>

This Thesis is protected by copyright and/or related rights. It has been brought to you by the The Research Repository @ WVU with permission from the rights-holder(s). You are free to use this Thesis in any way that is permitted by the copyright and related rights legislation that applies to your use. For other uses you must obtain permission from the rights-holder(s) directly, unless additional rights are indicated by a Creative Commons license in the record and/ or on the work itself. This Thesis has been accepted for inclusion in WVU Graduate Theses, Dissertations, and Problem Reports collection by an authorized administrator of The Research Repository @ WVU. For more information, please contact researchrepository@mail.wvu.edu.

INFORMATION TO USERS

This manuscript has been reproduced from the microfilm master. UMI films the text directly from the original or copy submitted. Thus, some thesis and dissertation copies are in typewriter face, while others may be from any type of computer printer.

The quality of this reproduction is dependent upon the quality of the copy submitted. Broken or indistinct print, colored or poor quality illustrations and photographs, print bleedthrough, substandard margins, and improper alignment can adversely affect reproduction.

In the unlikely event that the author did not send UMI a complete manuscript and there are missing pages, these will be noted. Also, if unauthorized copyright material had to be removed, a note will indicate the deletion.

Oversize materials (e.g., maps, drawings, charts) are reproduced by sectioning the original, beginning at the upper left-hand corner and continuing from left to right in equal sections with small overlaps. Each original is also photographed in one exposure and is included in reduced form at the back of the book.

Photographs included in the original manuscript have been reproduced xerographically in this copy. Higher quality 6" x 9" black and white photographic prints are available for any photographs or illustrations appearing in this copy for an additional charge. Contact UMI directly to order.

UMI

A Bell & Howell Information Company
300 North Zeeb Road, Ann Arbor MI 48106-1346 USA
313/761-4700 800/521-0600

**THERMAL STRESS PREDICTION FOR DIRECT-CHILL CASTING OF
A HIGH STRENGTH ALUMINUM ALLOY**

By

Jian Wan

A DISSERTATION

**Submitted to
The College of Engineering and Mineral Resources
at
West Virginia University**

**in partial fulfillment of the requirements
for the degree of**

**Doctor of Philosophy
in
Mechanical Engineering**

Department of Mechanical & Aerospace Engineering

**Morgantown, West Virginia
1998**

UMI Number: 9902322

Copyright 1998 by
Wan, Jian

All rights reserved.

UMI Microform 9902322
Copyright 1998, by UMI Company. All rights reserved.

This microform edition is protected against unauthorized
copying under Title 17, United States Code.

UMI
300 North Zeeb Road
Ann Arbor, MI 48103

**Copyright by
Jian Wan
1998**

ABSTRACT

THERMAL STRESS PREDICTION FOR DIRECT-CHILL CASTING OF A HIGH STRENGTH ALUMINUM ALLOY

By Jian Wan

Direct chill (D.C.) casting is one of the most important semi-continuous methods for the production of high strength aluminum alloys. The enormous unevenly cooling of ingots during the casting process can cause significant thermally induced stresses, which may result in solidification cracking. The control of the cracking during DC casting is a state-of-art technology, and many finite element models have been applied to simulate the solidification process during ingot casting. So far, most of the simulations can predict the thermal fields of the ingot accurately, but very few works can get satisfactory thermal stress profiles. One of the major difficulties is the lack of valid thermo-mechanical properties for constitutive modeling of as-cast ingots.

The mechanical properties of a high strength aerospace aluminum alloy 7050 was studied in the as-cast ingot form. A thermo-elastic-plastic constitutive model was adopted to summarize the ingot strength and deformation behavior over a wide temperature range from the melting point to room temperature. In addition, the dependence of ingot properties on the casting structure as well as the cooling history at different ingot locations were determined. The cooling history of 7050 ingots can be divided into two portions at every location. The solidification rate between liquidus (635°C/1175°F) and solidus (524°C/975°F) decides the cast microstructure, which exhibits various coarse grain structures with notable dendrite segregation. After solidification, the cooling rate of solid ingots will influence the formation of the precipitation phases and their morphology.

Both portions of the cooling history were considered as the parameters in the constitutive models. A finite element model (FEM) was developed to predict the thermal stress distribution in DC cast aluminum ingots by employing a commercial FEM code ABAQUS. The in-situ measured temperature profiles was input as the thermal conditions through a user subroutine, and the material constitutive model was employed in the modeling. In addition, fracture toughness of as-cast ingots was investigated experimentally through on-cooling K_{Ic} tests for material from the center and surface of Al-7050 ingot.

**THERMAL STRESS PREDICTION FOR DIRECT-CHILL CASTING OF
A HIGH STRENGTH ALUMINUM ALLOY**

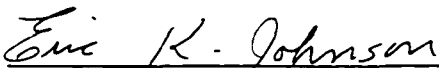
By

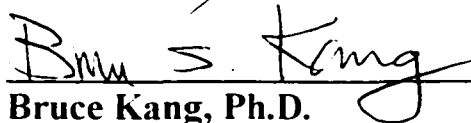
Jian Wan

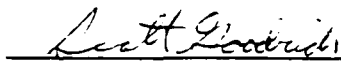
A DISSERTATION

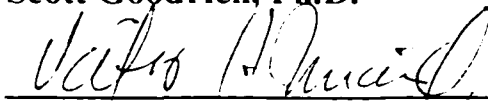
**Submitted to
West Virginia University
in partial fulfillment of the requirements
for the degree of
Doctor of Philosophy**

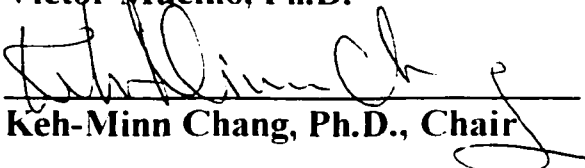
APPROVAL OF EXAMINING COMMITTEE


Eric Johnson, Ph.D.


Bruce Kang, Ph.D.


Scott Goodrich, Ph.D.


Victor Mucino, Ph.D.


Keh-Minn Chang, Ph.D., Chair

4/23/95

Date

ACKNOWLEDGEMENT

The completion of my research work and this dissertation can not be separated from the generous help of following people who deserve my appreciation and should share a little in the glory that comes with authorship.

My first sincere thanks must go to Professor Keh-Minn Chang, my research advisor, who provided thoughtful guidance to almost every tiny detail in my researches. His help did not limit in dissertation research. His goal is to build up a solid research ability in his students, from which I can benefit for my future career. I also would like to give my appreciation to all my committee members, Drs. Eric Johnson, Bruce Kang, Victor Mucino and Scott Goodrich, who gave me invaluable advice and help.

In addition, I would like to thank Jerry Harris, the project manager and my supervisor of my internship in Century Aluminum of WV, Inc., Jorge B. Deschappelles and Brad Whiteleather, for their generous help and support in the temperature profile measurement. I also truly appreciate the help in mechanical testing from Brain Joseph, Michael A. Thurston and Tim Channel of Touchstone Research Laboratory, WV.

Finally, I would like to thank Dr. Hwei-Min Lu and all other members in our research group, who provided their valuable time helping me in the research and preparation of dissertation. Thank you all.

TABLE OF CONTENTS

	Page
ACKNOWLEDGEMENT	vi
TABLE OF CONTENTS	vii
LIST OF TABLES	xi
LIST OF FIGURES	xiii
CHAPTER 1. INTRODUCTION	1
1.1 Statement of Problem	2
1.2 Objective of the Study	3
1.3 Outline of the Dissertation	4
1.4 Terminology	5
CHAPTER 2. LITERATURE REVIEW	7
CHAPTER 3. TECHNICAL APPROACHES	14
CHAPTER 4. IN-SITU TEMPERATURE MEASUREMENT	18
4.1 Experimental	18
4.2 Results and discussion	20
4.3 Summary	26
CHAPTER 5. METALLOGRAPHY ANALYSIS	28
5.1 Experimental	29
5.1.1 Section	29
5.1.2 Heat Treatment	30
5.1.3 Sample Preparation	30

	Page
5.1.4 Metallography	30
5.1.5 Quantitative Analysis	30
5.2 Results and Discussion	31
5.2.1 Fractograph	31
5.2.2 As-Cast Material	31
5.2.3 Tempering Effect	37
5.3 Summary	41
CHAPTER 6. THERMAL-MECHANICAL PROPERTIES	42
6.1 Experimental	45
6.1.1 Tensile Test for As-Received Material	45
6.1.2 Tensile Test for Natural Aged Apecimens	45
6.1.3 On-Cooling Tensile Test	45
6.1.4 Isothermal Aging and Hardness Test	48
6.1.5 On-Cooling Fracture Toughness Test	49
6.2 Results and Discussion	50
6.2.1 Tensile Properties of As-Received Material	50
6.2.2 Natural Aging Effect	50
6.2.3 On-Cooling Tensile Test	53
6.2.4 Isothermal Aging Hardness	61
6.2.5 Fracture Toughness	63
6.3 Summary	63
CHAPTER 7. CONSTITUTIVE MODELING	65

	Page
7.1 Temperature Effect	66
7.2 Solidification Rate	67
7.3 Continuous Cooling Rate	70
7.4 Modeling of Plasticity	74
7.5 Incremental Strain-Stress Relation	78
7.5.1 Elastic Strain-Stress Relation	79
7.5.2 Plastic Strain-Stress Relation	79
7.5.3 Thermal Strain Increment	80
7.6 Summary	81
CHAPTER 8. FINITE ELEMENT MODELING FOR THERMAL STRESS	82
8.1 FEM Modeling Procedure	82
8.2 Computational Domain	84
8.3 Boundary Conditions	84
8.4 Increment Strategy	86
8.5 Material Description	90
8.6 Results and Discussion	92
8.7 Summary	119
CHAPTER 9: CONCLUSION AND FUTURE WORK	121
9.1 Conclusion	121
9.2 Limitation	123
9.3 Suggestion for Future Work	123
REFERENCES	125

	Page
APPENDIXES: ABAQUS Input files	128
APPENDIX A: Input File for Constant Properties of Wrought Al-7050 Material Model	128
APPENDIX B: Input File for Temperature Dependent Properties of Wrought Al-7050 Material Model	139
APPENDIX C: Input File for Temperature Dependent Properties of As-cast Al-7050 Ingot Surface Model	142
APPENDIX D: Input File for Temperature Dependent Properties of As-cast Al-7050 Ingot Center Model	146
APPENDIX E: Input File for Cooling Rate Dependent Properties of As-cast Al-7050 Ingot Model	149

LIST OF TABLES

	Page
TABLE 5.1: Chemical Composition of Aluminum Alloy 7050	28
TABLE 5.2: Volume Fraction vs. Solidification Rate	36
TABLE 5.3: Average Grain Size vs. Distance from Ingot Surface	37
TABLE 5.4(a): Volume Fraction vs. Tempering Temperature	39
TABLE 5.4(b): Volume Fraction vs. Tempering Time	39
TABLE 6.1: Fracture Strength vs. Location	50
TABLE 6.2: Natural Aging Effect	51
TABLE 6.3: Strength at Different Ingot Locations at Elevated Temperatures	54
TABLE 6.4: Comparison of Elongation between Center and Surface at Elevated Temperatures	55
TABLE 6.5: Tensile Properties of Al-7050 at Room Temperature	57
TABLE 6.6: Tensile Properties of Al-7050 at 400°F with Different Continuous Cooling Rates	58
TABLE 6.7: Tensile Properties of Al-7050 at 200°F with Different Continuous Cooling Rates	60
TABLE 6.8: Tensile Properties of Al-7050 at 200°F with Different Aging Time	61
TABLE 6.9: Hardness Measured after Different Time Aging at Different Temperatures	62
TABLE 6.10: On-Cooling Fracture Toughness of Al-7050	63
TABLE 7.1: Qualitative Effects of Various Microstructure Parameters and Temperature on As-cast Mechanical Properties	65
TABLE 7.2: Regression Constants C_{T1} and C_{T2} for Different Solidification Rates	67

	Page
TABLE 7.3: Yield Strength of Al-7050 As-cast Ingot with Different Cooling Rates at Different Temperatures	68
TABLE 7.4: Regression Constants C_{s1} and C_{s2} for Different Temperatures	69
TABLE 7.5: Young's Modulus at Different Temperatures	77
TABLE 7.6: Tangential Modulus E_t At Different Temperatures	78
TABLE 8.1: Elastic Modulus of Al-7050T7451	90
TABLE 8.2: Yield Strength of Al-7050T7451	91

LIST OF FIGURES

	Page
FIGURE 1.1 : Direct Chill Casting	1
FIGURE 3.1 : The Finite Element Simulation System for D.C. Casting	15
FIGURE 4.1 : Devices Layout for In-situ Temperature Measurement	19
FIGURE 4.2 : Thermal Couples Distribution	19
FIGURE 4.3 : Thermal Couples Supporting Jigs	20
FIGURE 4.4 (a) : Cooling Curves in Steady State	22
FIGURE 4.4 (b) : Cooling Curves in Transient Stage	23
FIGURE 4.5 : Temperature Profile for Steady State	24
FIGURE 4.6 : Solidification Rates at Different Locations	25
FIGURE 4.7: Continuous Cooling from 850°F to 400°F	26
FIGURE 4.8: Continuous Cooling from 400°F to 200°F	27
FIGURE 5.1 : As-cast Ingot Pieces	29
FIGURE 5.2(a) : SEM Picture of Initial Area of Cracking Surface	31
FIGURE 5.2(b) : EDX of Cracking Surface	31
FIGURE 5.3 : Microstructures at Different Locations of Al7050 Ingot under SEM	33
FIGURE 5.4 : EDX Results at Different Phases of As-cast Al 7050	34
FIGURE 5.5 : Microstructures of As-cast Al 7050 at Different Distances from Ingot Surface under Optical Microscope	34
FIGURE 5.6 : Relation between Volume Fraction of Eutectic and Average Cooling Rate during Solification	36

	Page
FIGURE 5.7 : Relation between Grain Size and Location of Samples in the Ingot	36
FIGURE 5.8(a) : Microstructures of Al-7050 at Different Tempering Temperature for 2 Hours Followed by a Water Quench	38
FIGURE 5.8(b) : Microstructures of Al-7050 at Tempering Temperature of 850F for Different Periods of Time Followed by a Water Quench	38
FIGURE 5.9 : Relation between Volume Fraction with Tempering Temperature and Time	40
FIGURE 6.1: Testing System Layout for Thermal Mechanical Property Measurement	44
FIGURE 6.2: Fracture Strength of Specimens Sectioned from as-Received Ingot Pieces	50
FIGURE 6.3: The Effect of Natural Aging on Tensile Strength	51
FIGURE 6.4: The Effect of Natural Aging on Elongation	52
FIGURE 6.5: Yield Strength at Different Ingot Locations at Elevated Temperatures	54
FIGURE 6.6: Tensile Strength at Different Locations at Elevated Temperatures	55
FIGURE 6.7: Elongation at Elevated Temperatures for Center and Surface	56
FIGURE 6.8: Stress-Strain Curves at 600°F for Surface and Center	56
FIGURE 6.9: Tensile Properties of As-cast Al-7050 at Room Temperature	57
FIGURE 6.10: Fracture Surface of On-cooling Tensile Test for As-cast Al-7050 ingot at Room Temperature	58
FIGURE 6.11: Tensile Properties of Al-7050 at 400°F with Different Continuous Cooling Rates	59
FIGURE 6.12: Tensile Properties of Al-7050 at 200°F with Different Continuous Cooling Rates	60

	Page
FIGURE 6.13: Tensile Properties of Al-7050 at 200°F with Different Aging Time	61
FIGURE 6.14: Hardness Measured after Different Time Aging at Different Temperatures	62
FIGURE 6.15: On-Cooling Fracture Toughness Results of Al-7050	63
FIGURE 7.1: Temperature Effect on Yield Strength of Al-7050 As-Cast Ingot	66
FIGURE 7.2: Solidification Rate Effect on Yield Strength of Al-7050 As-cast Ingot at Different Temperatures	69
FIGURE 7.3: Effect of Continuous Cooling Rate from 400°F to 200°F on Yield Strength	72
FIGURE 7.4: Aging Effect at 200°F after Cooling from 400°F at 50°F/Min	73
FIGURE 7.5: Plasticity Model ($T_1 < T_2$): (a) Elastic-Linear Work-Hardening Model. (b) Elastic-Perfect Plastic Model	76
FIGURE 7.6: Relation of Elastic Modulus with Temperature	77
FIGURE 8.1: Procedures of Finite Element Modeling	83
FIGURE 8.2: Modeling Procedure of ABABUS	83
FIGURE 8.3: Computational Domain	84
FIGURE 8.4: Meshing and the Boundary Conditions	86
FIGURE 8.5: Temperature Incrementation Strategy	89
FIGURE 8.6: Comparison of Yield Strengths of Five Material Models	91
FIGURE 8.7: Comparison Of Elastic Modulus Of Five Material Models	92
FIGURE 8.8: Thermal Stress Distribution for Constant Properties of Wrought Material Model	99

	Page
FIGURE 8.9: Thermal Stress Distribution for Temperature-Dependent Properties of Wrought Material Model	103
FIGURE 8.10: Thermal Stress Distribution for Temperature-Dependent Properties of As-cast Ingot Surface Model	107
FIGURE 8.11: Thermal Stress Distribution for Temperature-Dependent Properties of As-cast Ingot Center Model	111
FIGURE 8.12: Thermal Stress Distribution for Cooling Rate Dependent Properties of As-cast Ingot Model	115
FIGURE 8.13: Comparison of Maximum Principal Stress of Model 3, 4 And 5	116
FIGURE 8.14: Comparison of Von Mises Stress of Model 3, 4 and 5	117
FIGURE 8.15: Normalized Von Mises Stress Distribution for Temperature Dependent and Cooling-Dependent Properties Models	118

CHAPTER 1

INTRODUCTION

Direct-chill (D.C.) casting is one of the most important methods for the production of high strength aluminum alloys. The main advantages of D.C. casting are permitting large dimension casting and having high productivity [1]. D.C. casting is a semi-continuous process which makes long ingots with different cross sections. Cooling water is sprayed below a water-cooled mold to extract the heat from the filling liquid metal and solidify it into an ingot. This process is schematically shown in Figure 1.1. Initially, the mold is closed by a bottom block. When the liquid metal fills to a certain height in the mold, the bottom block starts to move down at a slow steady rate, while cooling water is sprayed below the mold onto the surface of the emerging ingot. The bottom and each surface of the ingot solidify first, and become the "mold" for the remaining liquid metal.

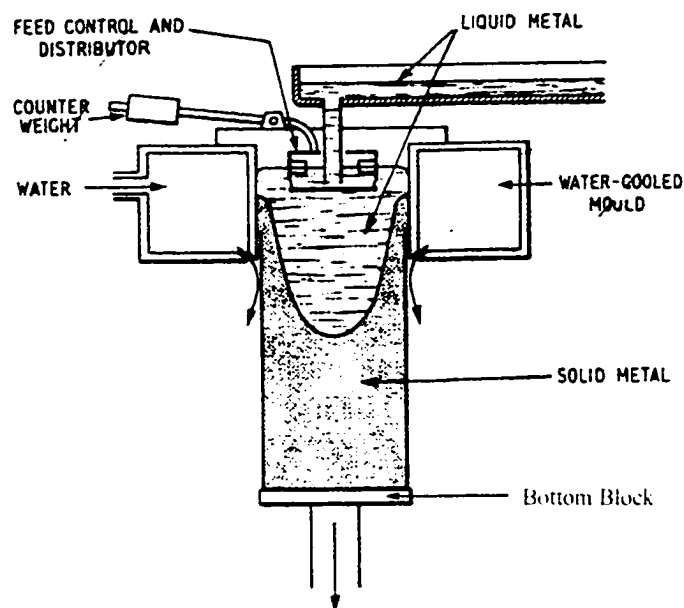


Figure 1.1: Direct Chill Casting

D.C. casting proceeds in three main stages: (1) the transient stage or start stage, during which the temperature field and the solidification front change with time; (2) the steady state or pseudo-stationary stage, during which the above parameters remain nearly constant; and (3) the end stage, during which melted metal pouring is stopped and the ingot cools down.

1.1 STATEMENT OF THE PROBLEM

During D.C. casting, the bottom and the surface of the ingot are rapidly chilled down by the mold, the bottom block and the impinging cooling water. However, the center of the ingot is still kept hot by the liquid metal. The great thermal unevenness builds up enormous thermal stress which causes the distortions of the ingot such as butt curl, butt swell and pull-in of lateral faces. These distortions are detrimental to the productivity of the process because they require butt saw and further ingot scalping before rolling. Furthermore, due to large thermal stress, hot cracks may initiate at the start phase of the casting, and propagate as the stress elevates. The most common one is the so-called "up-the-center" crack which propagates along the center line of the rolling surface. The casting cracks increase production cost and also bring safety concern.

[2]

Many efforts have been made in industry to minimize the thermally induced stress during casting, which include adjusting the casting parameters, such as drop rate, cooling water flow rate, distribution of cooling water around the mold, etc., according to practical experiences. In addition, distribution bags and head skimmers are used to improve the flow pattern of liquid metal in the mold. Insulation pads are placed on the center of the bottom block to reduce the

cooling of the ingot bottom through the bottom block. CO₂ gas is mixed into the cooling water to slow down the heat extraction from the ingot surface. The equipment called “top wipes”, which prevents cooling water from flowing down along the ingot surfaces, is also used to decrease the surface cooling. This causes the surfaces to become reheated, reducing the thermal stress.

However, the trial-and-error in practice is costly to achieve satisfactory results. In order to control the thermal stress and improve the casting, it becomes more and more important to fully understand the casting process. In recent years, finite element numerical modeling is actively applied to simulate the process of DC casting [3-15]. Most of the research concentrates on two subjects: (1) thermal analysis, and (2) stress and distortion calculation. The thermal analysis calculates the temperature distribution of the ingot during casting. Good fitting between thermal simulation and in-situ temperature measurement can be obtained by most of the works on the first subject [3-6]. Uncertainties still remain among the researchers on the stress and distortion analysis. Variation mainly concentrates on the description of the material behavior which will affect the results of the thermal stress calculation.

1.2 OBJECTIVE OF THE STUDY

The major objective of this research is to improve the thermal stress prediction by establishing a thermo-mechanical constitutive model which can describe the material behavior of D.C. cast aluminum ingot in the as-cast condition more accurately. In this constitutive model, dependency of material properties on both temperature and cooling history was emphasized. A high strength heat treatable aluminum alloy Al-7050 was adopted as the model alloy for comprehensive investigation. Special efforts were carried out to correlate the thermo-mechanical properties of

the as-cast ingot material with the cooling history it experienced during casting. New testing method, namely on-cooling tensile test, was implemented to measure the thermo-mechanical properties of the as-cast material at different temperature with different cooling rates. Based on the experimental results, a thermal-elastic-plastic constitutive model was developed. The constitutive model was employed in a finite element computational model to predict the thermal stress distribution of the ingot during casting. Different kinds of material properties were compared. Results showed significant differences between cooling-dependent model with constant and only-temperature-dependent models, which indicated the critical role the constitutive model played in the thermal stress calculation.

1.3 OUTLINE OF THE DISSERTATION

The material in the remaining chapters is organized as follows. In Chapter 2, a brief review of related work on thermal stress analysis of D.C. casting of aluminum ingots and thermo-mechanical property studies on high strength aluminum alloys will be given. Based on this review, integrated technical approaches including in-situ temperature measurement, metallurgical analysis, thermo-mechanical measurement and constitutive modeling, finite element thermal stress calculation will be discussed in Chapter 3. Chapter 4 and Chapter 5 will present the procedures and results of the in-situ temperature profile measurement of casting ingots and metallurgical analysis of as-cast ingot material, respectively. A series of designed mechanical testing were performed to obtain the required thermo-mechanical properties. The data will be presented in Chapter 6. The results in Chapter 6 quantitatively fitted into a thermal-elastic-plastic constitutive model will be presented in Chapter 7. In Chapter 8, numerical simulations of the thermal stress analysis at steady state will be presented. Steady state temperature profile measured in-situ in chapter 4 was used as the initial condition. Several

material constitutive models are to be compared in the simulations of the thermal-induced stresses. Finally, a summary of important finding in this study and some suggestions for the future work will be given in Chapter 9.

1.4 TERMINOLOGY

Solidification Rate Average cooling rate of ingot material from liquidus (1175°F/635°C) to solidus (975°F/524°C) of Al-7050 during direct chill casting. It is calculated by dividing the temperature difference between solidus and liquidus, which is 200°F or 111°C, by the time period the material takes to cool through this temperature range.

Continuous Cooling The cooling period of ingot material at temperature range from solidus (975°F/524°C) of Al-7050 to room temperature during direct chill casting.

Continuous Cooling Rate The cooling rate during continuous cooling period. The rate continuously changes during casting. The “continuous cooling rate” mentioned in Chapter 6 refers to the average cooling rate at different temperature ranges, such as from 850°F/454°C to 400°F/204°C and from 400°F/204°C to 200°F/93°C.

Temperature Dependent The thermal mechanical properties and the parameters in the constitutive model are functions of temperature. The effects of cooling history of the material during casting are not considered.

Cooling History Dependent The thermal mechanical properties and the parameters in the constitutive model are functions of both temperature and cooling history of the ingot material during casting. This dissertation describes the cooling history of as-cast ingot material as the combination of solidification and continuous cooling, and uses solidification rate and continuous cooling rate to express it quantitatively.

Cooling Dependent The “cooling dependent” mentioned in following chapters is the short term from “Cooling History Dependent”

As-received material It refers the ingot pieces having been natural aged in the aluminum plant after cracked from ingot during casting before taken to the lab for testing.

CHAPTER 2

LITERATURE REVIEW

Thermal stress simulation of D.C. casting has been studied extensively in recent years. Both steady state and transient stage were investigated. Numerous constitutive models describing material behavior were used by researchers.

In the stress calculation presented by S. C. Flood [7] *et al.*, linear elastic and non-linear elastic behavior with temperature dependence were compared. The results showed that not only the stress levels but also the stress distributions were different in two cases. Results of non-linear elastic model showed substantially lower stress level than that of linear-elastic model.

Inoue and Ju [8] simulated both temperature and stress field of a cylindrical ingot in D C casting. Temperature dependent elastic-viscoplastic material behavior was employed in their finite element stress field calculation. The total strain rate $\dot{\epsilon}$ is the sum of elastic and inelastic strain rate $\dot{\epsilon}^e$ and $\dot{\epsilon}^i$, as well as the thermal strain rate $\dot{\epsilon}^T$ and the strain rate $\dot{\epsilon}^m$ representing dilatation caused by phase change, shown as Equation 2.1.

$$\dot{\epsilon} = \dot{\epsilon}^e + \dot{\epsilon}^i - \dot{\epsilon}^T + \dot{\epsilon}^m \quad (\text{Eqn 2.1})$$

For elastic strain, Hook's law was adopted, expressed as,

$$\epsilon^e = \frac{1+\nu}{E} \sigma + \frac{\nu}{E} (tr \sigma) I \quad (\text{Eqn 2.2})$$

For thermal strain rate,

$$\dot{\varepsilon}^v = \alpha \cdot \dot{T} I \quad (\text{Eqn 2.3})$$

A unified viscoplastic model is employed to formulate the inelastic strain rate, expressed as,

$$\dot{\varepsilon}^v = \frac{1}{2\mu} \left(1 - \frac{\sigma_v}{(3J_2)^{1/2}}\right) s \quad (\text{Eqn 2.4})$$

where, s is deviatoric stress tensor, and the linear hardened static flow stress σ_v was expressed as,

$$\sigma_v = \sigma_{v0}(T) + H(T)\varepsilon^v \quad (\text{Eqn 2.5})$$

where, H is the hardening coefficient, ε^v and σ_{v0} stand for equivalent viscoplastic strain and initial yield stress, respectively. Both H and σ_{v0} depend on temperature. Material parameters in these constitutive equations were determined from the data of the tensile stress-strain curves under some strain rates at several temperature levels.

Fjær and Mo [9] presented their mathematical and numerical model named ALSPEN in 1990, which calculated the thermally induced stress and strain during D.C. casting. It was a two dimensional (2D) model applied on cylindrical ingots for extrusion billet. An isotropic elastic-viscoplastic material constitutive model was employed in the calculation. Similar with Inoue and Ju's model, the plasticity and the creep were treated in a "unified" manner as one quantity. The viscoplastic strain increment was given according to Prandtl-Reuss relations,

$$d\varepsilon_{vp} = \frac{3}{2} (\varepsilon_{vp}^{\dot{}} \cdot dt) \frac{s}{\sigma} \quad (\text{Eqn 2.6})$$

where, σ is the effective stress, and $\varepsilon_{vp}^{\dot{}}$ is the effective viscoplastic strain rate. Equation 2.7 was used to fit the experiment curves tensile tested for Al-6063 at a series temperature.

$$\sigma = c(T)(\alpha + \alpha_n)^{m_1} (\dot{\epsilon}_{vp})^{m_2} \quad (\text{Eqn 2.7})$$

where, α is the hardening parameter, c , n , m are material constants which are nonlinear functions of temperature.

Fjær and Jensen [10] implemented this “unified” elastic-viscoplastic material model mentioned by Equation 2.6-2.8 in the three dimensional (3D) version of the computer code ALSPEN to investigate the butt curl phenomena during the start-up phase of the aluminum sheet ingot casting of Al-6063. The modified MATMOD equations for Al-6063 and Lalli and DeArdo’s equations for Al-1050 were also implemented in 3D ALSPEN and results are compared. Stress calculated for Al-6063 showed about twice the magnitude of that for Al-1050. However, levels of butt curl are similar for all three models.

Fjær and Hånkonsen[11] showed the improvement of their stress model recently by presenting the ability to predict the lateral face pull-in phenomenon of the aluminum sheet ingot. Similar comparison was carried out between two kinds of temperature dependent elastic-viscoplastic material model associated with different aluminum alloys. For Al-1050, Lalli and DeArdo’s model was applied. For Al-3003, a modified MATMOD equations was used. In latter equations, effective viscoplastic strain rate $\dot{\epsilon}_{vp}$ was expressed as,

$$\dot{\epsilon}_{vp} = B\Theta(T) \left\{ \sinh \left[\frac{1}{a} \left(\frac{\sigma}{d^q} \right)^n \right] \right\}^n \quad (\text{Eqn 2.8})$$

where, $\Theta(T)$ is a function of temperature, and d is a internal variable. B , a , q , n are material constants which were evaluated through tensile tests at temperature ranging from 20°C to 600°C

and strain rates between 2×10^{-4} and 2×10^{-2} . Both 2D model, which used plane strain approximation and focused on the center cross-section of the rolling faces, and 3D model were implemented and compared in their research. Results from 2D and 3D showed close agreement near the center of the rolling faces, while large discrepancies existed when the cross section were close to the ingot narrow end where plane strain assumption became invalid.

In recent years, Drezet and Rappaz [12-15] studied extensively the distortions during DC casting, especially the lateral faces pull-in. They investigated the deformation and temperature field experimentally [12], and a transient thermomechanical model was developed. Based on the commercial finite element software ABAQUS, they built the 2D thermal/stress model, which focused the computational domain on cross-section located at the center of the rolling faces in their earlier study [13] and improved it to the comprehensive 3D model in their recent research [14]. Drezet and Rappaz [15] applied their model further to the optimization of the mold design based on the results of their simulations. However, the thermal-elastic-viscoplastic constitutive model implemented in their stress modeling showed little changes through out their papers. Superposition assumption of incremental deformation expressed by Equation 2.1 was adopted in their constitutive model (using strain increment instead of strain rate in Equation 2.1). So did the expressions for elastic and thermal strain increment described by Equation 2.2 and 2.3. The viscoplastic strain increment adopted Equation 2.6. The concept of the "coherency" temperature, above which the alloy was treated as a liquid and below which the alloy was treated as a solid, was also adopted in their modeling. Different equations for viscoplastic strain rate $\dot{\epsilon}_v$ were used for different temperature ranges. For material at temperature below solidus, Garafalo law was followed.

$$\dot{\varepsilon}_{vp} = A \left[\sinh\left(\frac{\sigma}{\sigma_0}\right) \right]^n \exp\left(-\frac{Q}{RT}\right) \quad (\text{Eqn 2.9})$$

where, A, σ_0 and n are alloy-dependent constants which were evaluated through creep tests. For material at temperature between solidus and coherence temperature, Norton-Hoff law was followed.

$$\dot{\varepsilon}_{vp} = k \cdot \left(\frac{\sigma}{\sigma_0}\right)^n \quad (\text{Eqn 2.10})$$

where, k, σ_0 and n are temperature-dependent constants which were evaluated through indentation test.

Magnin, *et al.* [16] determined the ductility of Al-4.5%Cu alloy over a wide range of temperature going from room temperature to the dendrite coherency temperature through tensile tests. The stress-strain curves measured for material in both semi-solid and solid states were used to establish an elastoviscoplastic constitutive model, expressed as,

$$\begin{aligned} \sigma &= K (\dot{\varepsilon}_{vp} + \dot{\varepsilon}_{vp}^i)^m (\varepsilon_{vp} + \varepsilon_{vp}^i)^n \quad \text{for plastic range} \\ \sigma &= E \varepsilon_e \quad \text{for elastic range} \end{aligned} \quad (\text{Eqn 2.11})$$

where, initial viscoplastic strain rate $\dot{\varepsilon}_{vp}^i$, initial viscoplastic strain ε_{vp}^i , m and n depend on material and temperature.

The results were introduced into a 2D axisymmetrical numerical model of D.C. casting and thermal stress in steady state was calculated. A hot cracking criterion in terms of plastic strain was proposed in their paper.

Microstructural considerations were involved in the constitutive modeling by some researchers. Estrin [17] developed a constitutive model which was based on dislocation density evolution during the deformation process. This model directly implemented the microstructural features of the material, such as the grain size, spacing between second-phase particles, etc. in the constitutive equations. Effect of second-phase particles on the creep behaviour was emphasized. Gehanno *et al.* [18] studied the mechanical behavior of Al-6xxx aluminum alloy at temperatures between 212°F/100°C and 572°F/300°C through different tests, such as creep test and tensile test. The resulted strain rate-stress relations were used to establish the constitutive equations with internal variables to describe high temperature mechanical behavior of industry aluminum alloys such as Al-6063. The value of the parameters in the constitutive model can be directly related to the microstructure features. Duval [19] also modeled the plastic behaviour of cold-rolled aluminum alloy 3104 based on its microstructures. Similar study were carried out by Chu and Granger [20] and Ha. *et al.* [21].

More constitutive models were presented in the studies of quenching residual stress, in which the material were only concerned within the solid range. Savamiphakdi and Kropp [22] developed a uncoupled thermo-elastic-plastic-creep model for thermal treatment of steel parts, in which mechanical properties were affected by temperature. Two methods were compared: (1) additional strain method which includes the additional strain into the constitutive description of the total strain rate, and, (2) material property modification method which modifies the material properties in the transformation temperature range. Franchet *et al.* [23] described the material during quenching as pseudoplastic at high temperature and as elastoplastic at low temperature.

The shrinkage caused by precipitation was considered. Becker *et al.* [24] described the deformation of a Al-4.6%Mg alloy bar during quenching as a combination of thermal strain, elastic strain and inelastic strain, similar as Equation 2.1. The constitutive model is temperature dependent. Denis *et al.* [25] also introduced transformation plasticity into the calculation of internal stresses as an additional strain related to the stress state. K. F. Wang *et al.* [26] applied temperature dependent material properties and a mixed hardening rule in their constitutive model for quenching analysis.

Most of the work in the above mentioned literature only consider the material properties as temperature dependent. Although as-cast materials were tested to setup the constitutive model by some of the researchers, the inhomogeneity of ingot material was neglected in all researches. As presented by Lu *et al.* [27], the microstructure of a D.C. cast ingot was significantly different from the surface to the center, which is a result of different cooling histories at different locations. Therefore, even at the same temperature, materials with different cooling histories may show different mechanical properties. Furthermore, the as-cast materials exhibit significant microsegregation making mechanical properties much different from that of the final product which has only minimum microsegregation. Without these considerations, accurate thermal stress analysis for as-cast ingot is difficult to achieve.

CHAPTER 3

TECHNICAL APPROACHES

Figure 3.1 shows a revised flow chart of finite element simulation needed for D.C. casting. The emphasis of this research are to verify and identify the microstructure difference in a D.C. casting, establish the constitutive model which reflects the thermo-mechanical properties of as-cast ingot with different microstructure, and validate the significance of microstructure factors on the computer simulation. The numerical simulation includes thermal modeling which calculates the temperature distribution of a casting ingot. The results will be an input of the stress modeling which calculates the stress distribution of the ingot by employing a commercial finite element software (such as ABAQUS [28]). Based on the simulation results, casting equipment and parameters can be optimized to improve the stress distribution and minimize the thermal stress in the casting ingot. The research presented in this dissertation are shown as the blocks with stars.

In order to calculate the boundary conditions for the thermal modelling, and provide direct input for stress calculation, temperature profile were measured in-situ during production ingot D.C. casting. As-cast aluminum ingot was metallurgically studied to investigate the effect of the cooling rate during casting on the ingot microstructures by correlating the metallographic results with the cooling curves from in-situ temperature profile measurement.

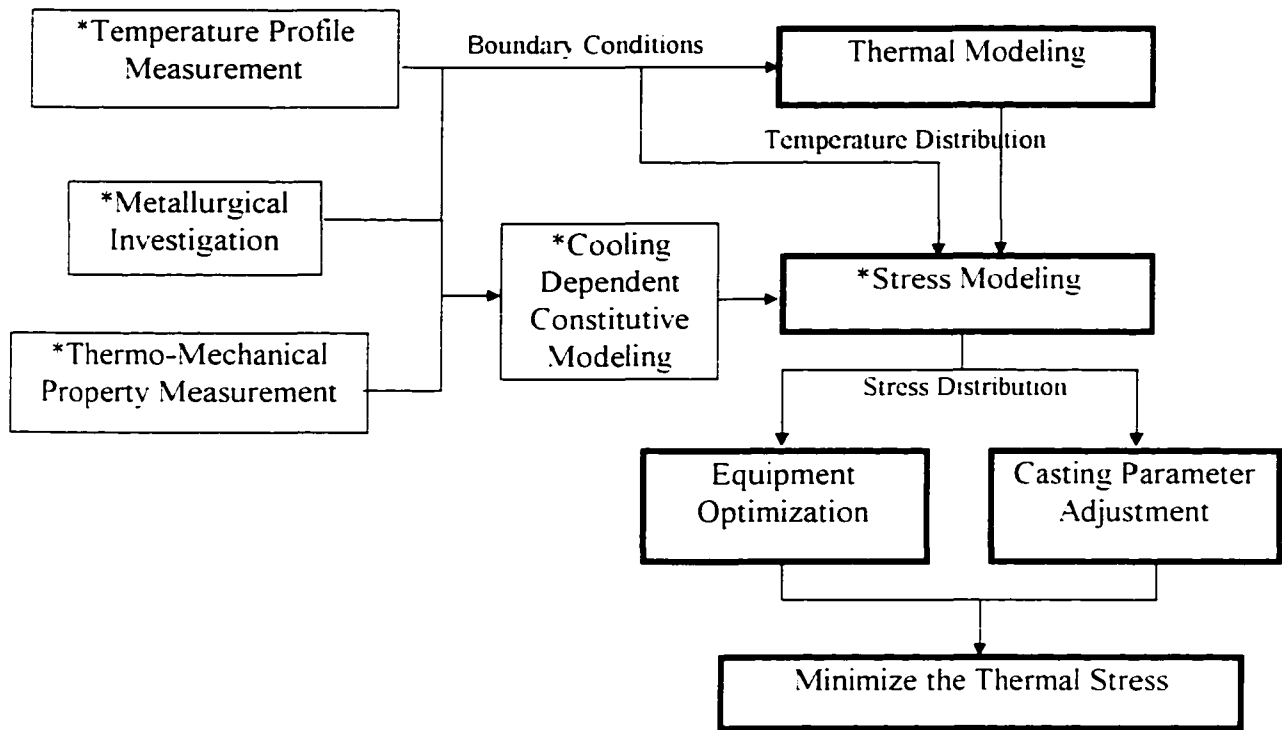


Figure 3.1 The finite element simulation system for D.C. casting

The cooling histories at every location during D.C. casting can be divided into two portions: 1) solidification between the liquidus and solidus, which determines the grain size and the amount of eutectic phases along grain boundaries; 2) continuous cooling, which affects the precipitation reaction both within grain and at grain boundary. The mechanical properties of the material are the combined result of these two cooling portions. In order to establish the correlations between cooling histories and the material properties of as-cast ingot, a series of mechanical tests were designed, which considered both temperature and cooling effects on the material properties. The tests includes several parts: isothermal aging and hardness tests, tensile test for as-received cracked ingot at room temperature, natural aging tensile test, on-cooling tensile test at elevated temperatures, on-cooling fracture toughness test. It is important to know that most high strength

aluminum alloys undergo a age-hardening reaction at room temperature. This natural aging process may confuse the real mechanical properties of as-cast ingot. As-received ingot pieces have been naturally aged for several weeks in the plant before taken to the lab for testing. The mechanical properties of these ingot pieces will not only reflect the effect of cooling during the ingot casting, but also the effect of natural aging. Natural aging and tensile tests were conducted to show this effect. On-cooling tensile tests were designed to eliminate this natural aging effect. It consisted of two sets. The first set mainly investigated the solidification rate and temperature effect through tensile tests at various temperatures for material from different location of ingot. The second set investigated the continuous cooling rate effect at different temperatures through a series of two-step on-cooling tensile tests. Isothermal aging and hardness tests were carried out to qualitatively investigate the effects of precipitation reaction at different temperatures. In order to attain useful information about failure criterion for casting ingot, on-cooling fracture toughness tests were implemented for both surface and center of the ingot to investigate toughness differences at different locations of ingot. In addition, tensile properties of Al-7050 at room temperature were investigated.

Based on the results of temperature profile measurement, metallurgical analysis and thermal mechanical property measurement, correlation between temperature history during casting and thermo-mechanical properties was established. According to this correlation, a thermal-elastic-plastic constitutive model was setup, which was implemented in the finite element modeling for thermal stress analysis. A two-dimensional plain strain model was built using commercial FEM code ABAQUS to calculate the thermal stress distribution in the longitudinal cross-section at the center of rolling faces of the casting ingot in steady state. An increment strategy for temperature

profile input was used through user subroutine for the steady state stress analysis. Five different kinds of material property models were used in the stress simulation separately and results were compared. These models are: 1) temperature-independent material properties for heat treated Al-7050 (Al-7050T7451) from literature; 2) temperature-dependent material properties for heat treated Al-7050 (Al-7050T7451) from literature; 3) temperature-dependent material properties for as-cast Al-7050 measured at the ingot surface; 4) temperature-dependent material properties for as-cast Al-7050 measured at the ingot center; 5) temperature-cooling rate dependent material properties for as-cast Al-7050 considering the measurement at different location of the ingot. The results were compared to illustrate the significance of microstructural effects on the stress analysis by computer simulation.

CHAPTER 4

IN-SITU TEMPERATURE MEASUREMENT

In order to determine the cooling histories at different locations of the ingot during casting, temperature fields were measured in-situ during a production casting of an aluminum 7050 ingot at Century Aluminum of WV, Inc. Various methods have been used by several researchers [29-33] The following presented experiments adopted the most commonly used thermocouple-casting method.

4.1 EXPERIMENTAL

The measurement was implemented by casting thermocouples (T/C's) into the withdrawing ingot during the casting. The thermocouples used in the measurement were type J (iron-constantan, temperature range from -346 °F to 2193 °F). A 60 channel data recorder was employed to acquire and convert the output voltage of the T/C's to temperature. The layout of the devices is shown in Figure 4.1. The T/C's were distributed along the two center lines of the ingot cross section, and around the corner of the ingot. The detailed locations of the T/C's are shown in Figure 4.2. There are eight T/C's along each center line. The four of them near the ingot surface were close to each other with half inch spacing. They measured the temperature changing near the surface which will be used in the boundary condition calculation for thermal modeling. The other four T/C's were mainly used to measure the temperature profile along the center line of the ingot. All T/C's were attached to L-shaped steel jigs, shown in Figure 4.3, which assured that the T/C's remained at the desired locations.

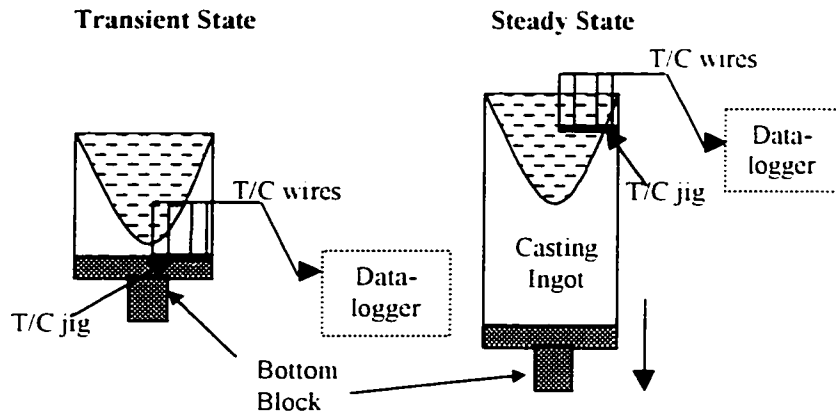


Figure 4.1: Devices Layout for In-situ Temperature Measurement

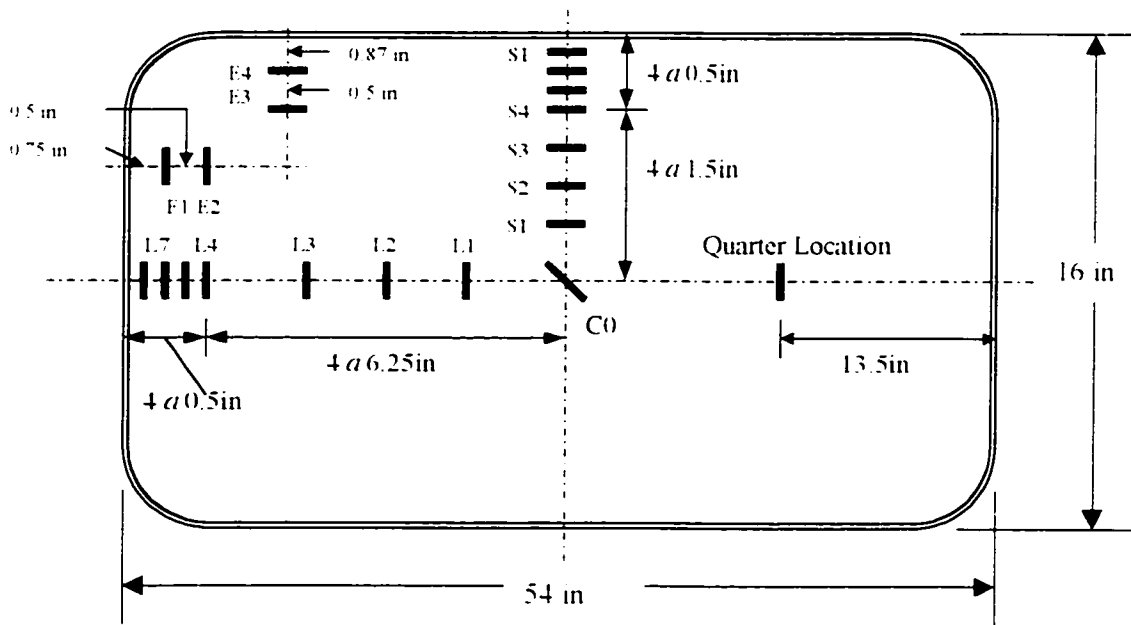


Figure 4.2: Thermocouples distribution

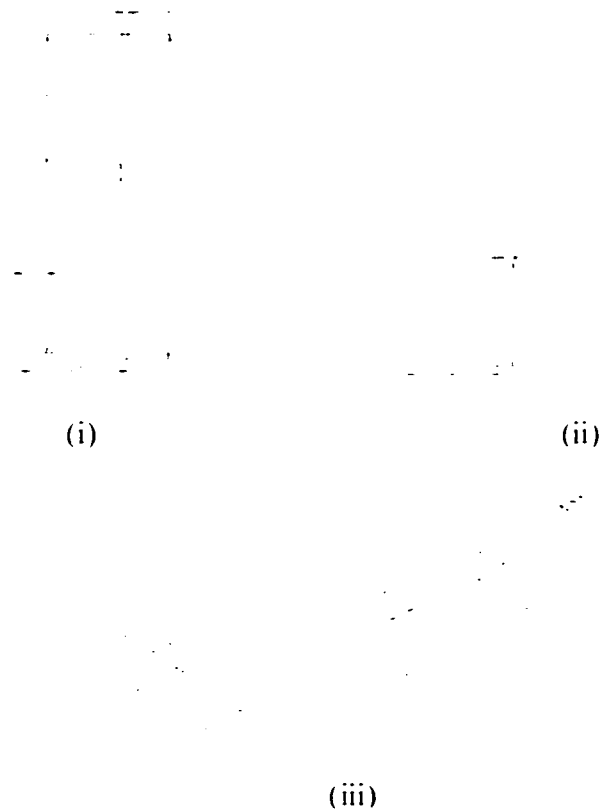


Figure 4.3 Thermocouple Supporting Jigs: (i) along center line for transient measurement, (ii) at corner of the ingot, (iii) along center line for steady state

Cooling histories in both transient and steady states were measured. For the transient measurement, T/C's were attached to a long jig and a short jig, then taped to the bottom block before casting, shown in Figure 4.1. For the steady state measurement, the jigs were put into the ingot from the top after the ingot length reached 30 inches. In both cases, T/C's moved with the withdrawing speed and temperatures were recorded by the data recorder as the ingot solidified and cooled down.

4.2 RESULTS AND DISCUSSIONS

Figure 4.4 shows the cooling curves measured in the transient and steady states. Using a casting rate of 1.9 in/min, cooling curves in the steady state can be converted to temperature profiles in

the cross-sections along the long and short axes. These are shown in Figure 4.5. As seen in the cooling curves of both the transient and steady states, faster cooling is observed near the surface and the corner of ingots, while slower cooling is observed near the ingot center.

For the steady state, the incubation time to start cooling increased as the location moves toward the center, and a liquid metal sump was developed. As shown in the transient cooling curves, the temperature measured at the ingot center dropped faster at the start. This indicates that there is extensive heat extraction from the bottom block at the starting stage. In addition, the crossover of the cooling curves was observed at the four locations near the center in transient measurement, which may relate to the occurrence of butt curl during the first several minutes of the casting.

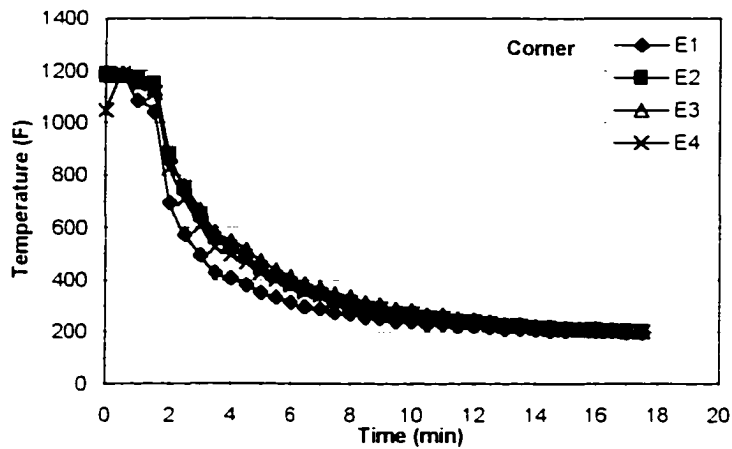
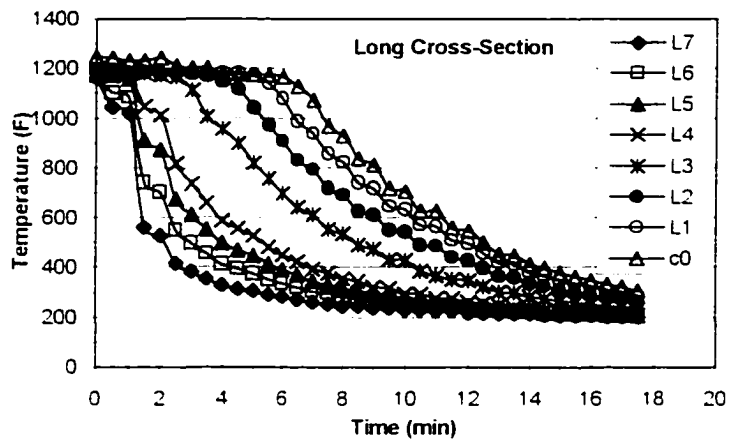
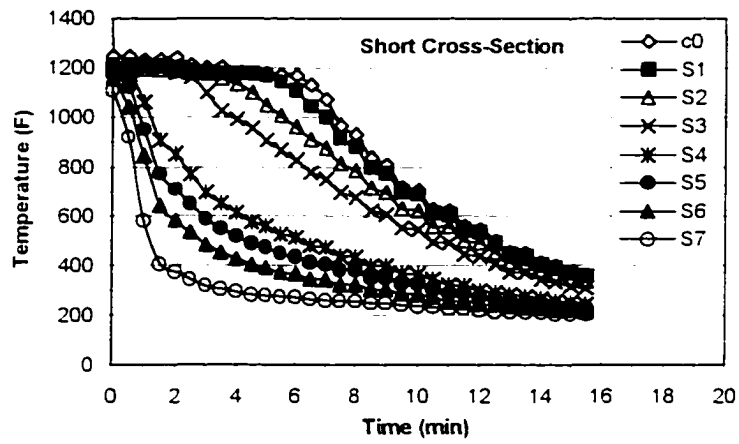


Figure 4.4(a): Cooling curves in steady state

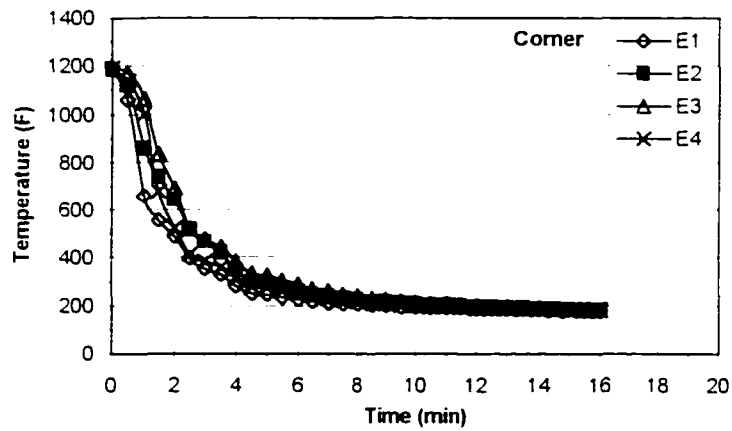
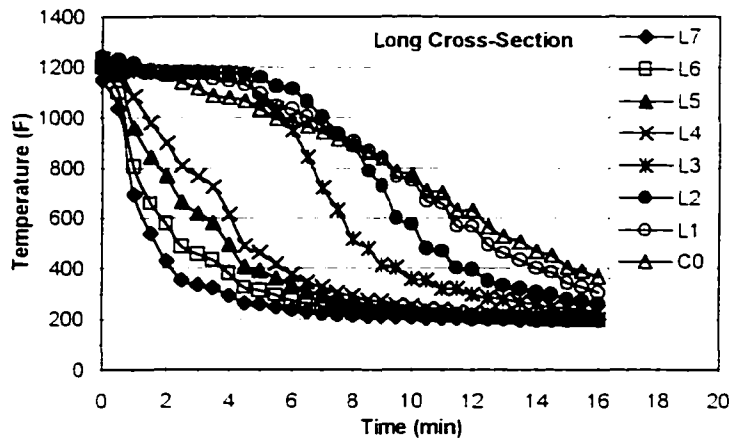
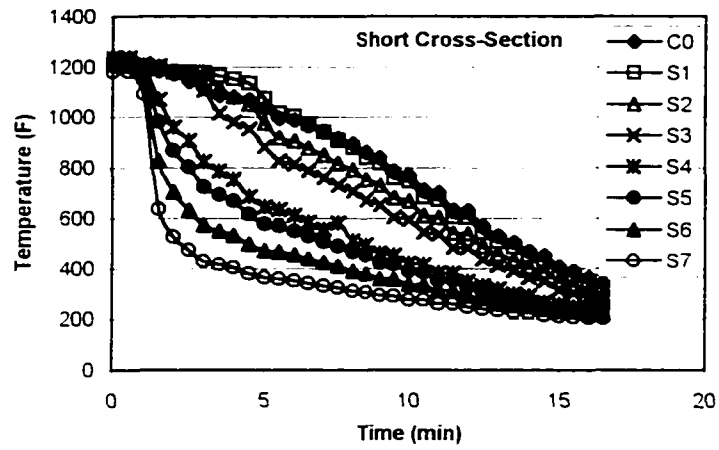
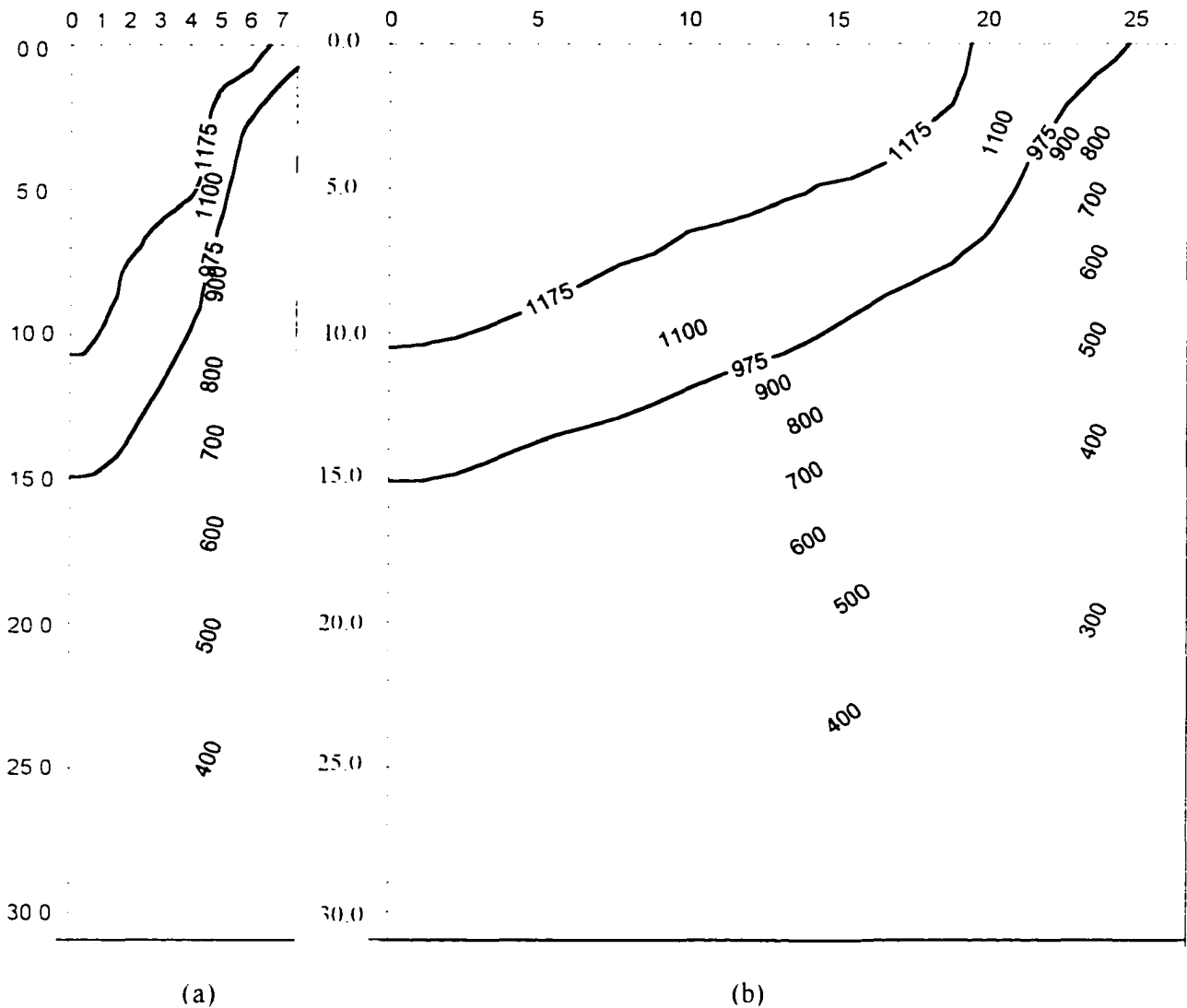


Figure 4.4(b): Cooling curves in transient stage



(a) (b)
 Figure 4.5: Temperature profile for steady state
 (a) cross-section along short axis (b) cross-section along long axis

As mentioned in Chapter 3, cooling history at each location can be divided into two portions: solidification and continuous cooling, which determine different characters of the microstructures and the mechanical properties of the as-cast ingot material.

The solidification rate used in this study is defined as the average cooling rate between liquidus (1175°F/635°C) and solidus (975°F/524°C). They were calculated from the measured

temperatures at different locations along short centerline of the cross-section during steady state measurement (shown in Figure 4.4(a)). Results are plotted in Figure 4.6 as a function of the distance from ingot surface. The solidification rate is extremely high ($\sim 4^\circ\text{C}/\text{sec}$) at ingot surface, but decreases rapidly as the distance from surface increases. It is almost constant beyond 3 inches deep from the ingot surface.

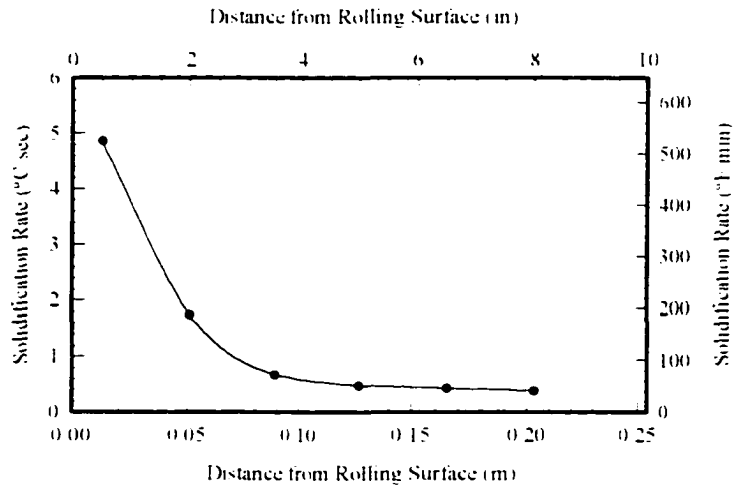


Figure 4.6: Solidification rates at different locations along short centerline during steady state

After solidification, cooling rate continuously changes during casting. For steady state, at higher temperature range (from solidus to $400^\circ\text{F}/204^\circ\text{C}$), average cooling rate follows the same trend as average solidification rate, with high rate within a short distance from ingot surface. Most locations inside the ingot cooled at almost the same rate (about $80^\circ\text{F}/\text{min}$ or $0.74^\circ\text{C}/\text{sec}$). At lower temperature range (from $400^\circ\text{F}/204^\circ\text{C}$ to $200^\circ\text{F}/93^\circ\text{C}$), all locations cooled slowly with ingot center showing slightly higher rate than surface. Figure 4.7 shows the average cooling rate from solidus to $400^\circ\text{F}/204^\circ\text{C}$ and from $400^\circ\text{F}/204^\circ\text{C}$ to $200^\circ\text{F}/93^\circ\text{C}$ as the function of distance from ingot center along the centerlines of ingot cross-section during steady state. Besides, the

cooling at every location becomes very slow when temperature reaches 200°F/93°C. It may take several hours for the whole ingot cooling to room temperature.

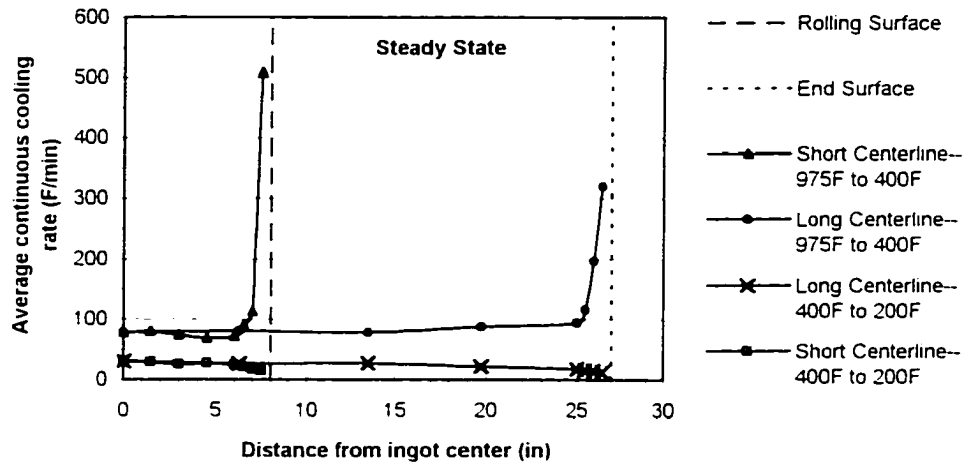


Figure 4 7: Average continuous cooling rate along the center lines of ingot cross-section during steady state

4.3 SUMMARY

In this chapter, the in-situ temperature profile measurement during production casting of Al-7050 ingot is described in detail. Both transient and steady states of casting process were measured. Cooling curves and temperature profile for the short and long cross-section of the ingot were obtained. The results show that different locations of ingot experience various cooling histories which change continuously from ingot surface to the center. The differences in cooling history can be further described as the differences in solidification rate and continuous cooling rate.

which influence the microstructure of the as-cast material and mechanical properties differently
Chapter 5 and Chapter 6 will present these influences in detail.

CHAPTER 5

METALLOGRAPHY ANALYSIS

Mechanical properties of the material depend on its microstructure. Since the aluminum ingot is not cooled evenly during the casting, significant differences of microstructures will be observed from location to location. To understand the effect of cooling rates on the properties of an as-cast high strength aluminum alloy requires a comprehensive analysis of microstructure through the whole cast ingot. In addition, the as-cast material exhibits notable microsegregation along grain boundaries, which is seldom observed in the wrought product. These characteristics of microstructure will definitely affect the mechanical behavior of the material. Based on such considerations, as-cast Al-7050 ingot pieces were studied at different locations under optical microscope, Scanning Electronic Microscope (SEM) and Energy Dispersion Analysis of X-ray (EDAX). The effects of the cooling history during casting on ingot microstructures were obtained by comparing the microstructures of materials with different cooling histories. The tempering effect was also studied by heat treatment and metallographic observation.

The nominal composition of Al-7050 is given in Table 5.1.

Table 5.1. Chemical Composition of Aluminum Alloy 7050

Element	Al	Zn	Mg	Cu	Zr
Wt. %	Balance	6.2	2.3	2.3	0.12

As-cast Al-7050 ingot pieces were provided by Century Aluminum of WV, Inc. The pieces came from ingots cracked during casting, as shown in Figure 5.1. The pieces were close to the center of the rolling surface. One has the dimension of about 16x8x5 in³, the other has the dimension of about 16x5x5 in³.

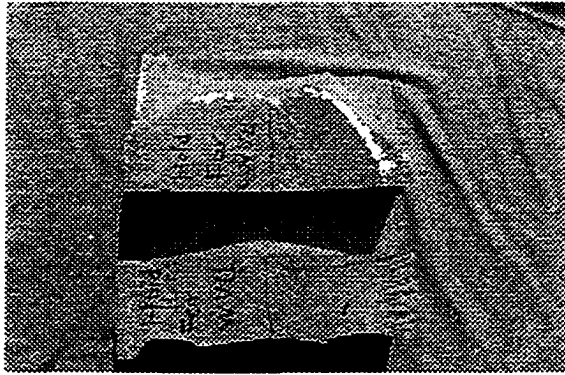


Figure 5.1: As-cast Ingot Pieces

5.1 EXPERIMENTAL

5.1.1 SECTION

The samples for metallography analysis were sectioned from the ingot piece at locations of 0, 0.5, 2, 3.5, 5, 6.5 and 8 inches away from the rolling surface respectively. The sample at 8 inches is located at the center between the two rolling faces. These are identical to the locations of the thermocouples which were cast into the ingot to measure the temperature. Because the ingot pieces were close to the center of rolling faces, the cooling histories of these samples were assumed to be the same as the measurement along the short center line of ingot cross-section.

5.1.2 HEAT TREATMENT

To analyze the tempering effect on the microstructure, the samples cut from ingot center were heated at 600°F (315°C), 650°F (343°C), 700°F (371°C), 800°F (427°C), 900°F (482°C), and 950°F (510°C) for 2 hours, followed with water quench. Tempering times were also studied by holding at 850°F (454°C) for 1 hour, 2 hours, 4 hours, 8 hours, and 16 hours, followed with water quench.

5.1.3 SAMPLE PREPARATION

The initial area of the crack surface sectioned from D.C. casting ingot pieces was washed by water and diluted HCL (5%) solution. The samples, including both as-cast and heat-treated, were first ground with 300, 600, and 800 grit sand papers, then polished using 1 micron alumina powder. The samples were etched with dilute Kellers reagent (2 ml HF (48%), 3 ml HCl (conc.), 5 ml HNO₃ (conc.), 190 ml water) (2:1) solution for 15 seconds.

5.1.4 METALLOGRAPHY

The crack surface and prepared samples were analyzed using Scanning Electronic Microscope (SEM), optical microscope with a computer controled digital camera and EDAX.

5.1.5 QUANTITATIVE ANALYSIS

Quantitative analyses were carried out from the pictures taken. The grain size was determined through the interception procedure according to ASTM E112 [34], and the volume fraction of eutectic phases was determined by systematic manual point count procedure according to ASTM E562 [34].

5.2 RESULTS AND DISCUSSIONS

5.2.1 FRACTOGRAPH

As shown in the SEM picture in Figure 5.2(a), the crack on the DC cast ingot pieces was intergranular. Microcracks can also be observed around the initial area of the crack along the grain boundary. Further evidence that cracking is highly related to the grain boundary segregated eutectic phases can be found in the EDAX results. The X-ray spectrum in Figure 5.2(b) was obtained by focusing the electron beam on one of the flat grain faces. A high Cu peak was exhibited. Similar EDAX results were also observed in the block-shaped eutectic phase at the grain boundary of the as-cast material shown in Figure 5.4.

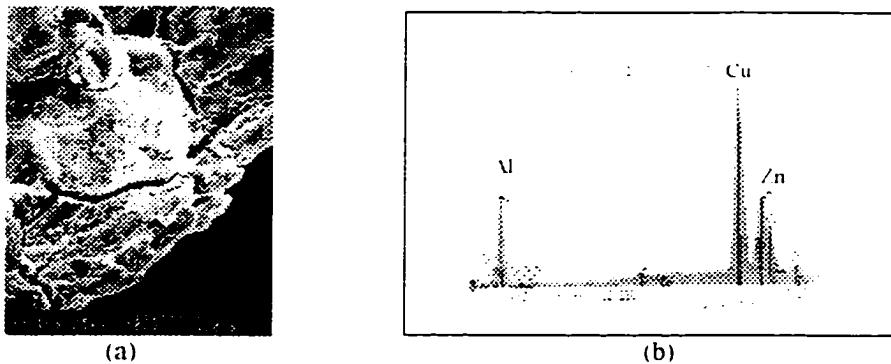
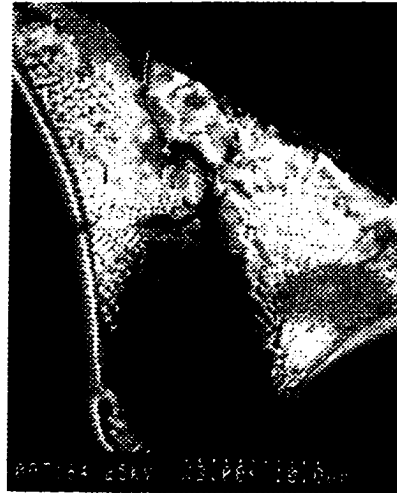
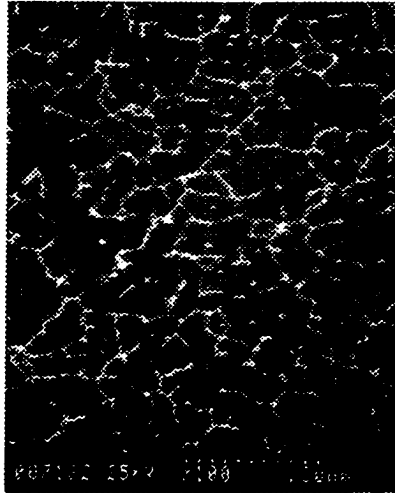


Figure 5.2: (a) SEM picture of initial area of crack surface
(b) EDAX of crack surface

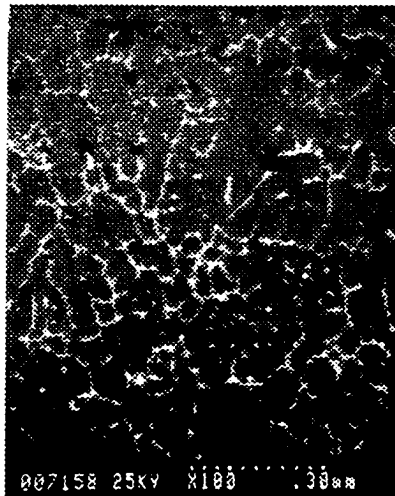
5.2.2 AS-CAST MATERIAL

Results of the as-cast material sectioned from different locations of Al-7050 ingot are shown in Figure 5.3, 5.4, and 5.5. In the EDAX results, 1000 points were counted and the highest peak was normalized to 1.

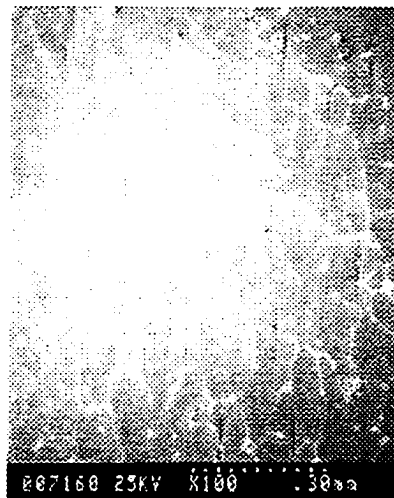
0.5 inches from
ingot surface



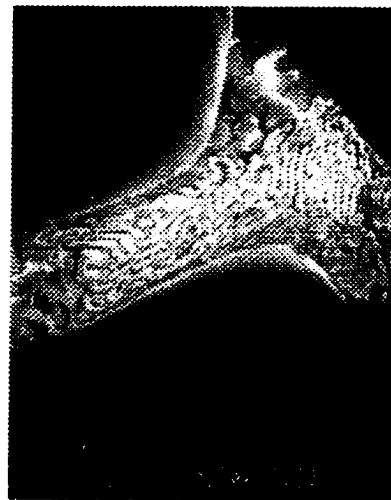
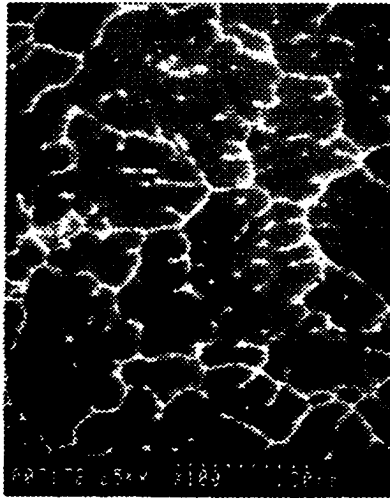
2 inches from
ingot surface



3 inches from
ingot surface



5 inches from
ingot surface



6.5 inches from
ingot surface

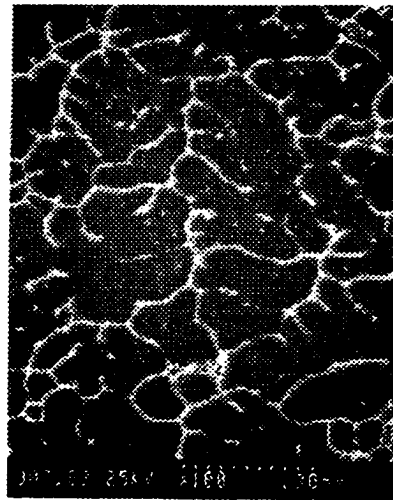
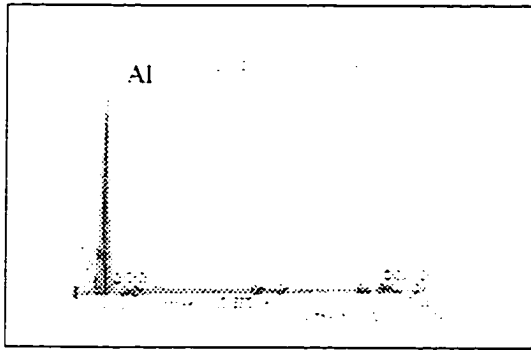
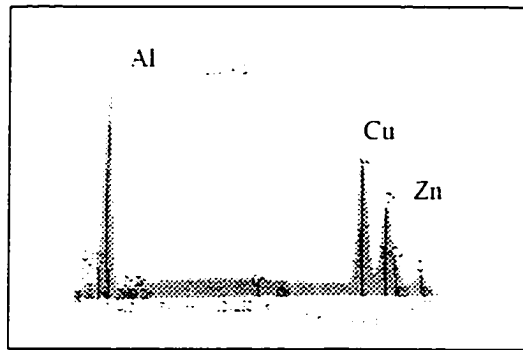


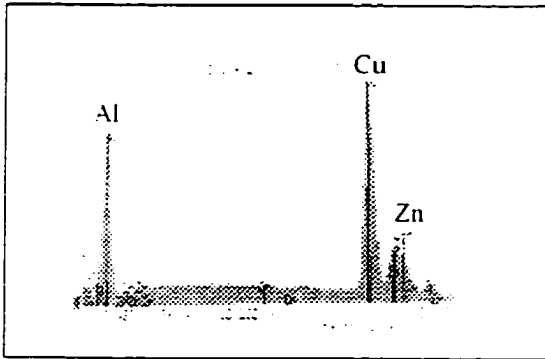
Figure 5.3: Microstructures at different locations of Al-7050 ingot under SEM



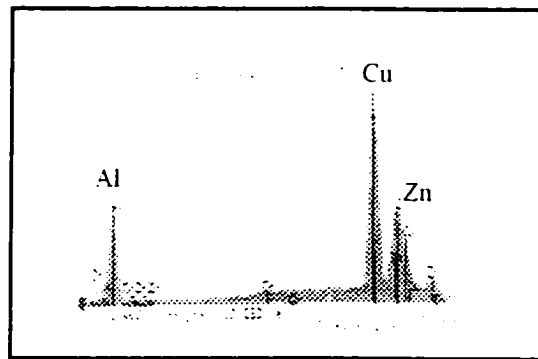
At Matrix



At Laminated Eutectic Phases



At Block Shape Eutectic Phases



At Crack Surfaces

Figure 5.4: EDAX results at different phases of as-cast Al-7050

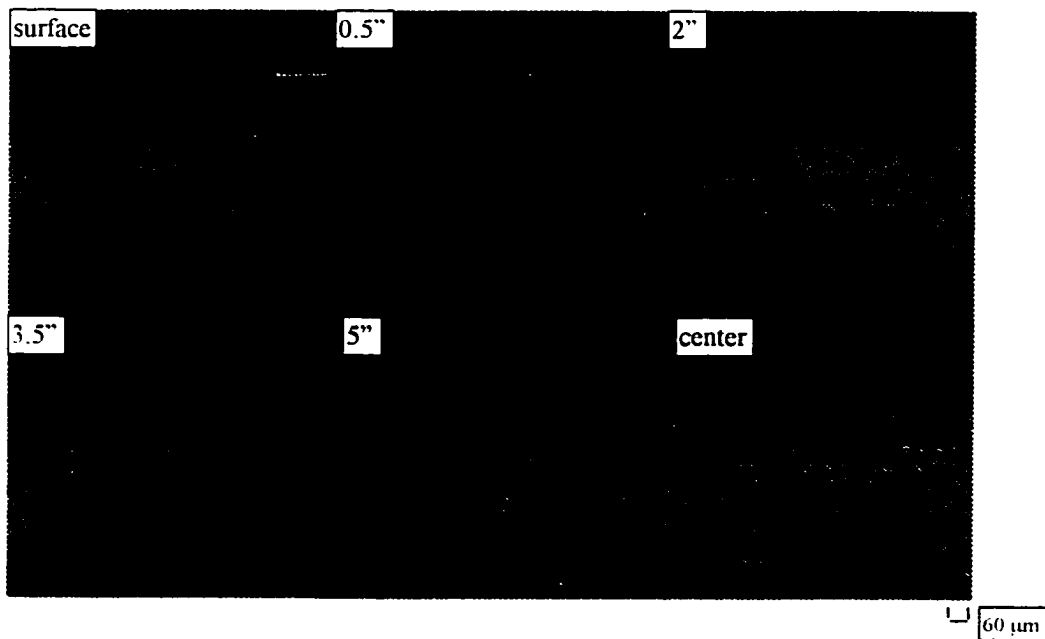


Figure 5.5: Microstructures of as-cast Al-7050 at different distances from ingot surface under optical microscope

Eutectic phases segregating along grain boundaries can be observed from the SEM pictures of as-cast Al-7050 at all locations. Early work [35][36] suggested that three major types of solidification terminal phases can be identified: (1) eutectic phases: Al – Al₂CuMg – MgZn₂, (2) impurity phases: α AlFeSi(\Rightarrow Al₇Cu₂Fe), Mg₂Si, (3) inclusion: ZrAl₃. After solidification, other phases, such as η (MgZn₂) phase, will precipitate within the grains as the solid ingot continuously cools down to room temperature.

The differences among the microstructures at different locations are significant, as seen in Figure 5.3. Needle-like η phase can be observed near the slowly-cooled center of the ingot but absent near the fast-cooled surface. The amount and morphology of the eutectic phases shows gradual changes from surface to center. Eutectic networks are dense but thin for the material near the surface of the ingot, while becoming loose and coarse near the center of the ingot. Results of volume fraction measurement of eutectic phases are shown in Table 5.2, comparing with the solidification rates described in Chapter 4. The relation between the volume fraction of eutectic phases and solidification rate are shown in Figure 5.6, which indicates that the amount of eutectic phases increases as the solidification rate decreases.

Table 5.2: Volume fraction of eutectic phases vs. solidification rate

Distance from surface (in)	6.5	2	0.5
Solidification Rate ($^{\circ}\text{F}/\text{min}$)	45.2 (0.4 $^{\circ}\text{C}/\text{sec}$)	187.1 (1.7 $^{\circ}\text{C}/\text{sec}$)	524.5 (4.9 $^{\circ}\text{C}/\text{sec}$)
Volume Fraction (%)	11.2	7.1	4.6

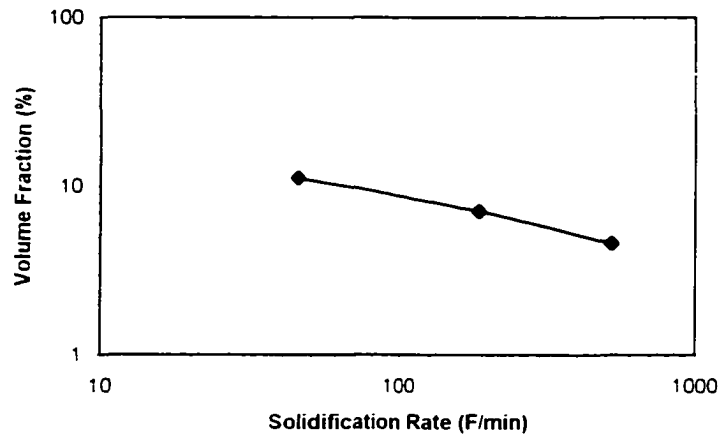


Figure 5.6: Relation between volume fraction of eutectic and average cooling rate during solidification

The cooling rate during solidification also notably affects the grain size. The results of quantitative measurement are listed in Table 5.3. Figure 5.7 indicates that higher cooling rate during solidification results in finer microstructure.

Table 5.3: Average grain size vs. distance from ingot surface and solidification rate

Average grain size (micron)	Distance from edge (in)	Solidification Rate ($^{\circ}\text{F}/\text{min}$)
140.9	0	524.5 (4.9 $^{\circ}\text{C}/\text{sec}$)
264.3	3.5	72.0 (0.67 $^{\circ}\text{C}/\text{sec}$)
323.5	5	50.5 (0.47 $^{\circ}\text{C}/\text{sec}$)
370.8	8	40.8 (0.38 $^{\circ}\text{C}/\text{sec}$)

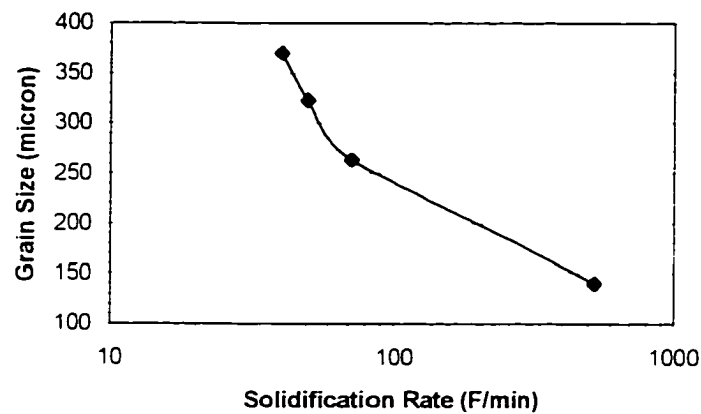


Figure 5.7: Relation between average grain size and solidification rate

5.2.3 TEMPERING EFFECT

Figure 5.8 (a) and (b) show that microstructure of as-cast Al-7050 vary with tempering temperature and time. Table 5.4 lists the results of quantitative study. The amount of eutectic phases decreased as tempering temperature elevates and tempering time increases as shown in Figure 5.9.

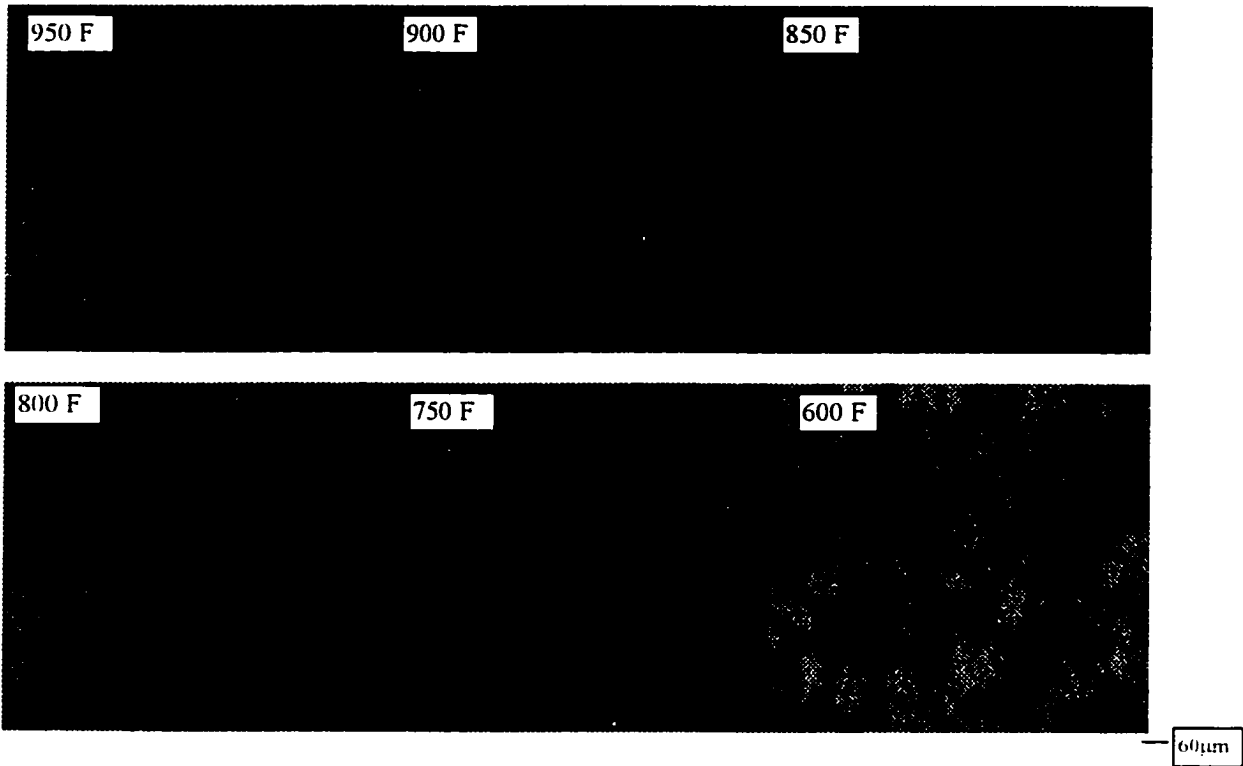


Figure 5.8 (a) Microstructures of Al 7050 at different tempering temperature for 2 hours followed by a water quench

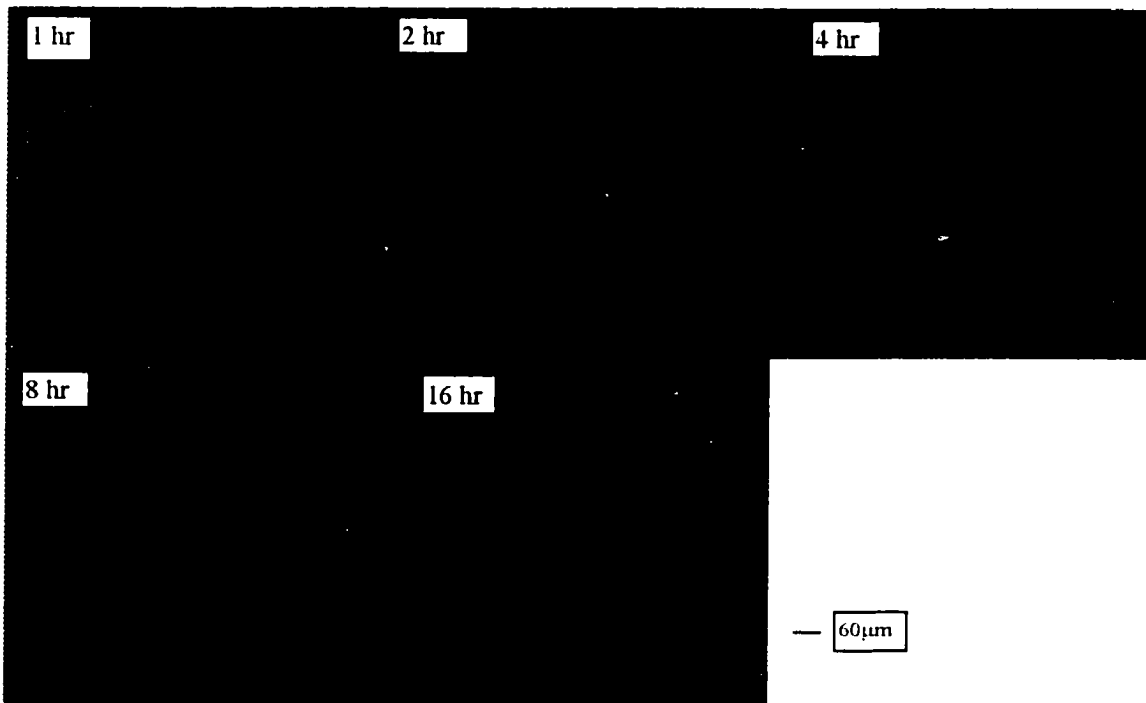


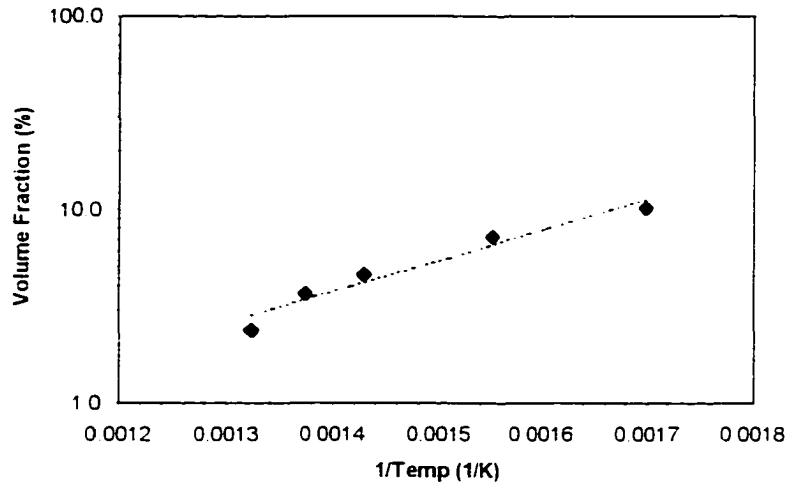
Figure 5.8(b): Microstructures of Al 7050 at tempering temperature of 850F for different periods of time followed by a water quench

Table 5.4(a) : Volume fraction eutectic phases vs. tempering temperature for 2 hour tempering

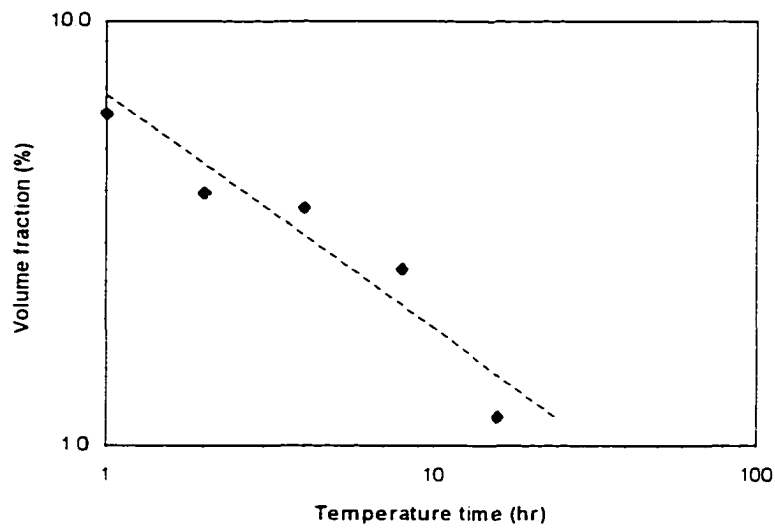
Tempering Temperature(°F)	Volume fraction (%)
600 (315°C)	10.1
700 (371°C)	7.2
800 (426°C)	4.6
850 (454°C)	3.7
900 (482°C)	2.4

Table 5.4(b): Volume fraction eutectic phases vs. tempering time

Tempering time for 850 °F(hr)	Volume fraction (%)
1	6.1
2	3.9
4	3.6
8	2.6
16	1.2



(a)



(b)

Figure 5.9: Relation between volume fraction with tempering temperature and time
 (a) volume fraction vs. 1/tempering temperature for 2 hr tempering time
 (b) volume fraction vs. tempering time at 850 F tempering temperature

5.3 SUMMARY

In this chapter, as-cast Al-7050 ingot pieces were metallurgically analyzed and results were correlated with the cooling history of ingot material during casting. Microstructures of as-cast ingot material show significant difference with that of wrought material. They exhibit various coarse grain size, notable grain boundary segregation and inhomogeneity through out the ingot. Results of quantitative analysis indicate that grain size and amount of eutectic phases increase as solidification rate decreases. Results of fractography and EDAX of the fracture surface of the cracked ingot indicate the strong correlation between casting crack tendency with grain boundary eutectic phases. Tempering effect on the microstructure was studied through a series of heat treatments and metallographical analysis of Al-7050 as-cast ingot material. Tempering reduces the amount of grain boundary eutectic phases, which will increase the fracture toughness of the material. This conclusion supports the higher recovery (successful rate) of the casting production by using "top wipe" equipment which prevents cooling water from going down along the ingot surface, thus reheats the ingot surface below it. The effect of this inhomogeneity of microstructure of as-cast ingot on its thermo-mechanical properties was further studied, which will be the major topic of Chapter 6.

CHAPTER 6

THERMAL-MECHANICAL PROPERTIES MEASUREMENT

The thermo-mechanical properties of the as-cast ingot material used in the thermal-stress modeling are critical to achieve an accurate prediction through the simulations. [17][27]. In addition, the failure criterion for the cracking requires the fracture toughness of the as-cast material. Chapter 4 shows the uneven cooling from location to location during D.C. casting of Al-7050 ingot. As a result, as-cast aluminum alloy 7050 has the structural characteristics much different from that of the wrought product, as shown in Chapter 5. In addition, the as-cast material exhibits various grain size and the amount of eutectic phases and precipitates throughout the ingot. This inhomogeneity determines the variation of thermomechanical properties of the aluminum casting ingot from location to location. All these indicate that the effect of cooling history during D C casting is important for stress modeling. It is necessary to evaluate this cooling effect along with temperature effect on the mechanical properties of as-casting ingot.

As mentioned in previous chapters, cooling rate during solidification mainly determines the grain size and eutectic phases of ingot material which will affect its strength and fracture toughness. The cooling rate during continuous cooling in solid ingot mainly determines the precipitation reaction, which may affect material strength through the ability to restrict the movement of dislocations.

In order to investigate the effects of cooling, a series of mechanical tests were designed. Tensile test at room temperature were conducted for the material from four different locations of the as-

received Al-7050 ingot to study the difference of mechanical properties at different locations of ingot. However, these properties do not represent the real properties of as-cast material, because the ingot pieces received have been naturally aged for several weeks in the plant before taken to the lab for testing. The mechanical properties of the material not only reflect the effect of cooling during the ingot casting, but also the effect of natural aging. Therefore, the natural aging and tensile tests were conducted to identify this natural aging effect, both for center and surface of the ingot. Because of this concern, on-cooling tensile tests were designed to redissolve the precipitates formed during continuous cooling and natural aging and simulate the as-cast condition of the ingot material during casting. The influence of the solidification rate was analyzed by comparing specimens from three typical locations of ingot, namely, center, 2 inches from surface and surface, which represent three different solidification rates, namely, 45°F/min (0.4K/sec), 187°F/min (1.7K/sec) and 524°F/min (4.9K/sec). According to the cooling histories described in section 4.2 and Figure 4.6 and 4.7, on-cooling tensile test, two-step on-cooling tensile test, and on-cooling plus aging tensile test were designed to investigate the continuous cooling effect on mechanical properties. Effect of precipitation reaction after solidification was also studied qualitatively through a series of isothermal aging and hardness test. In addition, several on-cooling K_{Ic} tests were implemented to measure and compare the fracture toughness of as-cast Al-7050 at surface and center locations.

The testing system for all tests employed a Model 810 Material Test System (MTS) which is controlled by a PC computer using a commercial software LabView[37]. Multi-zone parabolic heaters were employed for on-cooling tensile test, also controlled by LabView application

programs. The layout of the system is shown in Figure 6.1. The controlling program includes three main parts: 1) MTS mechanical testing control; 2) data acquisition; and 3) temperature control. For K_{IC} test and room temperature tensile tests, only 1) and 2) were used. The MTS controlling program sends the values of testing parameters (e.g. displacement rate of tensile test) to the MTS controller under closed-loop control to load the specimen. In the meantime, the load-displacement data is acquired and recorded by the computer. For on-cooling tensile tests, all three parts were applied. The temperature controlling program allows the user to maintain a constant temperature and cool at a certain rate. The heating controller regulates the parabolic heaters to heat the specimen. The thermocouples touching the specimen feed back the temperature for the closed-loop control of the heating.

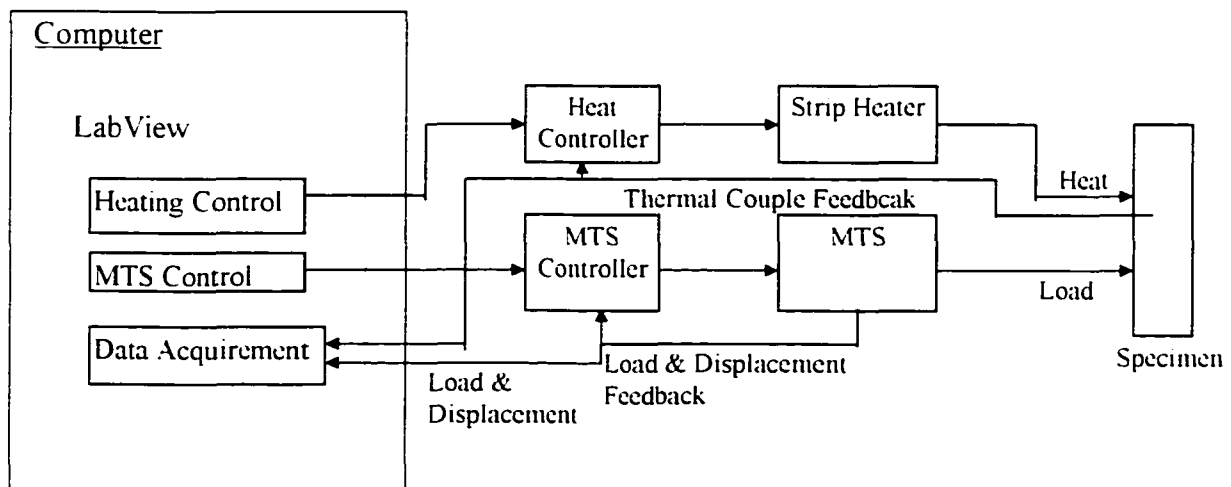


Figure 6.1: Testing system layout for thermal mechanical property measurement

6.1 EXPERIMENTAL

6.1.1 TENSILE TEST FOR AS-RECEIVED MATERIAL

Specimens were prepared from as-received Al-7050 ingot pieces at a series of locations, namely, 0, 2, 3, 5 and 8 inches from the ingot surface. Tensile tests were conducted on these specimens at room temperature. Results were compared with those obtained from natural aged specimens.

6.1.2 TENSILE TEST FOR NATURAL AGED SPECIMENS

Two groups of specimens were sectioned from the center and surface of the Al-7050 ingot. They were first heated to 850°F (454°C), which is above the solvus temperature of precipitates, and held for 20 minutes. Then, all the specimens were water quenched to room temperature. Through this treatment, the precipitates resulted from previous cooling histories were eliminated. Tensile tests were conducted after a series of time periods at room temperature. For the specimens from ingot center, natural aging time were 0.5 hour, 33 hours, 146 hours, and 486 hours. For the specimens from ingot surface, natural aging time were 0.5 hour, 48 hours, 179 hours, and 511 hours.

6.1.3 ON-COOLING TENSILE TEST

In order to eliminate the natural aging effect from as-received material, and also, to obtain the properties at elevated temperatures, on-cooling tensile tests were conducted. It includes following tests:

1. On-cooling tensile test at elevated temperatures with fast cooling rate

The purpose of this set of tests is to investigate both temperature and solidification rate effect.

The specimens were prepared from surface, 2 inches from surface and center of the Al-7050 ingot, which have different grain size and the amount of grain boundary eutectic phases result from different solidification rates. The procedures of the test are:

- Heat the specimen to 850°F (454°C) at 324°F/min (3°C/sec)
- Hold for 10 minutes at 850°F (454°C)
- Cool the specimen to the testing temperature at 324°F/min (3°C/sec)
- Stabilize for 2 minutes, and then test to failure
- Record the stress-strain curve

The testing temperatures were chosen to be 800°F (427°C), 600°F (316°C), 400°F (204°C), and 200°F (93°C).

2. On-cooling tensile test at room temperature with natural air cooling

The purpose of these tests are to compare the difference between surface and center of the Al-7050 as-cast ingot, which have significant difference in grain size and amount of eutectic phases. The procedures of the test are as following:

- Heat the specimen to 850°F (454°C) at 324°F/min (3°C/sec)
- Hold for 20 minutes at 850°F (454°C)
- Take the specimen out of the furnace, let it naturally cool to room temperature in lab air
- Conduct the tensile test at room temperature
- Record the stress-strain curves

The specimens were sectioned from both the surface and the center of Al-7050 as-received

ingot.

3. On-cooling tensile test at elevated temperatures with different cooling rates

The purpose of these tests is to investigate the effect of the continuous cooling on the mechanical properties of Al-7050. All specimens used in these tests were sectioned from center of Al-7050 as-cast ingot. It consists of three kinds of tests:

1) Continuous cooling effect on mechanical properties at 400°F (204°C). The procedures are as following:

- Heat the specimen to 850°F (454°C)
- Hold for 10 minutes
- Cool the specimen to 400°F (204°C) at three different rates, namely, 324°F/min (3°C/sec), 150°F/min (1.39°C/sec), 50°F/min (0.46°C/sec)
- Stabilize for 2 minutes, and then test to failure
- Record the stress-strain curve

2) Continuous cooling effect on mechanical properties at 200°F (93°C). The procedures consist of two steps of cooling, shown as following:

- Heat the specimen to 850°F (454°C)
- Hold for 10 minutes
- Cool the specimen to 400°F (204°C) at 200°F/min (1.85°C/sec)
- Cool the specimen to 200°F (93°C) at three different rate, namely, 50°F/min (0.46°C/sec), 30°F/min (0.28°C/sec), 10°F/min (0.09°C/sec)

- Stabilize for 2 minutes, and then test to failure
 - Record the stress-strain curve
- 3) On-cooling plus aging effect on mechanical properties at 200°F (93°C). The procedures, which consist of two steps of cooling and a series of time periods of aging, are as following:
- Heat the specimen to 850°F(454°C)
 - Hold for 10 minutes
 - Cool the specimen to 400°F (204°C) at 200°F/min (or 1.85°C/sec)
 - Cool the specimen to 200°F (93°C) at 50°F/min (or 0.46°C/sec)
 - Hold the specimen at 200°F (93°C) for a series of time periods, namely, 1 minute, 10 minutes, 30 minutes, and 60 minutes
 - Tensile test to failure
 - Record the stress-strain curve

6.1.4 Isothermal Aging and Hardness Test

For the same other conditions, the hardness of the material qualitatively reflects the amount and morphology of precipitates within the grains. A series of isothermal aging and hardness test were performed to qualitatively investigate the precipitation reaction at different temperatures. The procedures are shown as following:

- (1) Samples were all sectioned from center of ingot;
- (2) Heat the sample to 850°F(454°C);

- (3) Hold for 10 minutes;
- (4) Water quench;
- (5) Heat the specimen to the aging temperatures;
- (6) Hold for a series of time periods;
- (7) Water quench;
- (8) Measure the hardness of the material;
- (9) Record the hardness and aging time for all aging temperatures;

Step (2) to (3) dissolve the precipitates within grains. The precipitates will reappear during the aging by step (4) to (5). The amount and morphology of the precipitates depend on the aging temperature and aging time. The precipitation conditions are “frozen” by water quenching in step (6) to the room temperature, and represented by the measured hardness.

6.1.5 ON-COOLING FRACTURE TOUGHNESS TEST

Conventional K_{Ic} tests based on the ASTM standard E-399 were performed at room temperature to investigate the fracture toughness of as-cast ingot. The specimens were cut from surface and center of Al-7050 ingot. In order to eliminate the natural aging effect of the ingot material, all specimens were heated to 850°F (454°C), held for 20 minutes and naturally cooled at ambient temperature before tested.

6.2 RESULTS AND DISCUSSIONS

6.2.1 TENSILE PROPERTIES OF AS-RECEIVED MATERIAL

Table 6.1 shows the strength of as-received material measured as a function of location at room temperature. All specimens were failed intergranularly, with nil elongation. The fracture strength decreases as the distance from ingot surface increases as shown in Figure 6.2.

Table 6.1: Fracture strength vs. location

Location	Distance from surface (in)	UTS(ksi)
Surface	0	47.3
2" from surface	2	45.4
3.5" from surface	3.5	40.1
Center	7.5	35.5

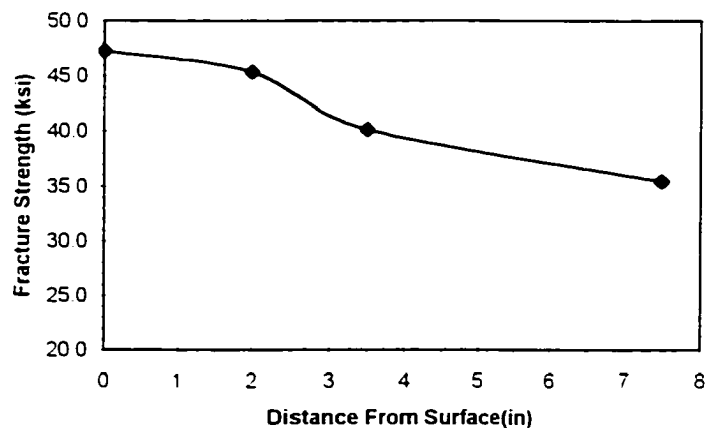


Figure 6.2: Fracture strength of specimens sectioned from as-received ingot pieces

6.2.2 NATURAL AGING EFFECT

Table 6.2 shows the tensile properties measured for the natural aged specimens. Both yield

strength and ultimate tensile strength increase with the aging time at ambient temperature, as shown in Figure 6.3. In addition, the difference between the tensile strength and the yield strength, i.e. strain hardening, decreases with increasing aging time. The material becomes more brittle as the alloy strength increases. This brittle-tendency is also shown by the decreasing of the elongation, as seen in Figure 6.4.

Table 6.2: Natural aging effect

Ingot Center				Ingot Surface			
Time (hr)	YS (ksi)	UTS(ksi)	Elong(%)	Time (hr)	YS (ksi)	UTS(ksi)	Elong(%)
0.5	11	24.5	4.84	0.5	12.5	32.0	9.77
33	23.5	29.7	1.00	48	29	37.8	1.88
146	26	27.2	0.19	179	31.6	41.4	2.03
486	30.3	31.0	0.18	511	34	38.4	0.54

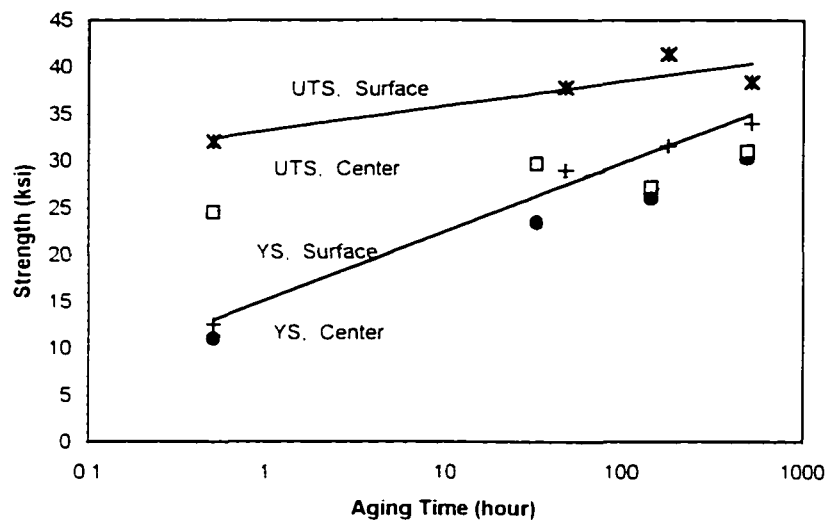


Figure 6.3: The effect of natural aging on material strength

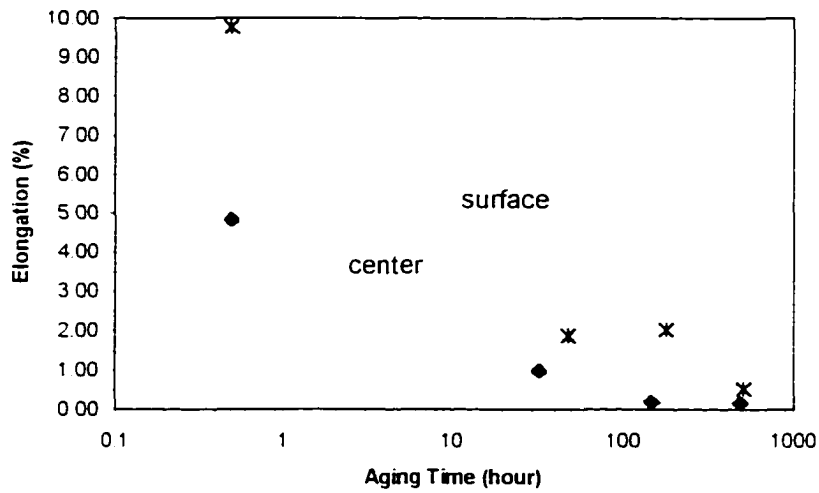


Figure 6.4: The effect of natural aging on elongation

By comparing Figures 6.2 and 6.3, the tensile properties of as-received material are similar to those of the specimen with a long natural aging time of 486 hours. These results indicate that the mechanical properties of as-received materials measured are the combination effect of the cooling during ingot casting and the natural aging afterward. The on-cooling tensile tests are thus required to eliminate the natural aging effect.

Further more, remarkable difference between surface and center of Al-7050 ingot can be seen from the results. Under the same aging time, the specimens from surface have higher strength and elongation than those from center. This is due to the finer grain size at ingot surface than ingot center.

6.2.3 ON-COOLING TENSILE TEST

1) On-cooling tensile tests at elevated temperatures with fast cooling

Table 6.3 and 6.4 lists the results of on-cooling tensile tests at elevated temperatures with fast cooling. For all three locations of ingot, namely surface, 2 inches from surface and center, which representing three different solidification rates, namely, 45°F/min (0.4 K/sec), 187°F/min (1.7 K/sec) and 524°F/min (4.9 K/sec), both yield and tensile strengths decreased as testing temperature elevated, as shown in Figure 6.5 and 6.6. By comparing the strength of specimens from different locations of the ingot, the effect of solidification rate can be seen. Yield strength decreased as the solidification rate decreased.

As shown in Figure 6.7, specimens from center showed higher elongation than those from surface at elevated temperatures, which is different from room temperature. The difference increased as temperature increased. There are two reasons causing this difference in ductility. Low yield strength at the center location can result in a high elongation, if the fracture strength remains the same. It requires more plastic deformation to strain harden the lower yield strength to fracture. The other factor, which is more significant at higher temperatures, relates to the strain softening during plastic deformation. Figure 6.8 shows the stress-strain curves tested at 600°F (316°C). Although with a lower yield strength, the material from the center shows more resistance to softening under stress, while the surface material failed soon after the softening occurred.

Table 6.3: Strength at different ingot locations at elevated temperatures

Temp(F)	Surface (4.9 K/sec)		2 in from surface (1.7 K/sec)		Center (0.4 K/sec)	
	YS(ksi)	UTS(ksi)	YS(ksi)	UTS(ksi)	YS(ksi)	UTS(ksi)
200	19.5	31.2	13.4	29.8	12.5	24.4
400	16.0	24.5	12.6	22.8	11.0	23.8
600	14.5	16.3	10.2	10.7	8.5	10.2
800	12.5	14.0	7.3	7.5	5.5	6.0

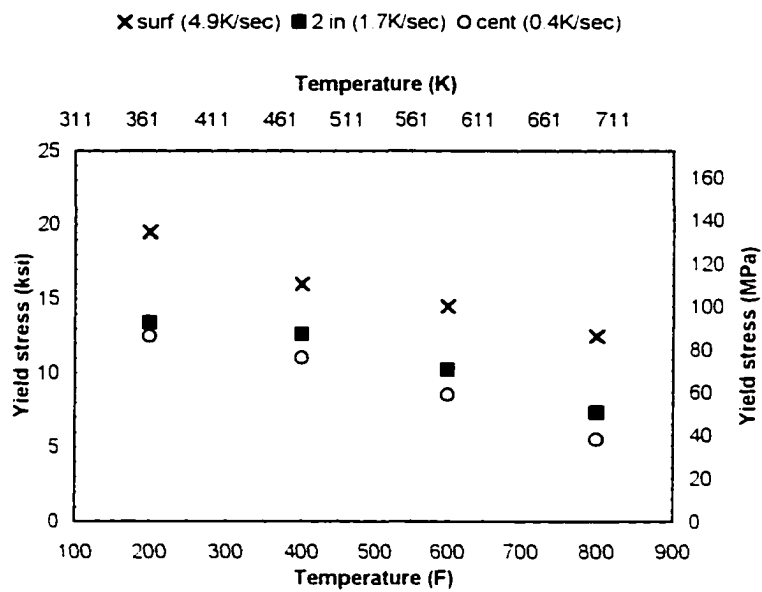


Figure 6.5: Yield strength at different ingot locations at elevated temperatures

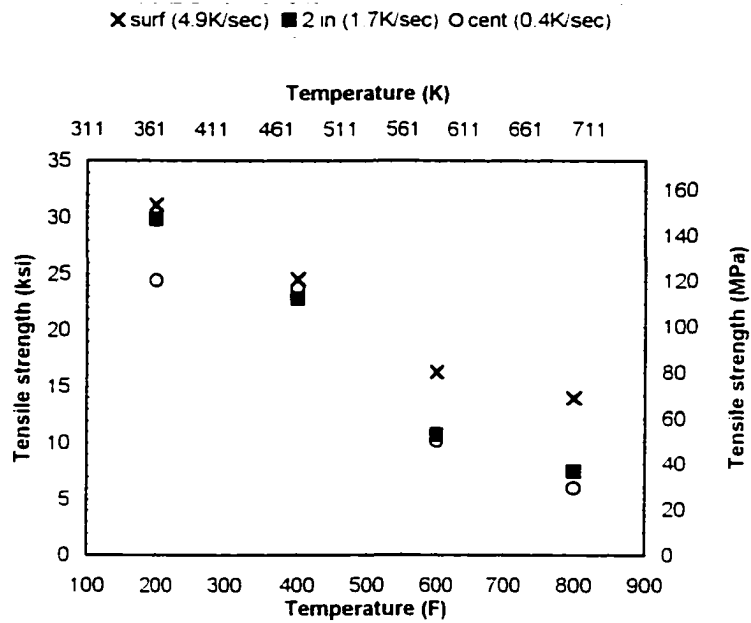


Figure 6.6: Tensile strength at different locations at elevated temperatures

Table 6.4: Comparison of elongation between center and surface at elevated temperatures

Temp (°F)	Elongation (%)	
	Center	surface
200	3.2	2.8
400	13.1	9.6
600	43.9	12.0
800	66.9	12.0

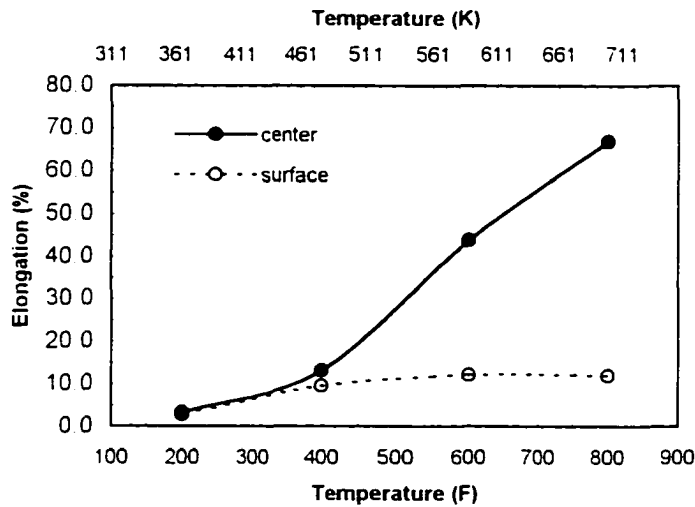


Figure 6.7: Elongation at elevated temperatures for center and surface

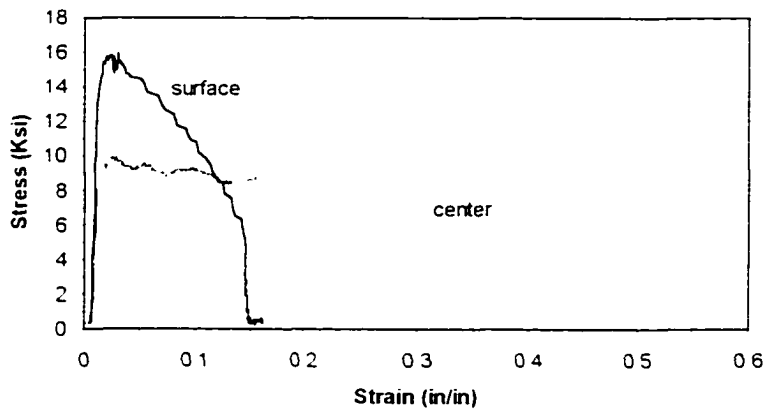


Figure 6.8: Stress-strain curves at 600°F for surface and center

2) On-cooling tensile test at room temperature with natural air cooling

Table 6.5 lists the tensile data measured by on-cooling tensile test at room temperature with natural air cooling. Material at surface of Al-7050 ingot has higher strength and elongation than that from ingot center at room temperature, as shown in Figure 6.9. Higher strength at ingot surface is caused by finer grain size and less amount of eutectic phases. The grain boundary eutectic phases increase the brittleness of ingot material at room temperature. Failures for both

ingot surface and center are intergranularly, as shown in Figure 6.10. Tensile ductility at room temperature decreases with increasing amount of eutectic phases, which is shown by the higher elongation at ingot surface than ingot center.

Table 6.5: Tensile properties of Al-7050 at room temperature

Location	YS(ksi)	UTS(ksi)	Elongation(%)
Center	18	27.8	1.5
Surface	20	30.7	2.1

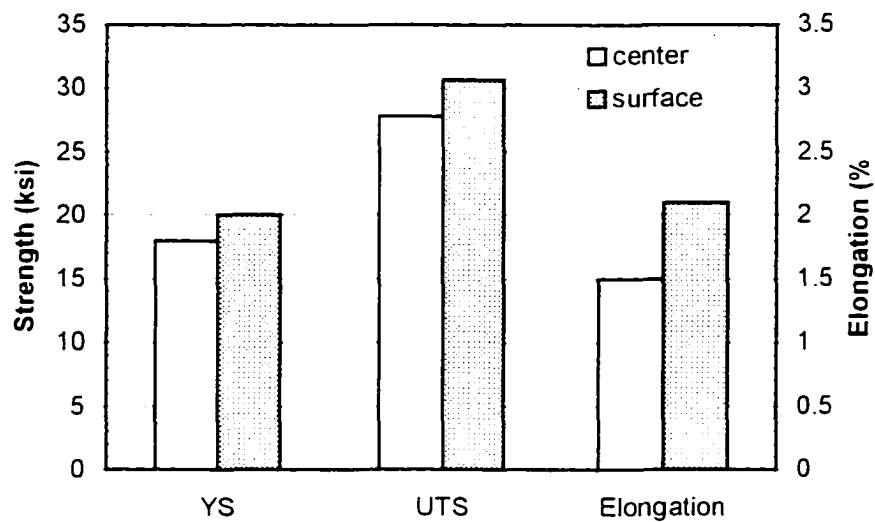


Figure 6.9: Tensile properties of as-cast Al-7050 at room temperature

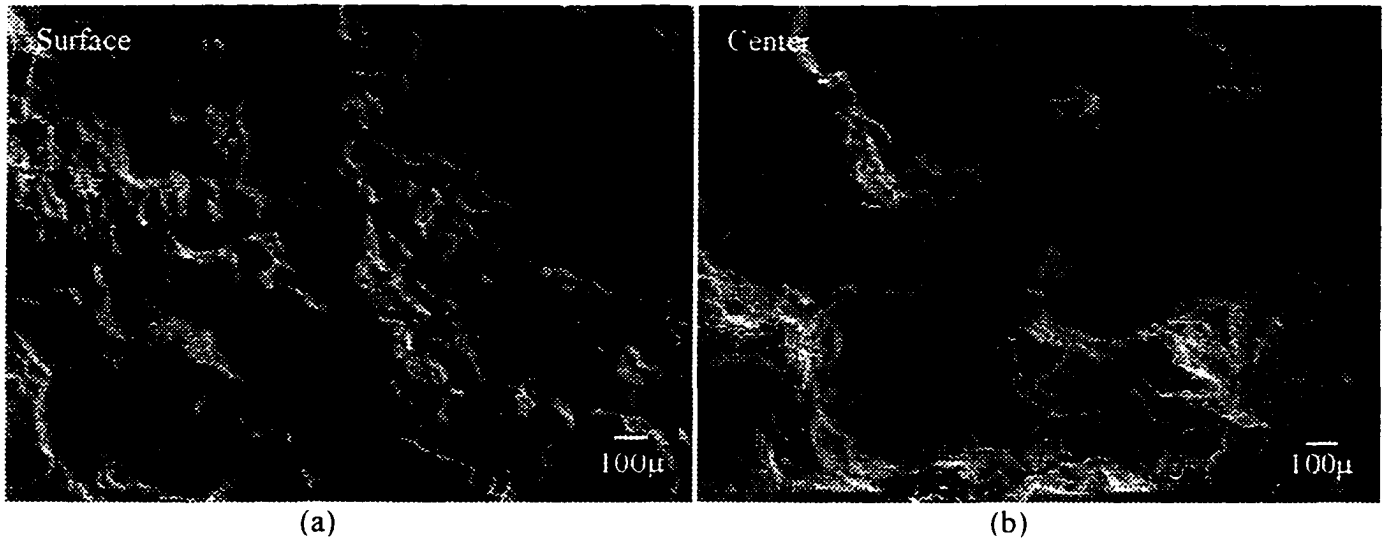


Figure 6.10: Fracture surface of on-cooling tensile test for as-cast Al-7050 ingot at room temperature : (a) specimen from ingot surface; (b) specimen from ingot center

3) On-cooling tensile test at elevated temperatures with different cooling rates

i) Continuous cooling effect at 400°F

Table 6.6 shows the results of on-cooling tensile tests with different cooling rate at 400°F (204°C). Tensile properties of Al-7050 have no significant change with different continuous cooling rates from 850°F (454°C) to 400°F (204°C), as seen in Figure 6.11. This indicates that precipitation during this period was not significantly affected by the cooling rates.

Table 6.6: Tensile properties of Al-7050 ingot center at 400°F with different continuous cooling rates

Rate (F/min)	YS(ksi)	UTS(ksi)	Elongation(%)
324	11.6	24.9	6.85
150	13.3	23.5	7.87
50	12.5	23.9	7.17

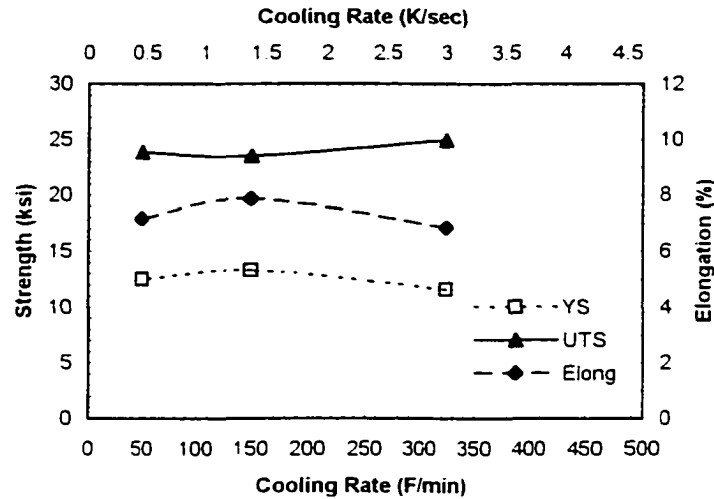


Figure 6.11: Tensile properties of Al-7050 ingot center at 400°F with different continuous cooling rates

ii) Continuous cooling effect at 200°F

Table 6.7 lists the results of on-cooling tensile tests with different cooling rate at 200°F (93°C). With the same cooling rate (200°F/min or 1.85°C/sec) from 850°F (454°C) to 400°F (204°C), the yield strength increased about 2 ksi as cooling rate from 400°F (204°C) to 200°F (93°C) decreased from 50°F/min (0.46°C/sec) to 10°F/min (0.09°C/sec), as shown in Figure 6.12. This indicates that during the temperature range between 400°F (204°C) and 200°F (93°C), amount of precipitates increases as cooling rate decreases. Elongation shows the trend of decreasing with decreasing of cooling rate, which may be because part of the precipitates formed along grain boundaries and increased the brittleness of the material. Tensile strength is defect-sensitive and does not show significant trend in the testing results.

Table 6.7: Tensile properties of Al-7050 ingot center at 200°F with different continuous cooling rates

Rate (F/min)	YS(ksi)	UTS(ksi)	Elongation(%)
50	12.8	23.8	2.56
30	14.6	25.2	2.65
10	15.2	24.2	2.15

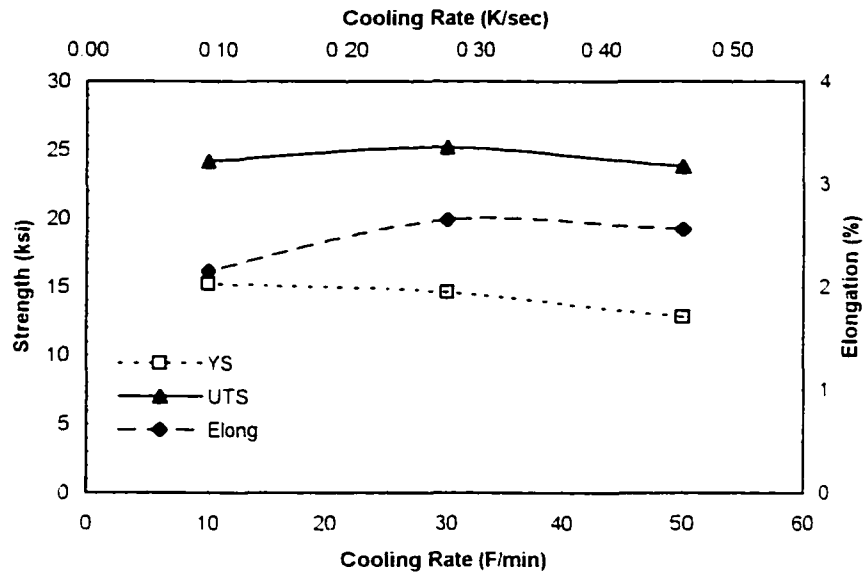


Figure 6.12: Tensile properties of Al-7050 ingot center at 200°F with different continuous cooling rates

iii) Continuous cooling plus aging effect at 200°F

Table 6.8 lists the results of on-cooling tensile tests after continuous cooling plus aging at 200°F (93°C). Aging time at 200°F (93°C) affected the yield strength of Al-7050 as-cast material, as shown in Figure 6.13. However, the increase slowed down for aging time longer than 30 minutes.

Table 6.8: Tensile properties of Al-7050 ingot center at 200°F with different aging time

Time (min)	YS(ksi)	UTS(ksi)	Elongation(%)
1	12.8	23.8	2.56
10	15.2	25.9	2.70
30	15.8	26.3	2.32
60	15.7	25.6	2.54

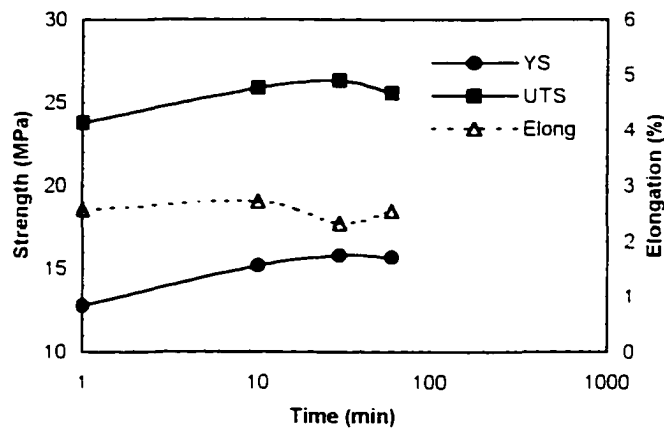


Figure 6.13: Tensile properties of Al-7050 ingot center at 200°F with different aging time

6.2.4 ISOTHERMAL AGING HARDNESS

Table 6.9 shows the results of hardness measured after a series of isothermal aging treatment for Al-7050 ingot section from same location. In contrast to homogenized wrought material, precipitation reaction was not remarkable because large amounts of solution elements were segregated along the grain boundary instead of dissolved within grains. Besides, as shown in Figure 6.14, precipitation mainly occurs at lower temperatures. When temperature was higher than 400°F (204°C), the material showed little hardening with aging time. This coincides with the results from the on-cooling tensile test, which indicates that material behavior is mainly

temperature dependent when above 400°F (204°C). Precipitation effect was most significant at 200°F (93°C) or lower, as shown in the hardness curves.

Table 6.9: Hardness of Al-7050 ingot center measured after different time aging at different temperatures

Time(min)	1	10	20	30	60	90
T=200°F/93°C	66.6	76.2	78.1	81.5	86.4	87.0
T=300°F/149°C	66.6	83.5	84.1	85.1	87.1	91.4
T=400°F/204°C	66.6	83.2	85.3	86.9	85.7	83.0
T=500°F/260°C	66.6	75.5	71.4	72.5	67.8	67.3
T=600°F/316°C	66.6	66.1	61.0	60.5	58.4	58.1
T=700°F/371°C	66.6	58.2	57.0	56.7	53.6	52.9
T=800°F/427°C	66.6	62.7	56.6	56.2	60.1	61.8

Hardness unit: HRE

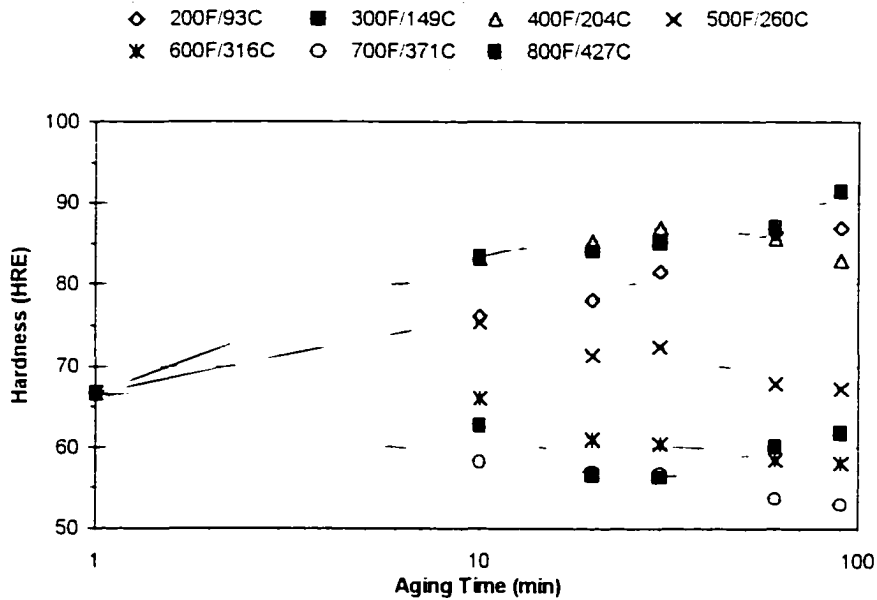


Figure 6.14: Hardness of Al-7050 ingot center measured after different time aging at different temperatures

6.2.5 FRACTURE TOUGHNESS

Table 6.10 lists the results of on-cooling fracture toughness of Al-7050 ingot at surface and center locations. Material from center of Al-7050 as-cast ingot has less fracture toughness than that from ingot surface at room temperature, as shown in Figure 6.15. This also indicates that the amount of grain boundary eutectic phases affects the fracture toughness of the ingot material. At room temperature, fracture toughness decreases as amount of eutectic phases increases.

Table 6.10: Fracture toughness of Al-7050 as-cast ingot at room temperature

Location	Center	Surface
Fracture Toughness (ksi·√in)	10.8	12.8

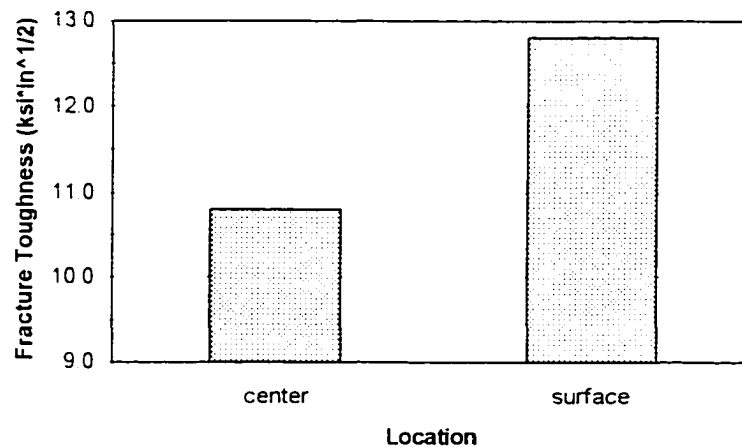


Figure 6.15: On-cooling fracture toughness results of Al-7050 as-cast ingot

6.3 SUMMARY

In this chapter, thermo-mechanical properties of as-cast Al-7050 ingot material were measured through a series of testing methods designed to identify and eliminate the natural aging effect on

the as-received ingot pieces and simulate the as-cast conditions during ingot casting. The effects of temperature and solidification rate were obtained through a series of on-cooling tensile tests with fast cooling for specimens sectioned from three typical locations from ingot which experienced three different solidification rates during casting. Strengths of the materials decreased with increasing temperature for all three locations. At the same temperature, material with lower solidification rate showed lower strengths.

The effect of precipitation reaction resulted from continuous cooling was studied through two-step on-cooling tensile test, and isothermal aging and hardness test. Results show that material properties are mainly temperature dependent at higher temperature range (above 400°F/204°C). At lower temperature (below 400°F/204°C), yield strength increases as cooling rate decreases. Precipitates formed by aging effect when the specimens were held at 200°F (93°C). The strengths increase with longer aging time.

Room temperature fracture toughness of as-cast Al-7050 ingot material was investigated through on-cooling fracture toughness tests. Due to the higher amount of eutectic phases formed in the center because of the slower solidification rate during casting, ingot center shows lower fracture toughness than ingot surface. This result coincides with the phenomena of "up-the-center" crack often occurred in ingot casting. In order to establish the cooling dependent constitutive model, results from on-cooling tensile tests will be further discussed and expressed quantitatively in Chapter 7, based on which a cooling-dependent constitutive model will be established.

CHAPTER 7

CONSTITUTIVE MODELING

In contrast to the homogeneous characteristics of wrought materials, as-cast Al ingots show a significant variation of mechanical properties from location to location. The experiment results shown in previous chapters indicate that the grain size, the amount of eutectic phases, and the amount of precipitates play important roles on the mechanical behavior of the cast material. They have different effects on strength, tensile ductility, and fracture toughness. A qualitative summary which shows the influence of various microstructure parameters and temperature on the mechanical properties of as-cast materials is given in Table 7.1. All the microstructure parameters listed here are determined by the cooling histories during the casting, which makes it possible to relate the cooling rate of the casting process with the mechanical properties of the casting ingot in the constitutive model. Two cooling portions, i.e. solidification rate and continuous cooling rate, will have various impacts on the as-cast properties.

Table 7.1: Qualitative effects of various microstructure parameters and temperature on as-cast mechanical properties

	Strength	Tensile Ductility	Fracture Toughness
Smaller Grain Size & Less Eutectic Phase	+	+ (Low Temperature) - (High Temperature)	+ (Less Eutectic Phase)
More Precipitation	+	-	-
Higher Temperature	-	+	?

("+": improve, "-": reduce, "?": not clear so far)

7.1 TEMPERATURE EFFECT

Temperature is a very important factor determining the mechanical properties of Al-7050 ingot. As shown in above results, the higher the temperature, the lower the strength of the material. Furthermore, at elevated temperatures, ingot material behaves much different from that at room temperature. The failure of the material transferred from intergranular brittle fracture to ductile fracture for testing above 400°F (204°C). The strain hardening decreases rapidly as temperature is elevated.

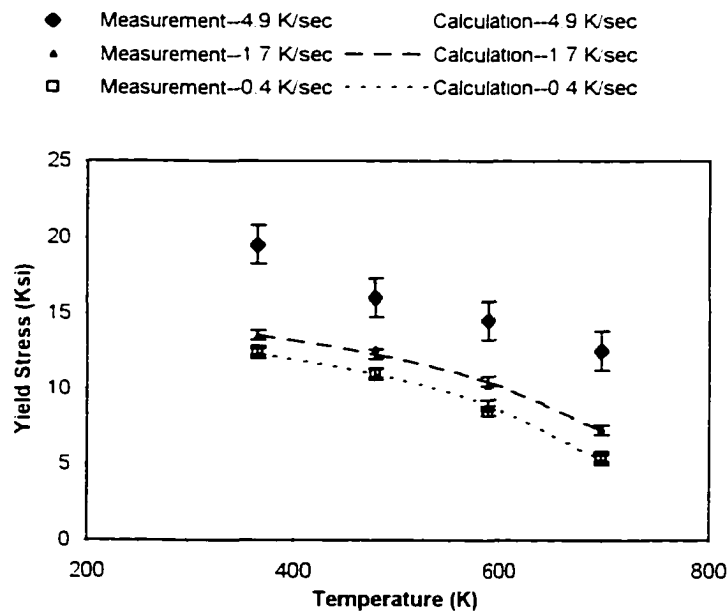


Figure 7.1: Temperature effect on yield strength of Al-7050 as-cast ingot

Figure 7.1, replotting the results of on-cooling tensile tests, shows the temperature effect on the yield strength of Al-7050 as-cast ingot. Unit of temperature used Kelvin. For each solidification

rate, the relations between the yield strength and temperature can be described as Equation 7.1.

Table 7.2 shows the values of the regression constants for different solidification rates.

$$\sigma_y = C_{T1} + C_{T2} \cdot \ln\left(1 - \frac{T}{T_m}\right) \quad (\text{Eqn 7.1})$$

where,

σ_y : yield strength of the material, unit is ksi

C_{T1} , C_{T2} : regression constant, unit is ksi

T : current temperature of the material, unit is K

T_m : solidus of Al 7050, 796.9K (975°F)

Table 7.2: Regression constants C_{T1} and C_{T2} for different solidification rates

Solidification Rate (K/sec)	4.9	1.7	0.4
C_{T1} (ksi)	20.944	16.134	15.251
C_{T2} (ksi)	4.276	4.229	4.725

7.2 SOLIDIFICATION EFFECT

The cooling rate during solidification determines the grain size and the amount of grain boundary segregation. A fast solidification rate occurs on the ingot surface, at which a fine grain size and a less amount of eutectic phases are resulted. Correlate the solidification rate and yield strength. Table 7.3 and Figure 7.2 can be obtained. Relation between yield strength and solidification rate was assumed to be linear, which can be expressed as Equation 7.2. Table 7.4 shows the values of regression constants for different temperatures.

$$\sigma_v = C_{s1} + C_{s2} \cdot \dot{T}_v \quad (\text{Eqn 7.2})$$

where,

σ_v : yield strength of the material, unit is ksi

C_{s1} : regression constant, unit is ksi

C_{s2} : regression constant, unit is ksi*sec/K

\dot{T}_v : solidification rate, unit is K/sec

Table 7.3: Yield strength of Al-7050 as-cast ingot with different solidification rate at different temperatures

Yield Strength (ksi)	Rate (K/sec)		
	4.9	1.7	0.4
Temp=366.3K	19.5	13.4	12.5
Temp=477.4K	16	12.6	11
Temp=588.6K	14.5	10.2	8.5
Temp=699.8K	12.5	7.3	5.5

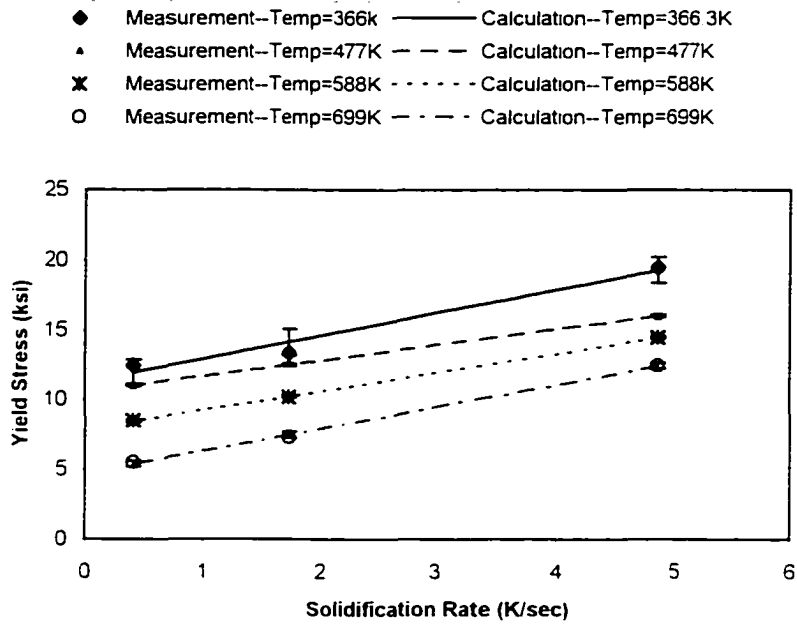


Figure 7.2: Solidification rate effect on yield strength of Al-7050 as-cast ingot at different temperatures

Table 7.4: Regression constants C_{s1} and C_{s2} for different temperatures

Temperature (K)	366.3	477.4	588.6	699.7
C_{s1} (ksi)	11.290	10.585	7.898	4.712
C_{s2} (ksi*sec/K)	1.645	1.120	1.356	1.593

Combining the effects of both solidification rate and temperature, the relation can also be described as Equation 7.3.

$$\sigma_y = C_1 + C_2 \cdot \dot{T}_s + C_3 \cdot \ln\left(1 - \frac{T}{T_m}\right) \quad (\text{Eqn 7.3})$$

where,

σ_y : yield strength of the material, unit is ksi

C_1 : regression constant, with the value of 14.1 ksi

C_2 : regression constant, with the value of 1.429 ksi*sec/K

C_3 : regression constant, with the value of 4.41ksi

\dot{T}_s : solidification rate, unit is K/sec

T : current temperature of the material, unit is K

T_m : solidus of Al-7050, 797K

7.3 CONTINUOUS COOLING EFFECT

Continuous cooling mainly determines the precipitation reaction of as-cast materials. The slower the cooling rate is, the more the precipitates form. The effects of precipitates on the mechanical properties of as-cast materials can be qualitatively seen from the effect of natural aging. More precipitates formed will result in higher strength and lower ductility and cracking resistance. The decreasing in ductility and cracking resistance is caused by the formation of precipitates along grain boundaries.

As mentioned in Chapter 4 and Chapter 6, continuous cooling of Al-7050 ingot can be further divided into four parts: 1) from 850°F (454°C) to 400°F (204°C); 2) from 400°F (204°C) to 200°F (93°C); 3) 200°F (93°C) to room temperature; 4) aging at room temperature. Continuous cooling rate effects are different during these cooling periods. As the results show, precipitates do not significantly form during the cooling period from 850°F (454°C) to 400°F (204°C) for Al-7050 as-cast ingot material. This indicates that at the temperature range above 400°F (204°C), the material properties of the ingot are mainly temperature dependent, and the effect of continuous cooling rate is negligible. During the cooling period from 400°F (204°C) to 200°F (93°C), slow cooling rate starts to affect the amount of precipitates, as shown by the increasing of the yield strength of the material. After the ingot material reaches 200°F (93°C), it will take hours to cool the cast ingot to room temperature. During this period, the strengths of the material are increased by the aging effect. However, this aging effect is not as pronounced as the isothermal aging after quenching. The cooling rate during casting is much slower than quenching for most portions of ingot and much less solid solutions of alloy elements retained within grains. Thus, the strength of the material soon reaches maximum after about 30 minutes of aging in the two-step-on-cooling-and-aging tests, as shown in Figure 6.17. The fourth period was not further studied because in most cases during production, the cast ingots will be sent for further heat treatment (stress relief) or remelted (if cracked) before they reach to room temperature.

The relation between cooling rate from 400°F to 200°F and yield strength of the material is described as Equation 7.4. The calculated curve is shown in Figure 7.3.

$$\sigma_y = C_1 + C_2 \cdot \ln(2 - \dot{T}_c) \quad (\text{Eqn 7.4})$$

where,

σ_y : yield strength of the material, unit is ksi

C_1 : regression constant, with the value of 8.15 ksi

C_2 : regression constant, with value of 11.206 ksi/ln(K/sec)

\dot{T}_c : continuous cooling rate from 477.4K(400°F) to 366.3K(200°F), unit is K/sec

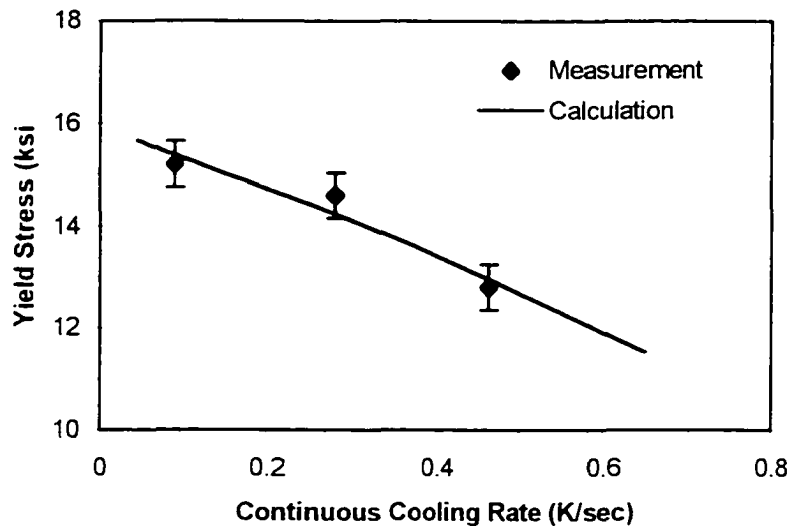


Figure 7.3: Effect of continuous cooling rate from 400°F to 200°F on yield strength of center of ingot

The effect of aging at 200°F after cooling from 400°F at 50°F/min on the yield strength of the material is described as Equation 7.5. The calculated curve is shown in Figure 7.4.

$$\sigma_y = k \cdot \ln(t) + \sigma_0 \quad (\text{Eqn 7.5})$$

where.

σ_y yield strength of the material, unit is ksi

σ_0 strength constant, = 13.026 ksi

k: constant, =0.755 ksi/ln(minute)

t: aging time at 200°F, unit is minute

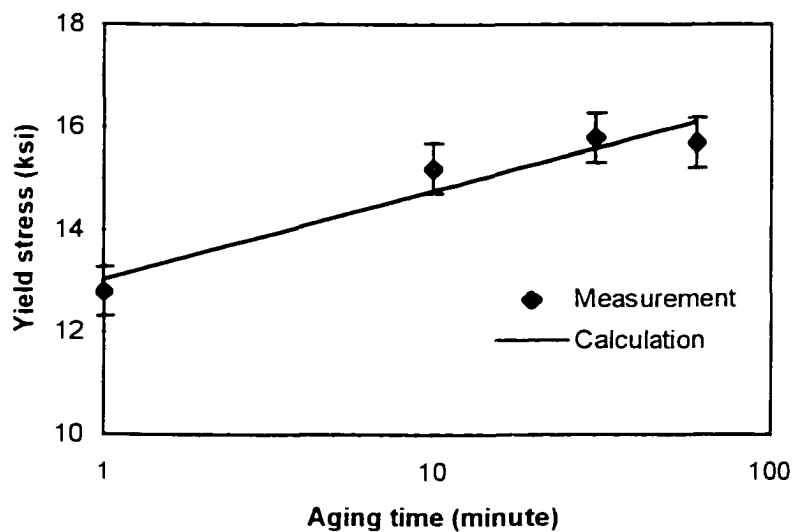


Figure 7.4: Aging effect at 200°F after cooling from 400°F at 50°F/min

Applying Equation 7.4 into 7.3 by assuming the equation is suitable for every locations of ingot, which needs to be improved by more testing for other locations other than just center, a general description of yield strength considering both solidification rate and continuous cooling rate is obtained, shown as Equation 7.6.

$$\left\{ \begin{array}{l} \sigma_y = C_1 + C_2 \cdot \dot{T}_s + C_3 \cdot \ln\left(1 - \frac{T}{T_m}\right) \quad \text{for } 477.4\text{K} \leq T < 796.9\text{K} \\ \\ \sigma_y = C_0 + C_2 \cdot \dot{T}_s - C_3 \cdot \ln\left(1 - \frac{T}{T_m}\right) + C_4 \cdot \ln(2 - \dot{T}_c) \quad \text{for } 366.3\text{K} \leq T \leq 477.4\text{K} \end{array} \right. \quad (\text{Eqn 7.6})$$

Where,

σ_y : yield strength of the material, unit is ksi

C_1 : regression constant, with the value of 14.1 ksi

C_2 : regression constant, with the value of 1.429 ksi*sec/K

C_3 : regression constant, with the value of 6.95 ksi

C_4 : regression constant, with the value of 4.41 ksi

C_0 : regression constant, with the value of 11.206 ksi/ln(K/sec)

\dot{T}_s : solidification rate, unit is K/sec

\dot{T}_c : continuous cooling rate from 477.4K (400°F) to 366.3 (200°F), unit is K/sec

T : current temperature, unit is K

7.4 MODELING OF PLASTICITY

In order to be applied to the constitutive modeling, the deformation behavior model of as-cast material has to be selected first according to the experimental results.

Strain hardening of as-cast Al-7050 ingot material decreased rapidly as temperatures elevated. At temperature above 600°F, material showed little strain hardening. Therefore, two models were adopted to describe the uniaxial deformation behavior for different temperature ranges. Elastic-linear work-hardening model [38] was applied for temperature below 600°F, while elastic-perfect-plastic model [38] was used for temperature above 600°F.

In the elastic-linear-work-hardening model, the continuous stress-strain curve is approximated by two straight lines, which can be expressed as Equation (7.7a) and Figure 7.6(a).

$$\left\{ \begin{array}{ll} \varepsilon = \frac{\sigma}{E(T)} & \text{for } \sigma \leq \sigma_y(T, \dot{T}_s, \dot{T}_c) \\ \varepsilon = \frac{\sigma}{E(T)} + \frac{1}{E_s(T)}(\sigma - \sigma_y) & \text{for } \sigma > \sigma_y(T, \dot{T}_s, \dot{T}_c) \end{array} \right. \quad (\text{Eqn 7.7a})$$

where,

E : Young's modulus, which is the functions of temperature T ;

E_s : slope of strain-hardening range, which is the function of temperature T ;

σ_y : yield strength of the material, which is the function of temperature T , solidification rate \dot{T}_s , and continuous cooling rate from 400°F to 200°F, \dot{T}_c .

Strain-hardening is neglected in the elastic-perfect plastic model, which can be expressed as Equation (7.7b) and Figure 7.6b.

$$\left\{ \begin{array}{ll} \varepsilon = \frac{\sigma}{E(T)} & \text{for } \sigma < \sigma_y(T, \dot{T}_v, \dot{T}_c) \\ \varepsilon = \frac{\sigma}{E(T)} - \lambda & \text{for } \sigma = \sigma_y(T, \dot{T}_v, \dot{T}_c) \end{array} \right. \quad (\text{Eqn 7.7b})$$

where,

E = Young's modulus, which is the functions of temperature T ,

σ_y = yield strength of the material, which is the function of temperature T , solidification rate

\dot{T}_v , and continuous cooling rate from 400°F to 200°F, \dot{T}_c ;

λ is a non-zero scalar.

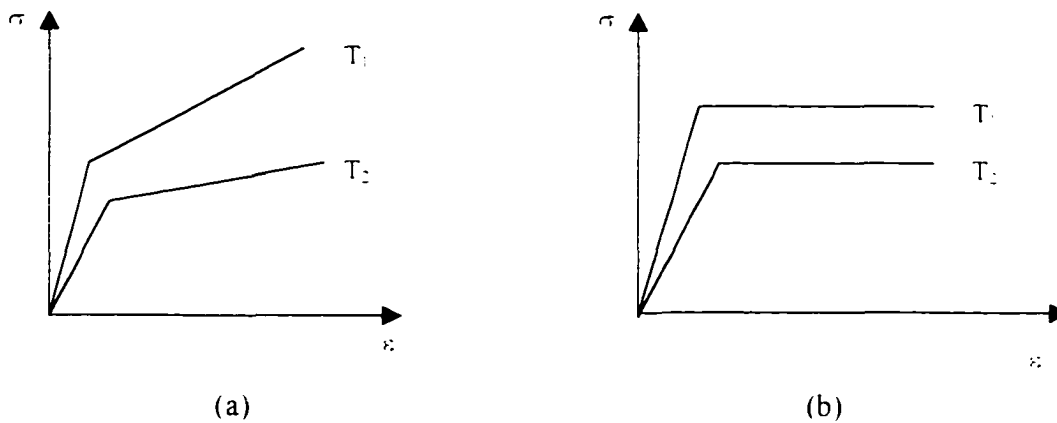


Figure 7.5: Plasticity model ($T_1 < T_2$): (a) Elastic-linear work-hardening model. (b) Elastic-perfect plastic model

Young's modulus measured at different temperatures are shown in Table 7.5 [39]. Compared with the data in other literatures [41], the trend can be described as Equation (7.8). The fitting curve is shown in Figure 7.7.

Table 7.5: Young's modulus at different temperature

Temperature	Young's modulus (Mpsi)
70°F(294.1K)	7.24
200°F(366.3K)	11.70
400°F(477.4K)	9.71
600°F(588.6K)	5.92
800°F(699.7K)	6.56

$$E(T) = C_1 + C_2 \cdot \ln\left(1 - \frac{T}{T_m}\right) \quad (\text{Eqn 7.8})$$

where,

E: elastic modulus, unit is Mpsi

T: current temperature of the material, unit is K

T_m : solidus of Al-7050, $T_m = 796.9\text{K}$ (975°F)

C_1, C_2 : regression constants, $C_1 = 13.08$ Mpsi, $C_2 = 3.644$ Mpsi

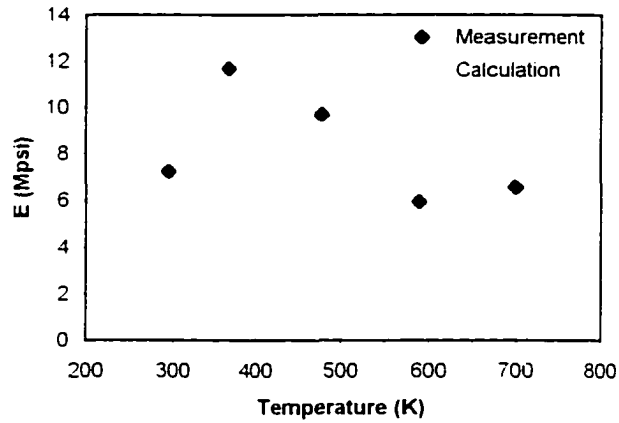


Figure 7.6: Relation of elastic modulus with temperature

$E_i(T)$ for elastic-linear work-hardening model can be obtained through regression analysis for the stress-strain curves measured in on-cooling tensile tests, in which slopes were calculated for the

data in the hardening range of the curves. Table 7.6 shows the results calculated for the specimens for the ingot surface and center tested at different temperatures. E_t for temperatures above 600°F is set to be zero. Averages of the two locations were used for the following numerical thermal stress simulation. The values were linearly interpolated for the intermediate temperatures

Table 7.6: Tangential modulus E_t at different temperatures

Temperature	E_t (ingot center) Mpsi	E_t (ingot surface) Mpsi	Average Mpsi
70°F(294.1K)	1.539	1.716	1.627
200°F(366.3K)	1.174	1.032	1.103
400°F(477.4K)	0.291	0.248	0.269
600°F(588.6K)	0	0	0

7.5 INCREMENTAL STRAIN-STRESS RELATION

Based on the plasticity models, a thermo-elastic-plastic constitutive model can be established. For the convenience of its application in the finite element modeling, the strain-stress relation will be described in the incremental form. The constitutive model is based on classical small deformation theory, i.e., the total strain increment can be assumed as the superposition of the elastic strain increment, plastic increment, and thermally induced strain increment, which can be written as,

$$d\varepsilon = d\varepsilon^e + d\varepsilon^p + d\varepsilon^t \quad (\text{Eqn 7.9})$$

in which, $d\varepsilon$ is the total strain increment, $d\varepsilon^e$ is the elastic strain increment, $d\varepsilon^p$ is the plastic strain increment which is non-zero only when plastic deformation occurs, $d\varepsilon^t$ is the thermal strain increment.

7.5.1 ELASTIC STRAIN-STRESS RELATION

According to Hooke's law, elastic strain-stress relation can be expressed as,

$$d\epsilon_{ij}^e = \frac{1+\nu}{E} ds_{ij} - \frac{1-2\nu}{3E} d\sigma_{kk} \delta_{ij} \quad (\text{Eqn 7.10})$$

in which, ν is poisson ration, ds_{ij} is deviatoric stress increment. E is expressed by Equation 7.8.

7.5.2 PLASTIC STRAIN-STRESS RELATION

Von Mises model (J_2 Theory) is adopted to describe the plastic strain-stress relation for the as-cast aluminum alloy. The von Mises yield criterion can be expressed as

$$f = \sqrt{J_2} - k = 0 \quad (\text{Eqn 7.11})$$

where,

J_2 is invariant of the stress deviator tensor which can be written as,

$$J_2 = \frac{1}{2} s_{ij} s_{ij} \quad (\text{Eqn 7.12})$$

k is the yield strength in pure shear, and can be expressed by uniaxial yield strength σ_y in Equation 7.7(a) and 7.7(b) as,

$$k = \frac{\sigma_y}{\sqrt{3}} \quad (\text{Eqn 7.13})$$

Based on the von Mises yield criterion, the incremental stress-plastic strain relations for elastic linear work-hardening and elastic-perfectly plastic can be derived as following Equation (7.14a) and (7.14b) [38], respectively.

For material at temperature below 600°F, elastic-linear work-hardening plastic stress-strain relation will be used, which can be expressed as Equation 7.14a.

$$d\epsilon_{ij}^p = \frac{3}{4} \frac{E - E_t}{E \cdot E_t} s_{ij} \left(\frac{dJ_2}{J_2} \right) \quad (\text{Eqn 7.14a})$$

where,

E : elastic modulus, which is the function of temperature T described in Equation 7.8,

E_t : slope of strain-hardening range, which is the function of temperature T described in Table 7.6,

s_{ij} : stress deviator tensors.

For material at temperature above 600°F, elastic-perfect plastic stress-strain relation will be used, which can be expressed as Equation 7.14b.

$$d\epsilon_{ij}^p = \frac{s_{mn} de_{mn}}{2k^2} s_{ij} \quad (\text{Eqn 7.14b})$$

where,

s_{ij}, s_{mn} : stress deviator tensors;

e_{mn} : strain deviator tensors;

k is described in Equation 7.12, which is also a function of temperature T , solidification rate \dot{T}_s , and continuous cooling rate from 400°F to 200°F, \dot{T}_c .

7.5.3 THERMAL STRAIN INCREMENT

Thermal strain increment can be calculated by Equation 7.15.

$$d\epsilon_{ij}^T = \alpha \cdot dT \cdot \delta_{ij} \quad (\text{Eqn 7.15})$$

in which, α is the coefficient of thermal expansion of the material, dT is temperature increment, δ_{ij} is the Kronecker symbol.

7.6 SUMMARY

In this chapter, yield strength of Al-7050 as-cast ingot material was expressed as the function of temperature and solidification rate. The elastic modulus and tangential modulus were described as the functions of temperature. Based on these relations, a thermal-elastic-plastic constitutive model was established, in which the elastic-linear strain hardening model was adopted to describe the behavior of ingot material at temperature below 600°F (316°C) and elastic-perfectly plastic model for material at temperature above 600°F (316°C). Incremental stress-strain relation was derived. The total strain increment was the superposition of the elastic, plastic and thermal strain increment. The Equations (7.10), (7.14), and (7.15) of the constitutive model can be employed into the stress analysis either separately through commands ELASTICITY, PLASTICITY, and THERMAL EXPANSION in ABAQUS [28], or through user subroutine provided by ABAQUS to describe the material behavior. The former method was adopted in the following thermal stress calculation. The latter one is more flexible but more complicated to be fulfilled.

CHAPTER 8

FINITE ELEMENT THERMAL STRESS MODELING

8.1 FEM MODELING PROCEDURE

A general finite element modeling system is schematically described by the flow chart in Figure 8.1 [40]. The model is first meshed using the desired type of elements, which have certain physical and mechanical properties. For non-linear problems, the load is applied incrementally. For each incremental loading, iterations are employed to calculate the responses of the material. The stiffness matrix is recalculated for each iteration, and convergence is determined according to a preset criterion. If the convergence is reached, the program proceeds to the next increment. After all increments are finished, the calculation is complete and results are output.

Many commercial finite element modeling (FEM) packages are available. ABAQUS was one of the most powerful codes for nonlinear calculations at the time of this research. The procedures of modeling in ABAQUS are shown in Figure 8.2. An input file has to be provided by the user to define the meshing scheme, material properties, load, boundary conditions, initial conditions, etc. ABAQUS compiles and implements the iterations as described above, and the convergent results are output. The post processor of ABAQUS can also read these results and converts them to graphic formats such as profiles and curves.

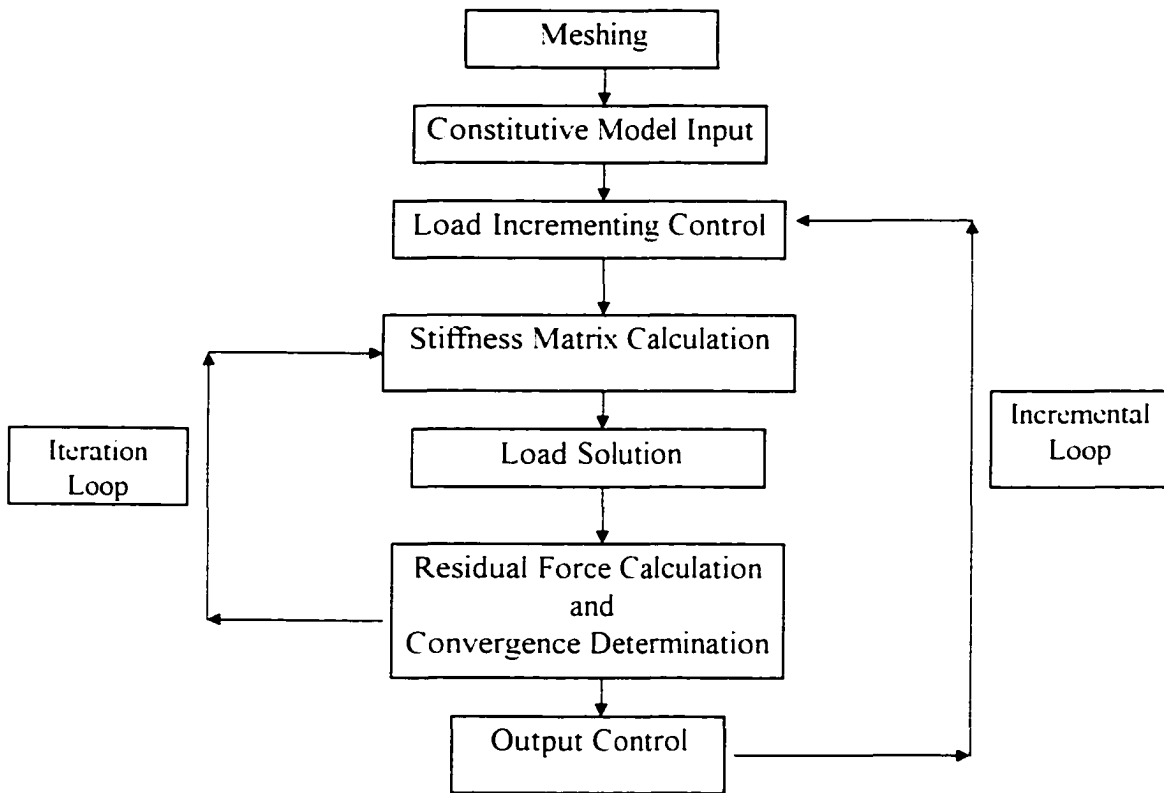


Figure 8.1 : Procedures of finite element modeling

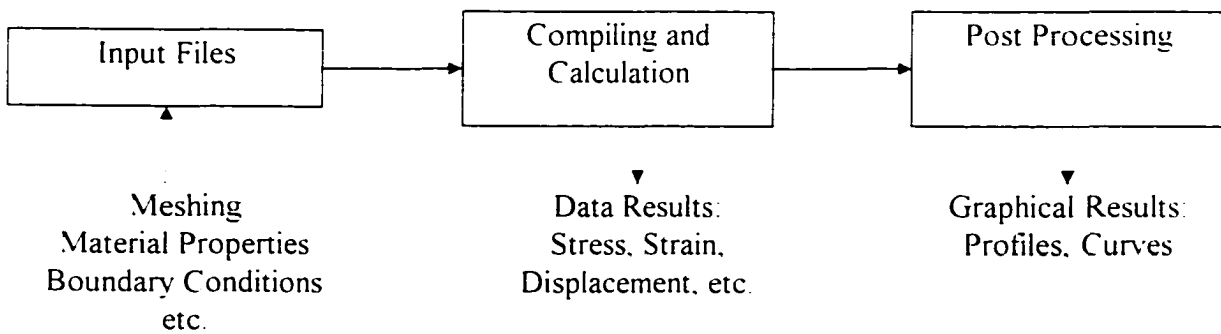


Figure 8.2 : Modeling procedure of ABABUS

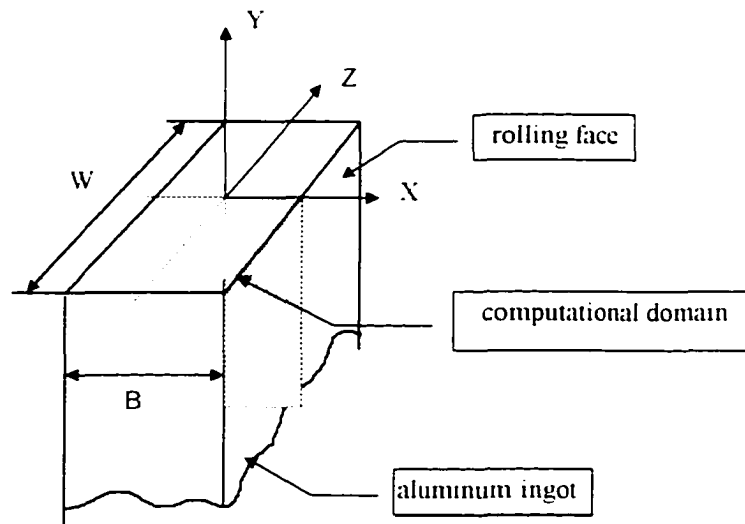


Figure 8.3: Computational domain

8.2 COMPUTATIONAL DOMAIN

Because of the symmetry of the ingot, it is possible to use a two-dimensional model to represent the most critical part of the ingot, which is the longitudinal cross-section at the center of the rolling faces where most “up-the-center” cracks occurred. The computational domain is shown in Figure 8.3.

8.3 BOUNDARY CONDITIONS

As shown in Figure 8.4, the meshing of the model is according to the distribution of thermocouples and the time steps in the temperature profile measurement. The liquid part of the cross-section was neglected to simplify the problem. Only half of the cross-section was considered

due to symmetry. "Slider" restraints were put on the center-line which only allowed the boundary to move in the Y-direction. The top, bottom and right side of the model are free of restraint. The weight of the material itself was not considered to simplify the calculation.

Plane strain approximation was employed in the two-dimensional model. In real life, the cross-section in the computational domain is not exactly under a plane strain condition, because the material layer adjacent to it will shrink as well during cooling instead of keeping stationary. However, the error brought by this assumption is limited due to two reasons: 1) the dimension in the Z direction is long; 2) the solidification takes place from outside inward. Therefore, the thick solid shell outside will be a strong obstacle for the shrinkage of the center layer, making the stress condition very close to the plane strain condition. Two-dimensional model will be a good foundation for the future three-dimensional model.

The cooling was the main "load" in the model, which determines strain and stress in the ingot. The temperature data measured in the in-situ measurement were curve-fitted using 6-order polynomial to obtain smooth cooling curves, which allow adjustable calculation increment, necessary for convergence. The cooling curves can also come from the results of thermal modeling.

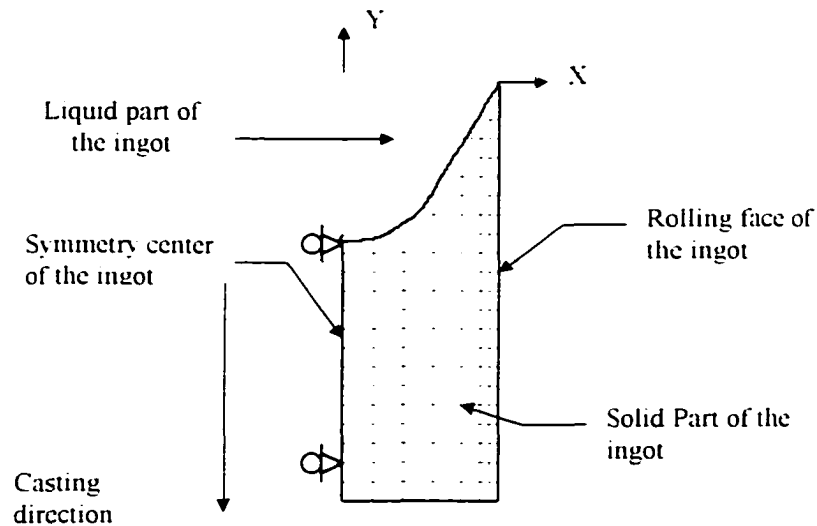


Figure 8.4: Meshing and the boundary conditions

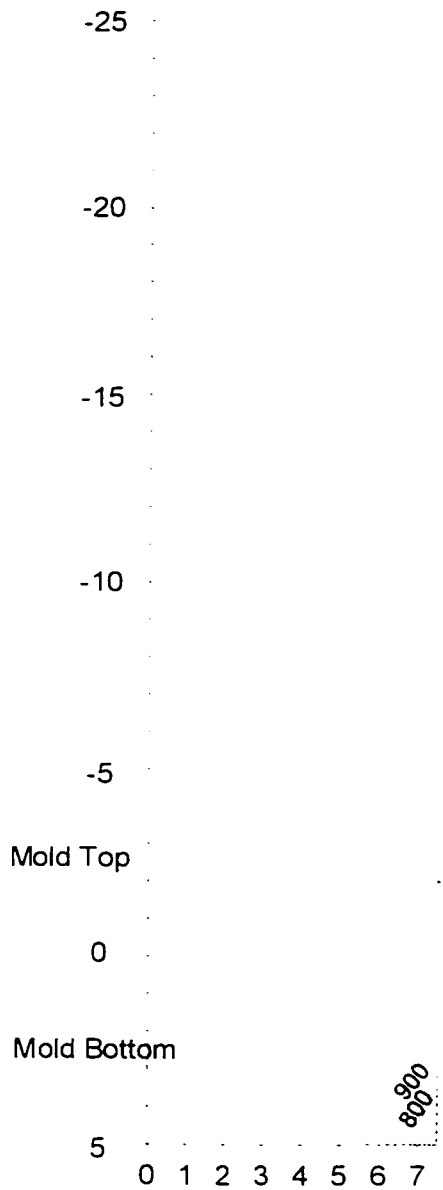
8.4 INCREMENT STRATEGY

In the above two-dimensional model, material in the same x coordinate experiences the same cooling history from pour-in temperature to room temperature, according to the definition of thermal steady state. The nodes at different Y locations represent the intermediate points on the cooling curve. In order to describe the gradually increased thermal load using steady state temperature profile, a temperature increment strategy was designed.

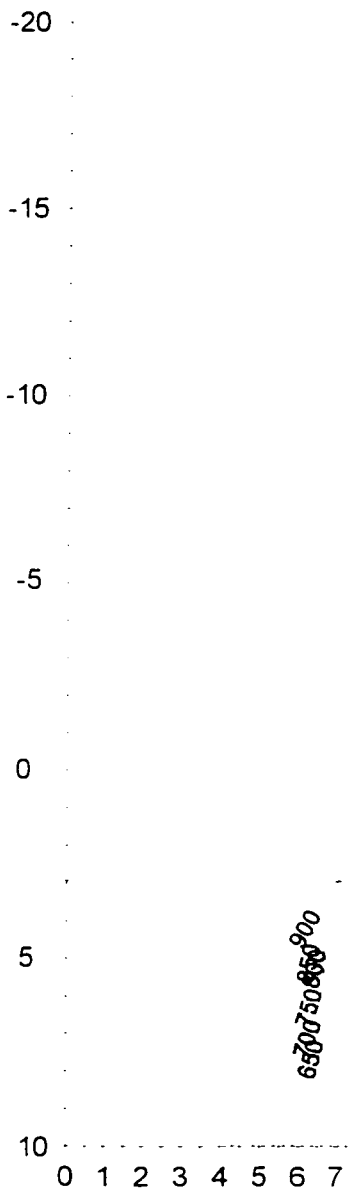
The strategy is shown in Figure 8.5, which shows the temperature profiles in the computational domain at a series of increments during calculations. The left side of each profile is the center of the ingot. The unit in the left and bottom axis is inch. The mold lines represent the top and bottom levels of the casting mold. At the beginning, the temperature of the whole 30-inch ingot model was solidus temperature. The casting processing can be viewed as the drop of this 30-inch model through the cooling mold. The material at the bottom cools first, and the nodes below the mold

have the corresponding thermal profile as in-situ measurement. When the whole 30 inch model drops below the mold (increment = 30), the temperature distribution becomes a complete steady state profile, and each element of the material experiences the cooling history which reflects the same cooling path of each ingot material moving from top of the ingot to the current location during steady state of ingot casting. A user subroutine was programmed to realize this increment strategy. These cooling histories built up unique thermal stress inside the ingot, which depends on the pattern of these histories and the thermo-mechanical behavior of the as-cast ingot material.

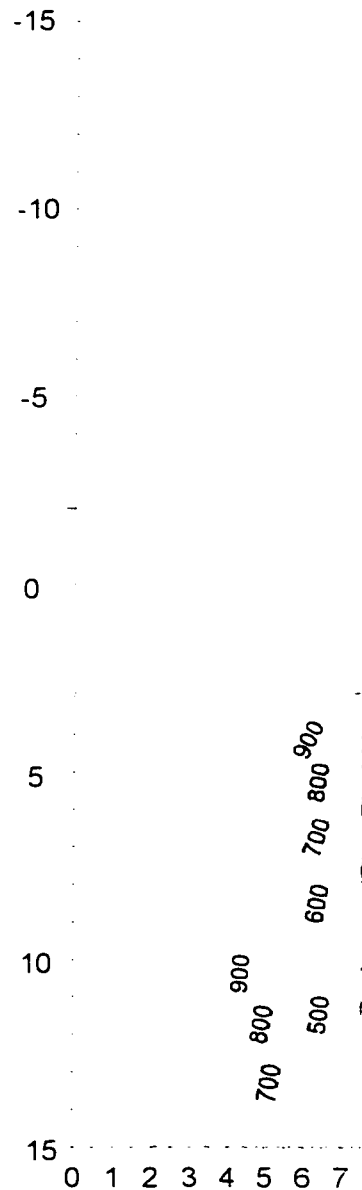
Increment = 5
(time = 2.5 min)



Increment = 10
(time = 5 min)



Increment = 15
(time = 7.5 min)



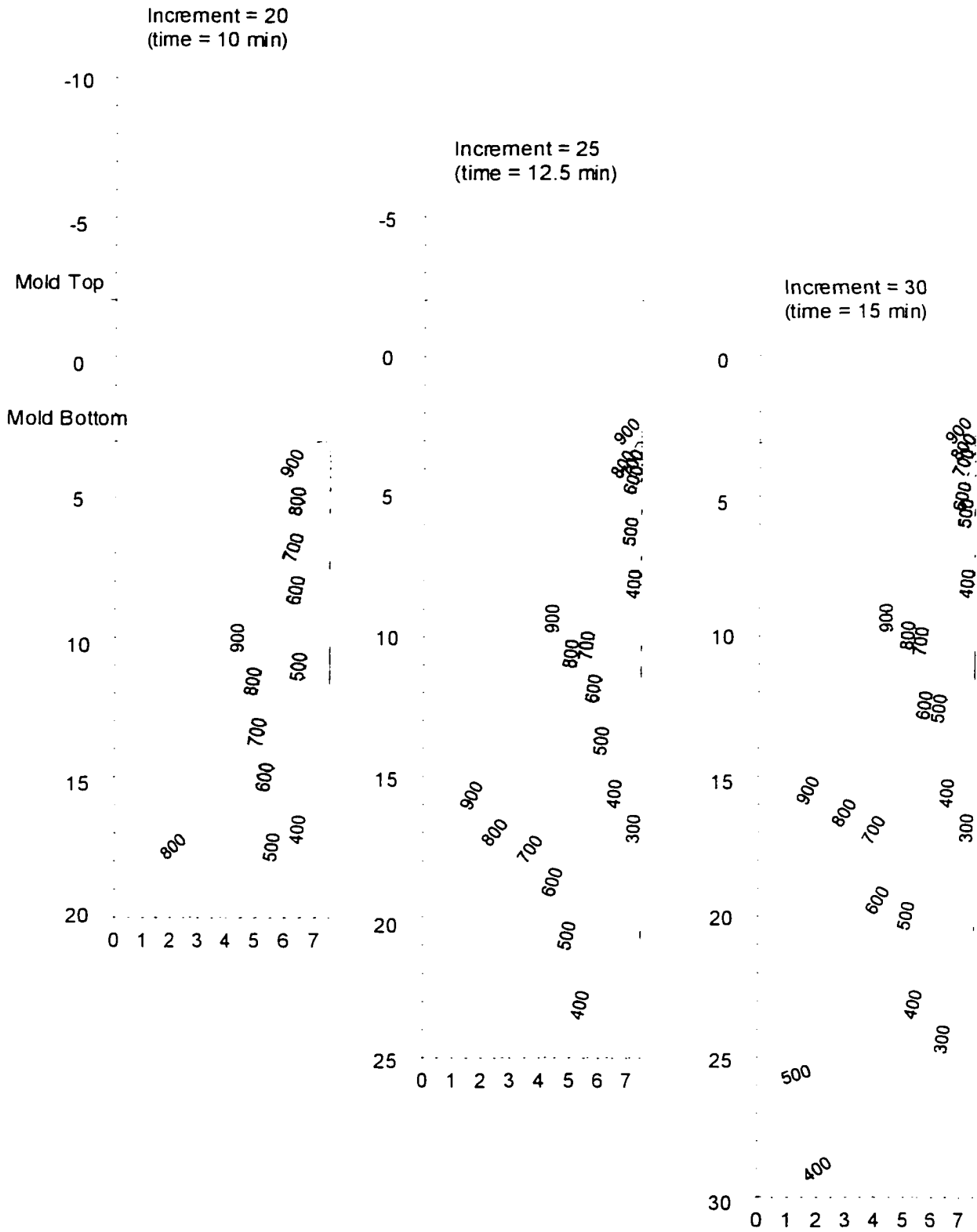


Figure 8.5: Temperature incrementation strategy

8.5 MATERIAL DESCRIPTION

In order to show the critical role the material description played for thermal stress calculation, different material properties were compared in the modeling. Five models will be used in the calculations. They are:

Model 1: temperature-independent material properties for heat treated Al-7050T7451 [41], with constant elastic modulus $E=10.3$ Mpsi and constant yield strength $\sigma_y = 73$ ksi.

Model 2: temperature-dependent material properties for heat treated Al-7050 [41], shown in Table 8.1 and 8.2.

Model 3: temperature-dependent material properties for as-cast Al-7050 measured at the ingot surface, shown in Table 6.3.

Model 4: temperature-dependent material properties for as-cast Al-7050 measured at the ingot center, shown in Table 6.3.

Model 5: temperature-cooling rate dependent material properties for as-cast Al-7050 described in Chapter 7. However, the cooling rate only considers solidification rate in following calculation.

The elastic modulus used for model 3, 4 and 5 are from Table 7.5. Figure 8.5 and 8.6 compares these different material models.

Table 8.1 Elastic modulus of Al-7050T7451 [41]

Temperature	Elastic modulus (Msi)
70°F (294.1 K)	10.3
250°F (394.1 K)	9.4
350°F (449.7 K)	8.7
500°F (533 K)	8.4
975°F (796.9 K)	0

Table 8.2 Yield strength of Al-7050T7451 [41]

Temperature	Yield strength (ksi)
70°F (294.1 K)	73
212°F (373 K)	62
300°F (421.9 K)	56
400°F (477.4 K)	42
500°F (533 K)	21
975°F (796.9 K)	0

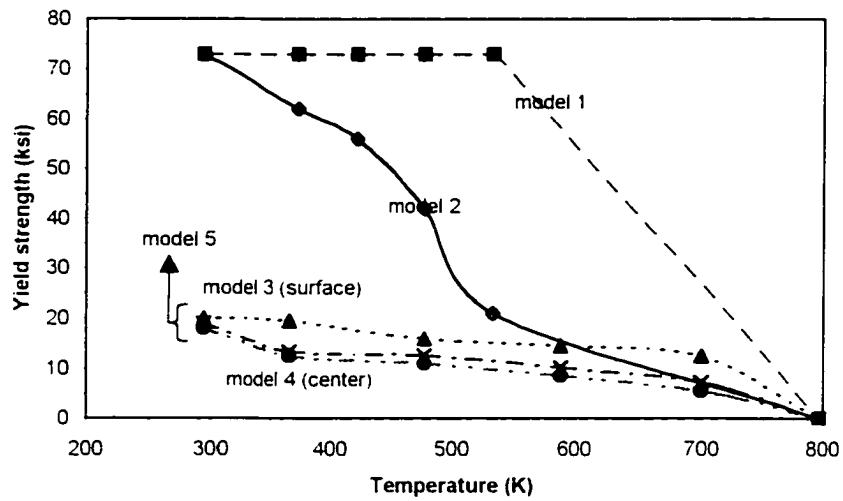


Figure 8.6: Comparison of yield strengths of five material models

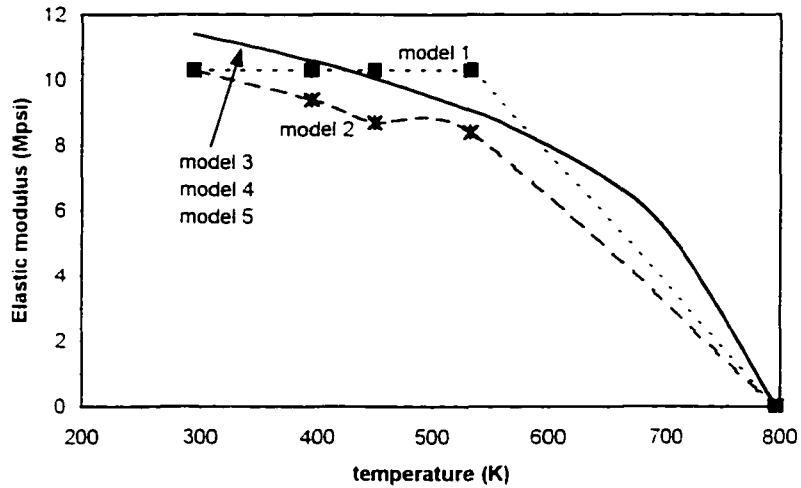


Figure 8.7: Comparison of elastic modulus of five material models

8.6 RESULTS AND DISCUSSION

Figure 8.8 to 8.12 show the calculated thermal stress distribution at different increments along the short cross-section for all five material models. The vertical axis at the left side of the profiles is Y-axis which is along the dropping direction with zero representing ingot top. Bottom of the mold locates at 3 inch in the vertical axis. The Y-axis is also the symmetry line of ingot longitudinal cross section described in Figure 8.3. The horizontal axis at the top is X-axis which is from the center of ingot toward the surface. The right side of the profile is the free surface of the ingot. The unit for both axes is inch. The unit for the profiled stress is ksi. Three kinds of stresses were calculated, namely, s_{33} which is in Z-direction (reference Figure 8.3), perpendicular to the computational domain, maximum principal stress and von Mises stress. The stress in the Z-direction is the major driven force for the casting crack propagation. As shown in the results, after first several increments, a very high tensile stress occurred at the outer surface two to three inches below the mold where the cooling water was impinged for all material models. When ingot

material moved farther from the mold, different material models showed different thermal distribution and stress level. In all five cases, the maximum location of both Z-direction stress and maximum principal stress tend to move from ingot surface toward ingot center, while maximum von Mises stress remain at ingot surface. This means the material experienced higher and higher tension at the ingot center when dropping during cast, although ingot surface got the highest of the distortion.

The toward-center movement of maximum tensile stress is because of the solidification sequence of aluminum ingot during the casting. After the ingot just emerged from the bottom of the mold, material of ingot surface was cooled rapidly by the impinging water. The sudden shrinkage of the ingot surface was hindered by the still-hot ingot inside material which shranked much less. Thus, high tension occurred in the material close to the surface, which is generally called "queching stress". With ingot material moving down, material inside the ingot start to cool down and reduce the volume. However, the already solidified outside ingot material prevented this shrinkage, which built higher and higher tension in the ingot center, generally called "center stress". With ingot increasing the length, the center tensile stress will increase dramatically and become a enormous driving force for up-the-center casting crack propogation.

By comparing the results from the five models, differences of level and distribution of the stresses can be observed. This is because both level and distribution of the stresses are highly related to the strength level of ingot material. Material with higher yield strength can stand higher stress caused by the thermal strain, while material with lower strength yields at a certain stress level and has to pass the load to the nearby material. The results of model 1 and model 2, which used wrought

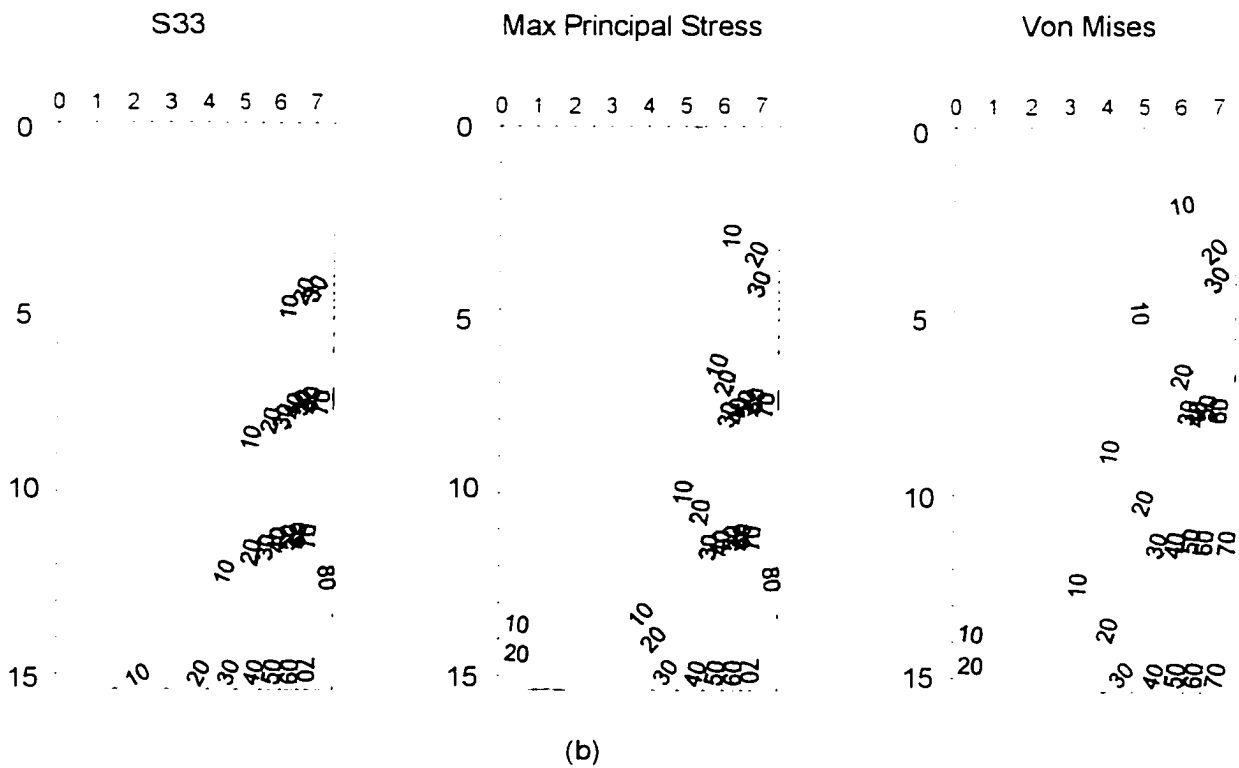
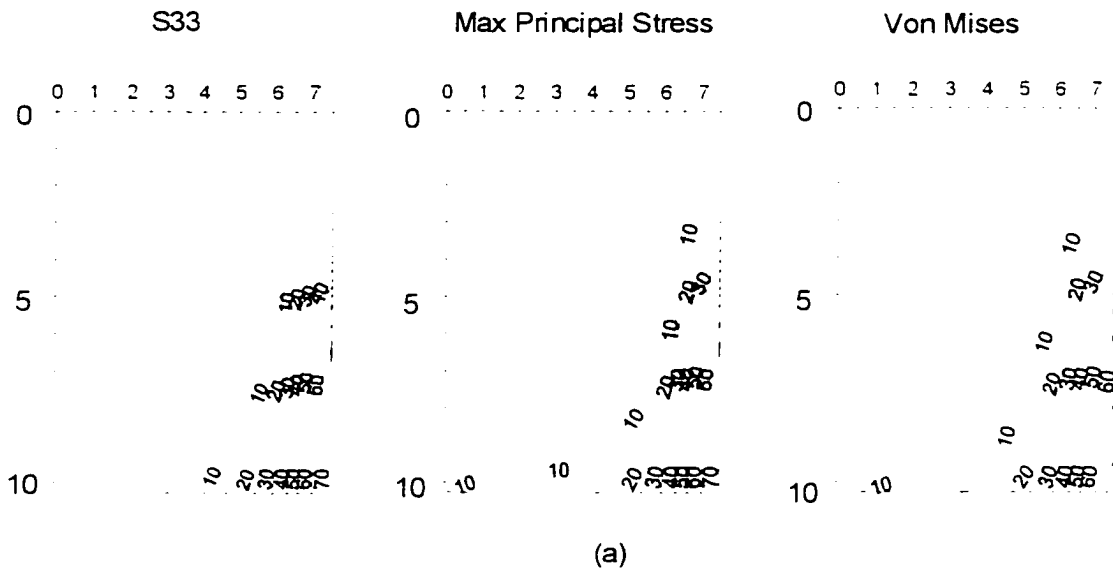
material properties, show much higher stress level than model 3, 4 and 5, which used as-cast material property with much lower material strengths. Model 3, which using ingot surface material properties, also produced higher stress levels than model 4, which using ingot center material properties. In addition, the toward-center movement of tensile stress tends to be slower when using higher material strengths.

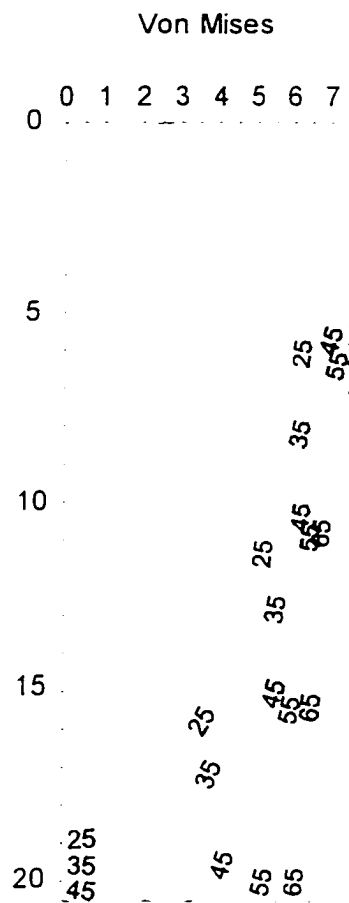
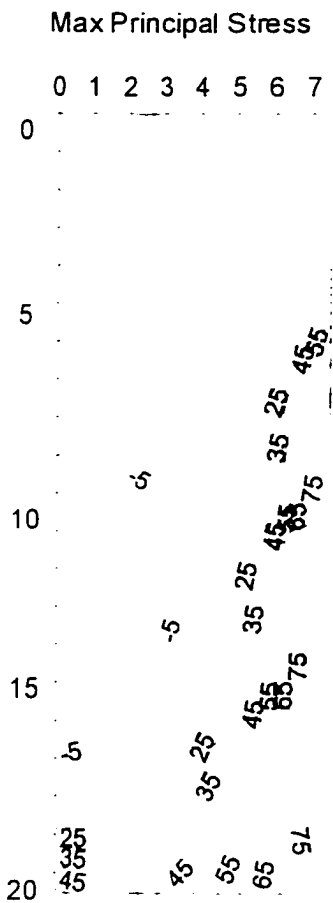
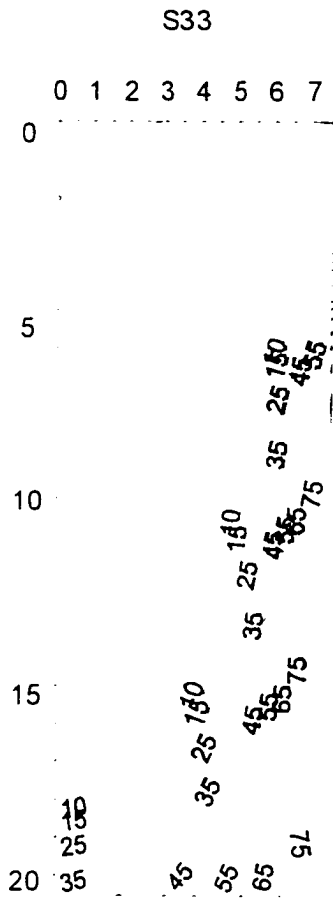
The distribution of the material properties in the ingot also influences the calculation of thermal stress remarkably. Results of model 1 and model 2 have significant difference both in stress level and distribution. Result of model 1 using constant properties show much higher stress level than model 2 using temperature-dependent properties, especially the stress at ingot center. The differences are due to the different material property distribution used in the two models. In model 2, material strengths are lower at higher temperatures, while strengths remain constant for all temperatures in model 1.

The stress distribution patterns of model 3, 4 and 5 are similar, showing evident inward movement of maximum tensile stress. However, the stress levels are much different when compared at each location of the ingot. In the results of temperature dependent models, the Z-direction stress and maximum principal stress showed the same level for center stress and quenching stress. At the same location in the result of cooling-dependent property model, the center stress was still 4 ksi lower than quenching stress. For von Mises stress distribution, the stress level difference between ingot center and surface is much higher from cooling-dependent model than those from two temperature-dependent models. All these differences are due to different strength distribution assumed in three models. In cooling-dependent property model, material at ingot center

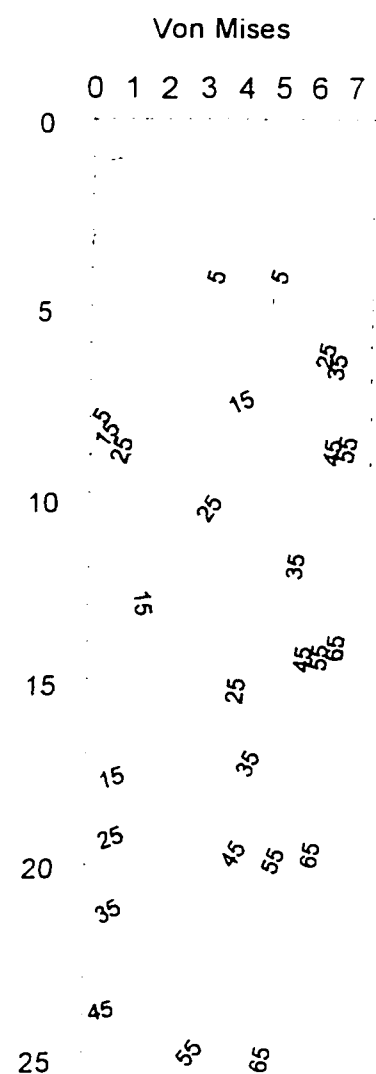
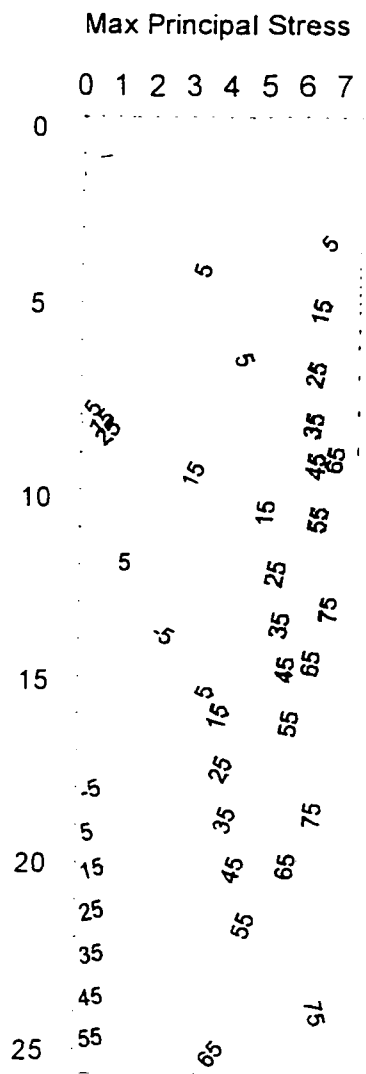
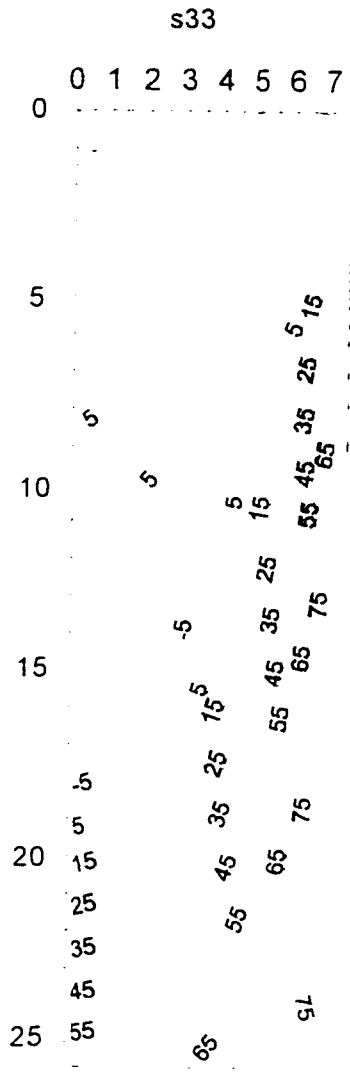
experienced lower solidification rate, which resulted lower material strengths, than ingot surface. Thus, even at same temperature, ingot center material can carry lower stress load than ingot surface.

Figures 8.13 and 8.14 plot the maximum principal stress and von Mises stress of a ingot material point moving along ingot surface and center as the function of casting time, respectively. Results of cooling-dependent property model and temperature-dependent (ingot surface and ingot center) property model are compared. As shown in Figure 8.13, for material moving along the ingot center, both maximum principle stress and von Mises stress from cooling dependent property model are close to those from temperature-dependent center property model. Maximum principal stress resulted from temperature-dependent surface property model shows significantly higher stress level than the other two with about 64% higher at the peak value. The time reached to the peak value also 1 minute later. Von Mises stress from surface property model is remarkably different from cooling dependent model, with about 46% higher for the maximum value. As shown in Figure 8.14, for material moving along ingot surface, the results from cooling-dependent model is closer to those from temperature-dependent surface property model. The difference between center property model and cooling-dependent model can reach 39% of peak value for maximum principal stress of model 4 and 26% of the peak value for von Mises stress of center property model.





(c)



(d)

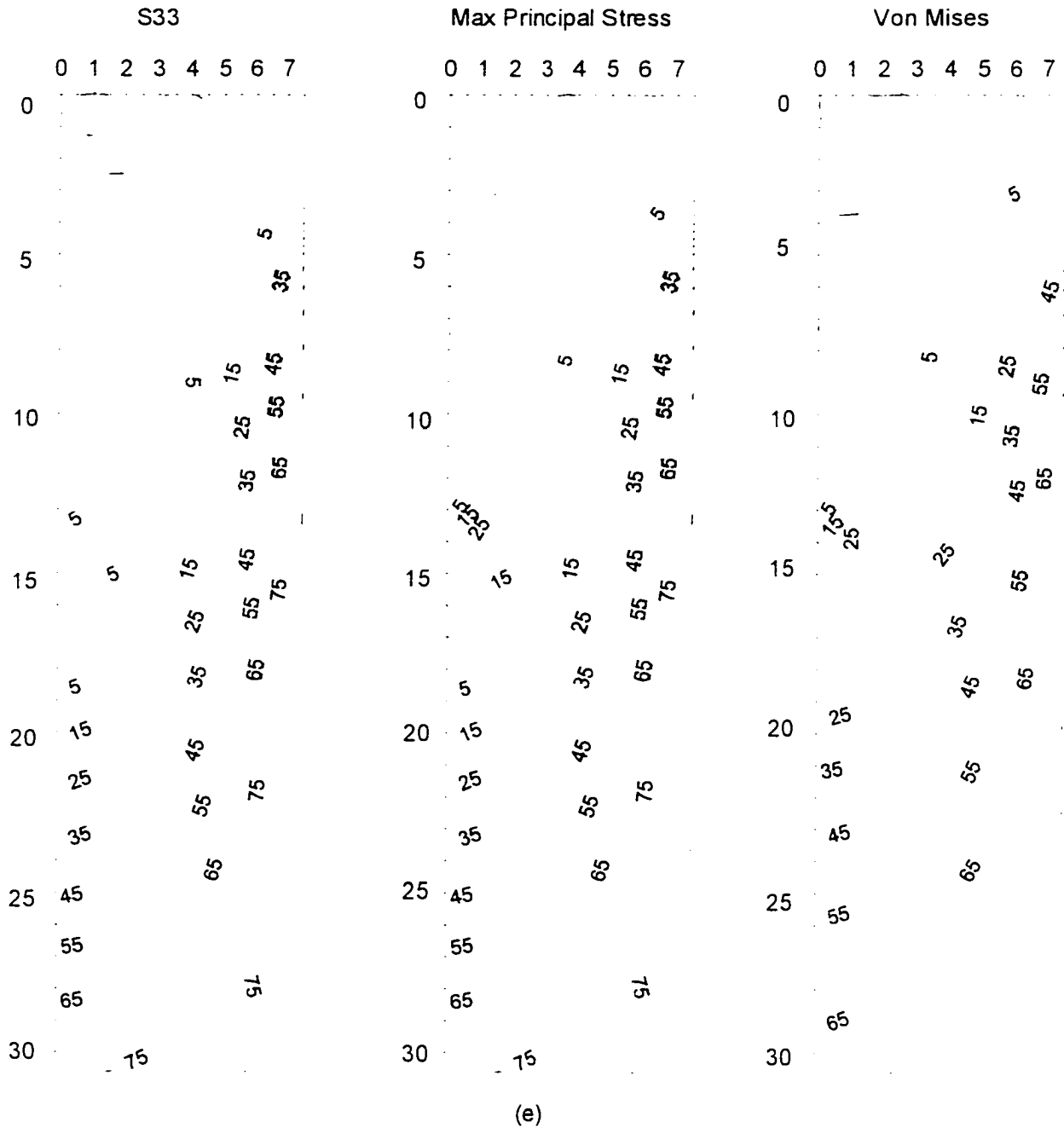
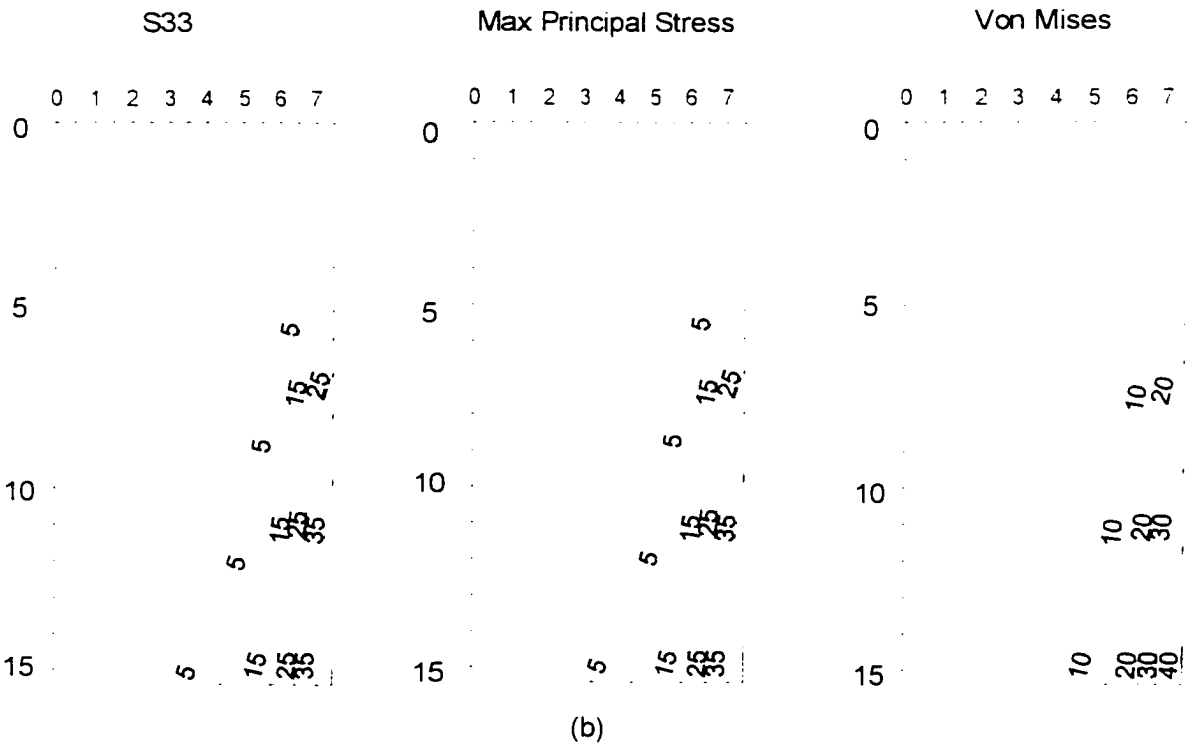
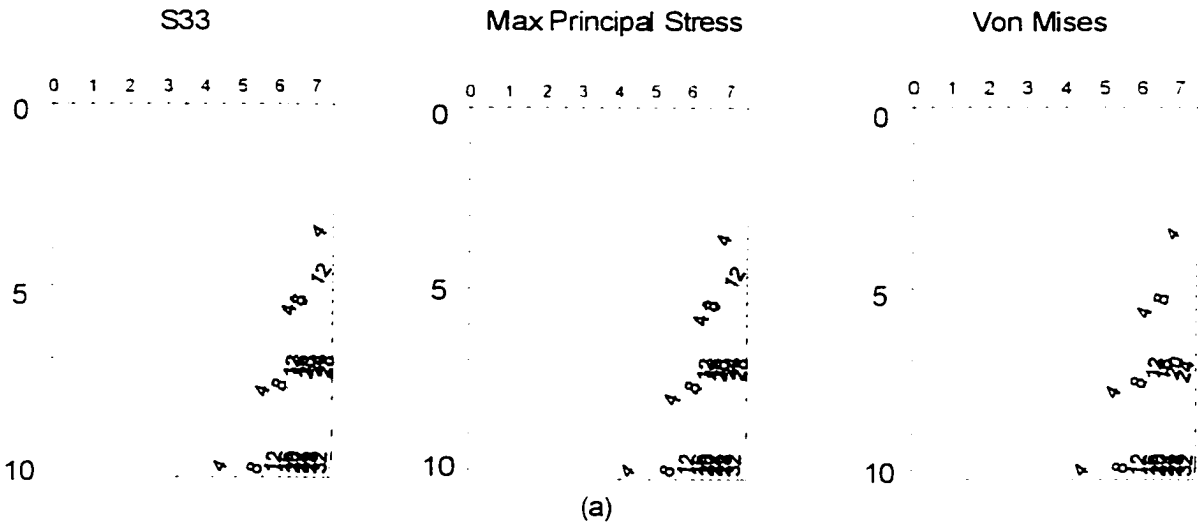
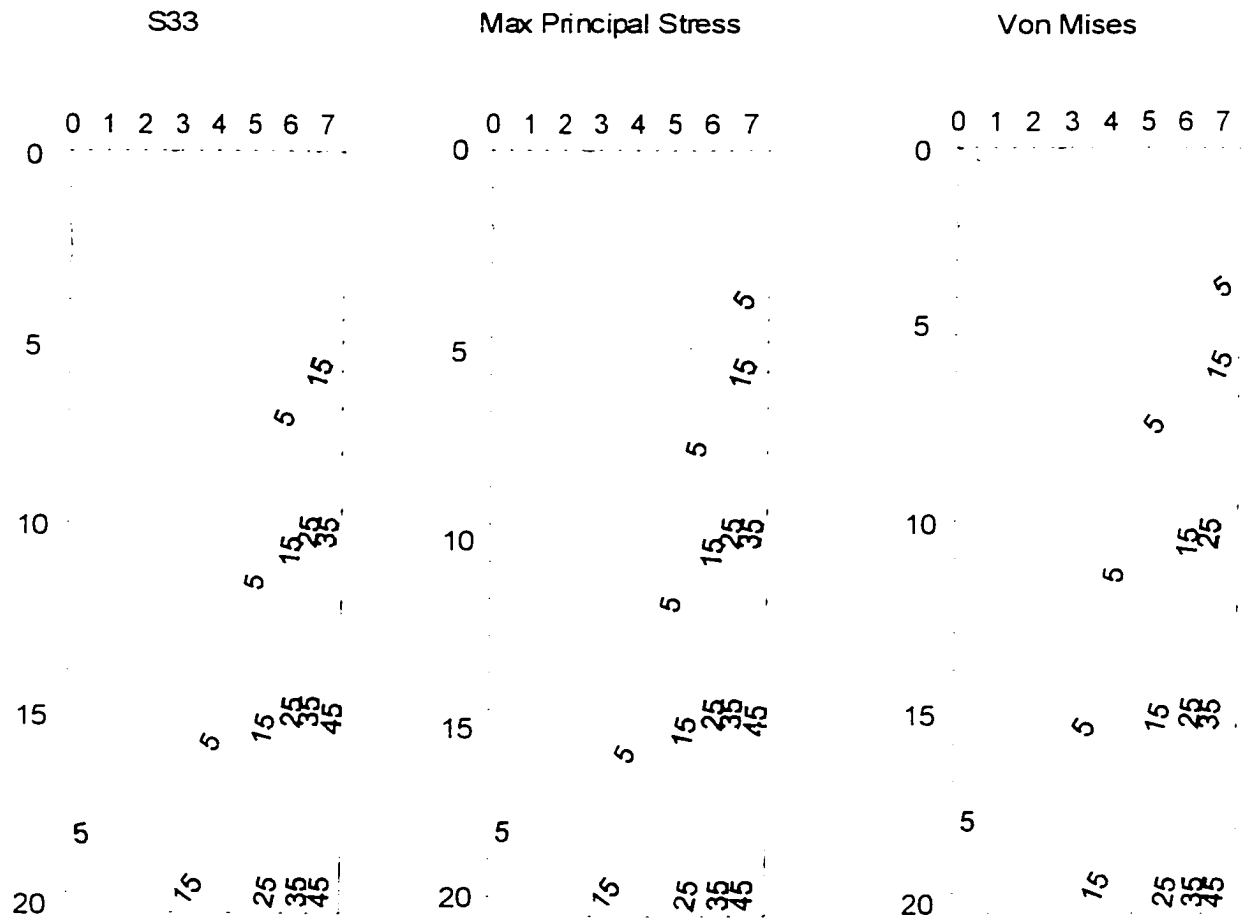


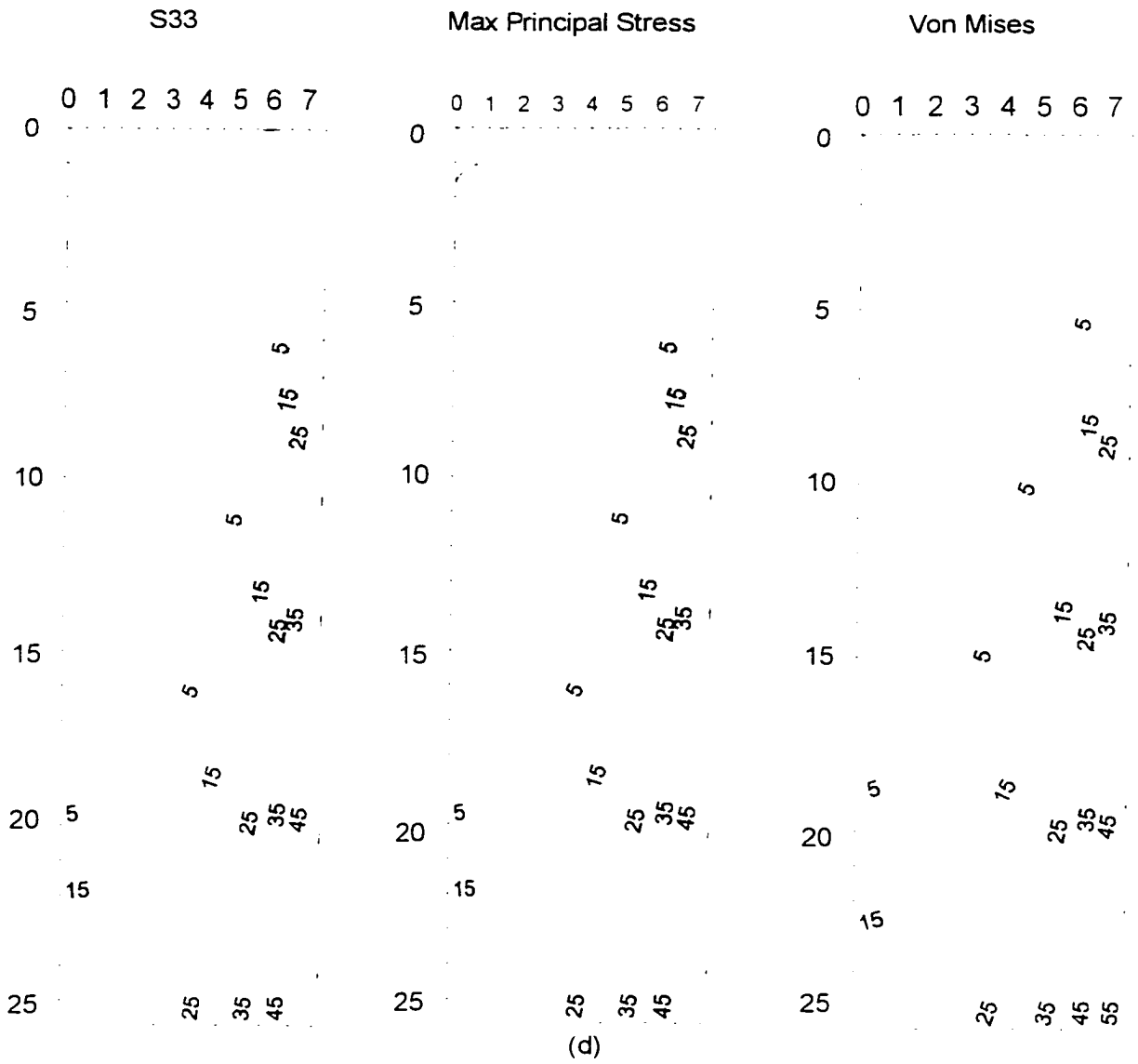
Figure 8.8: Thermal stress distribution for constant properties of wrought material model:

(a) increment=10, (b) increment = 15, (c) increment = 20, (d) increment =25, (e) increment =30





(c)



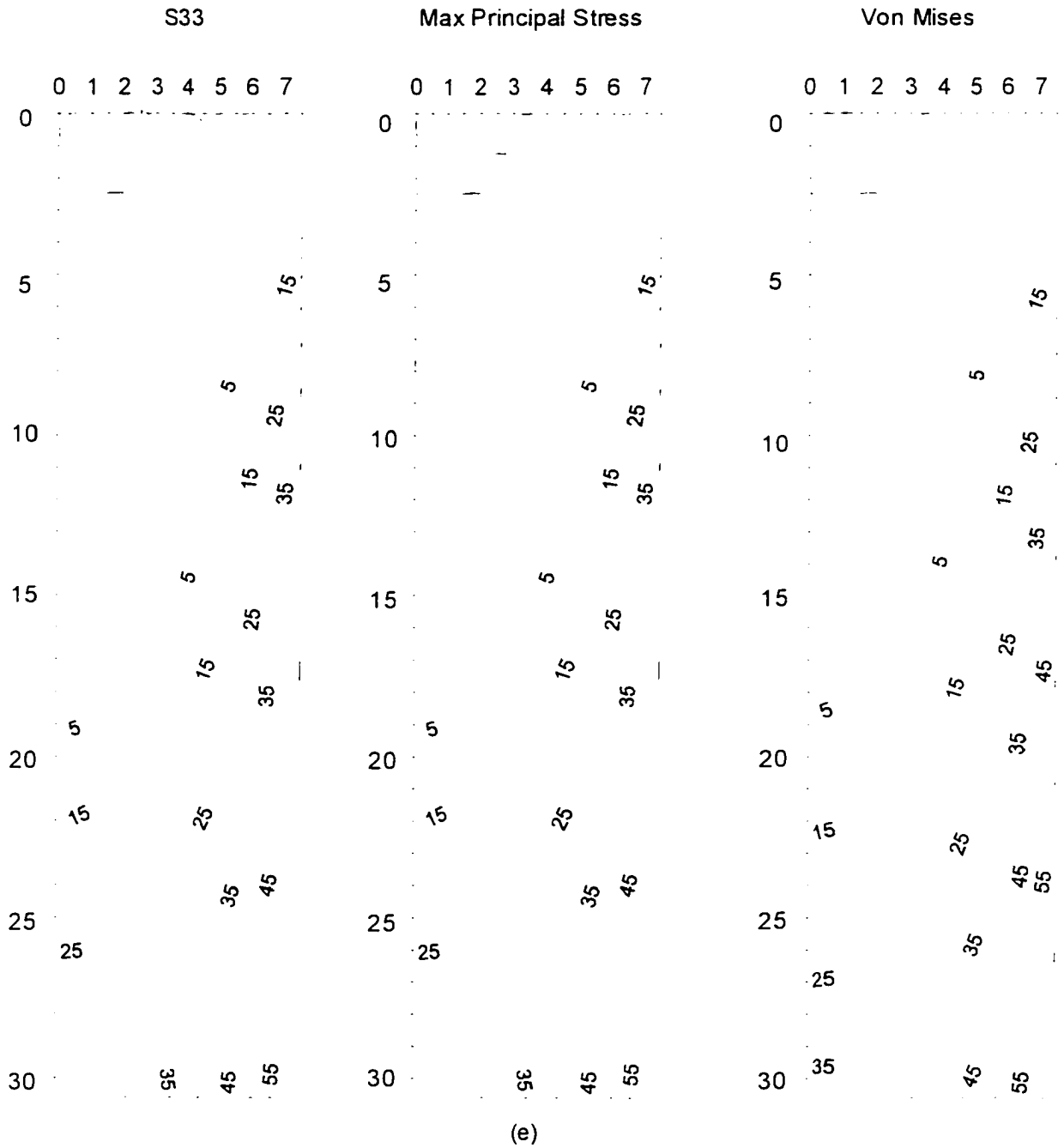
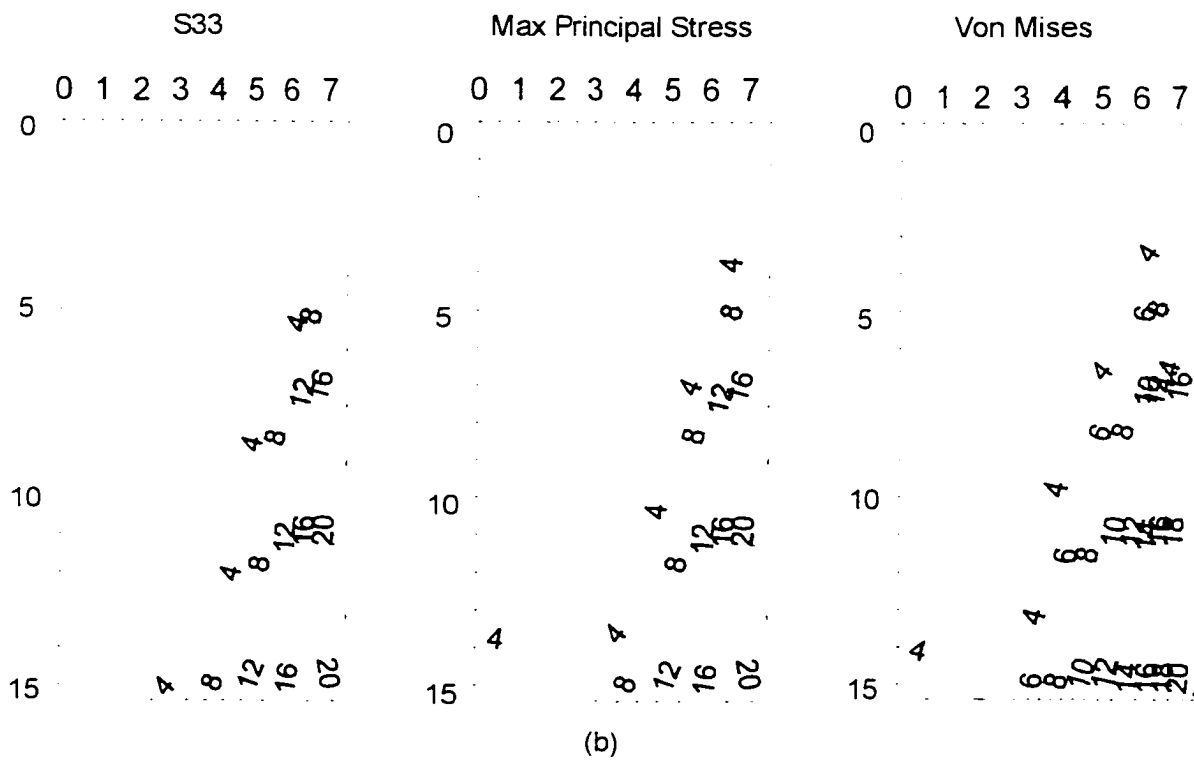
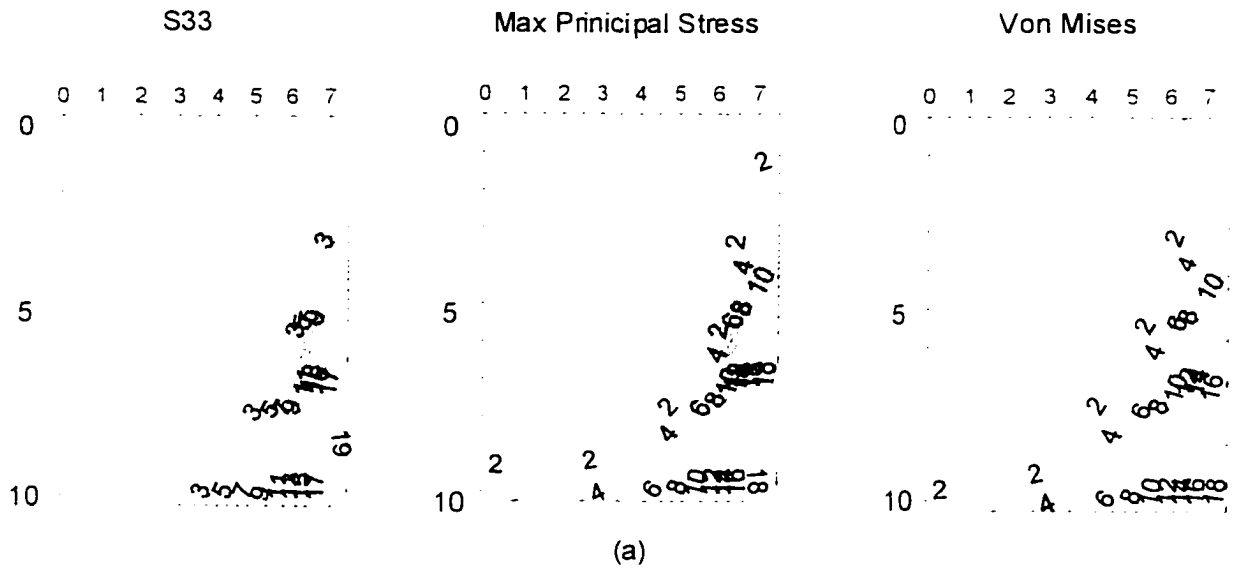


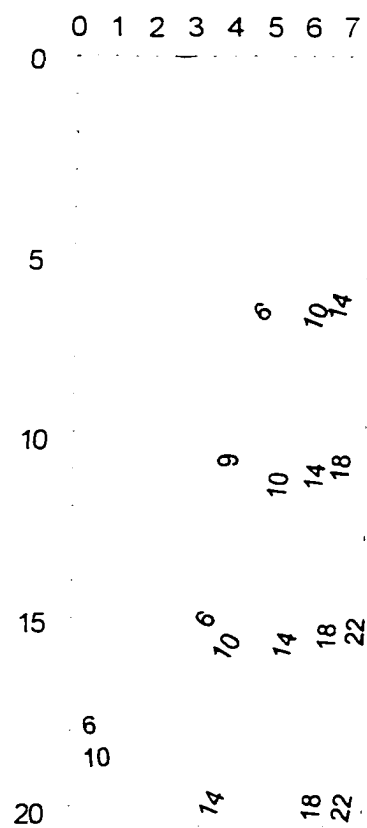
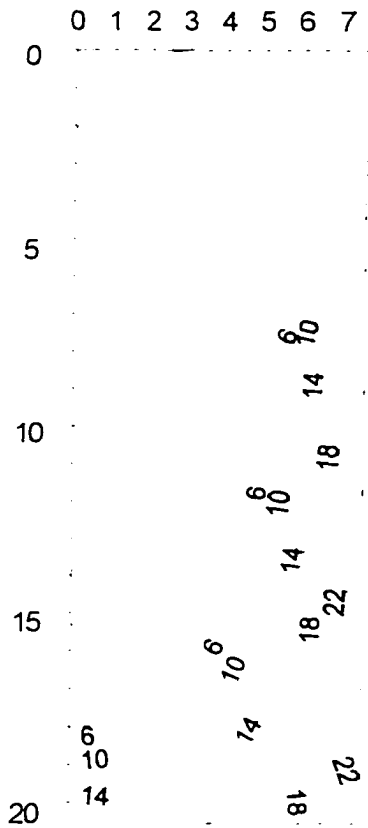
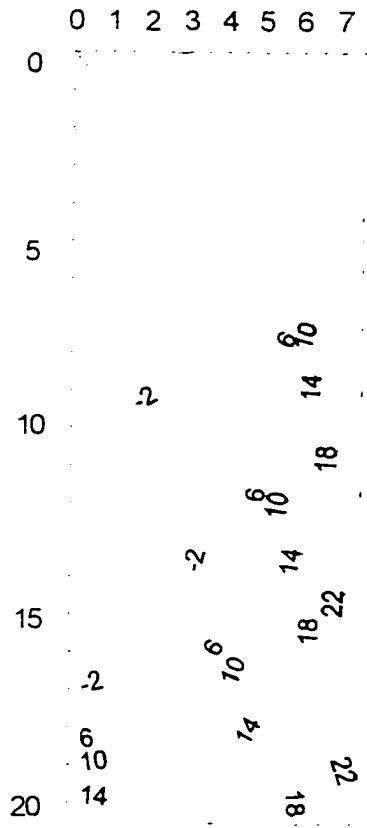
Figure 8.9. Thermal stress distribution results for temperature-dependent properties of wrought material model: (a) increment=10; (b) increment=15; (c) increment=20; (d) increment=25; (e) increment=30



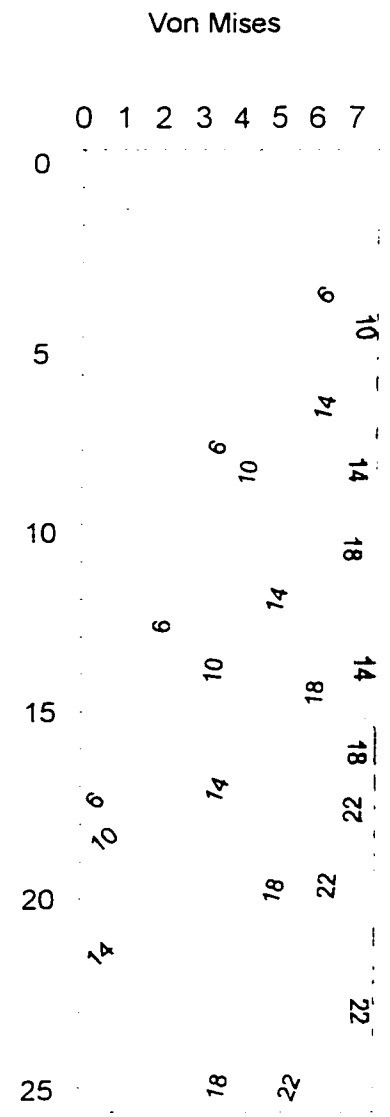
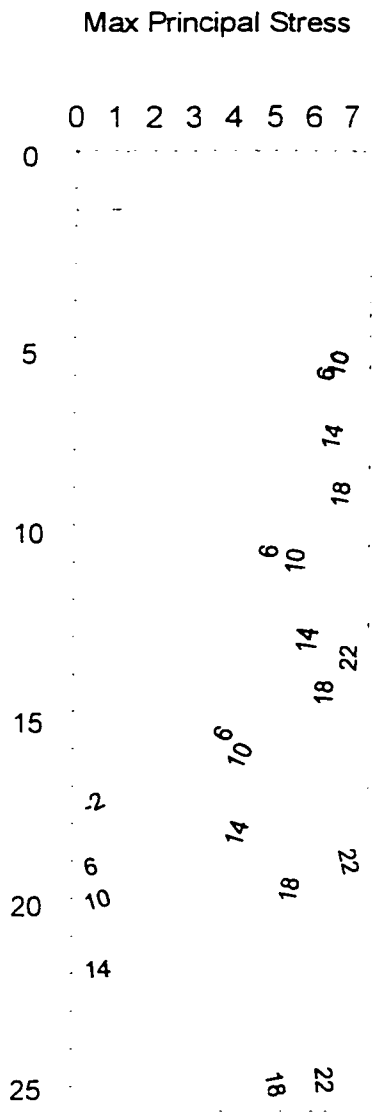
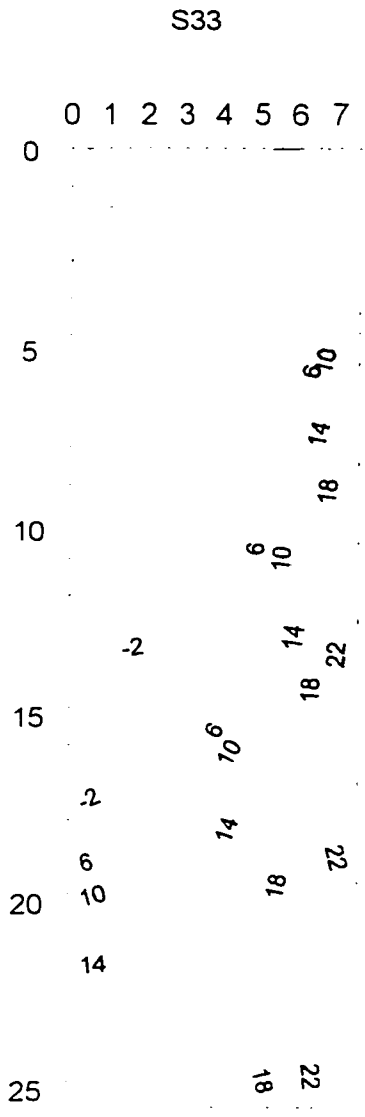
S33

Max Principal Stress

Von Mises



(c)



(d)

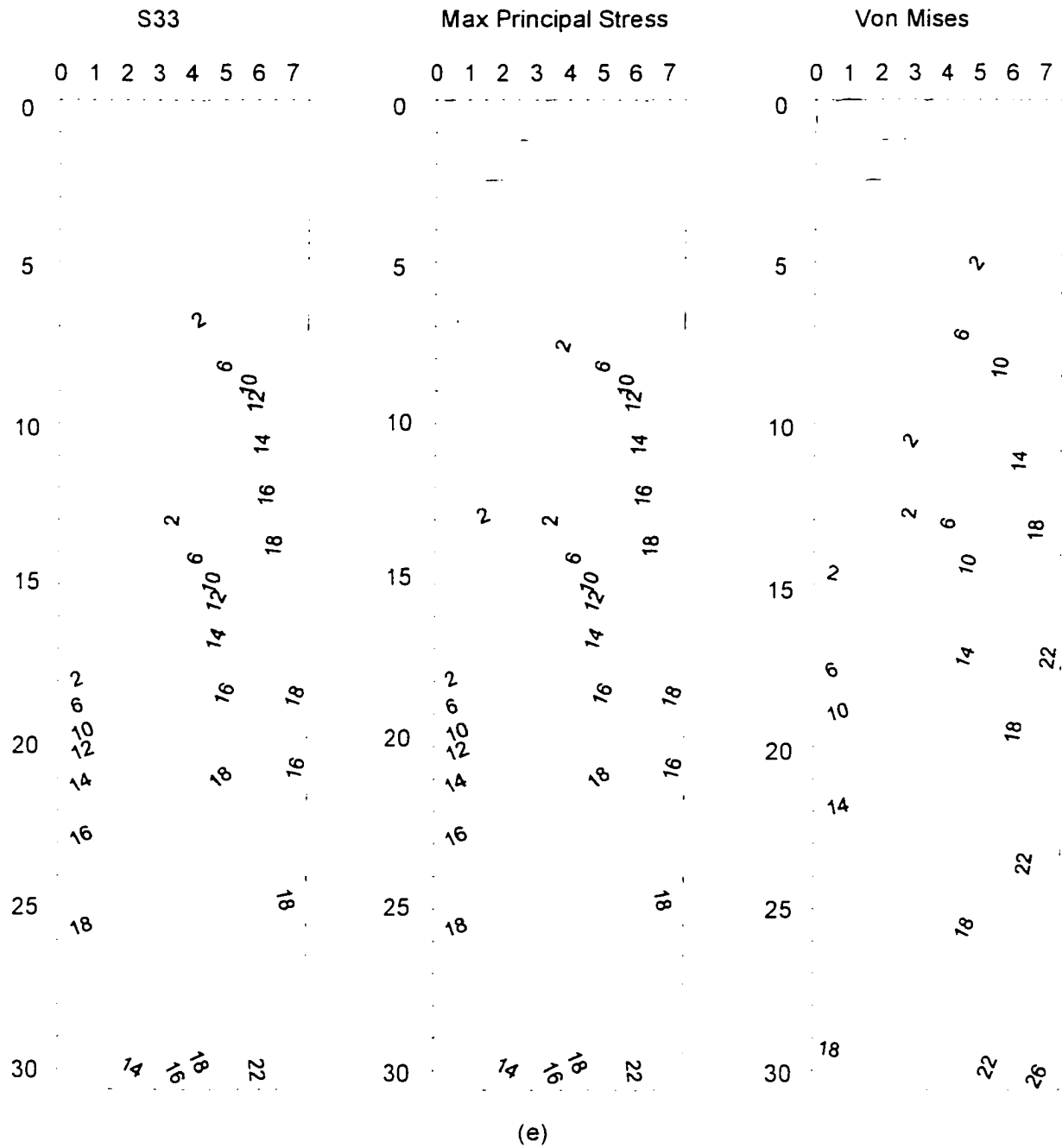
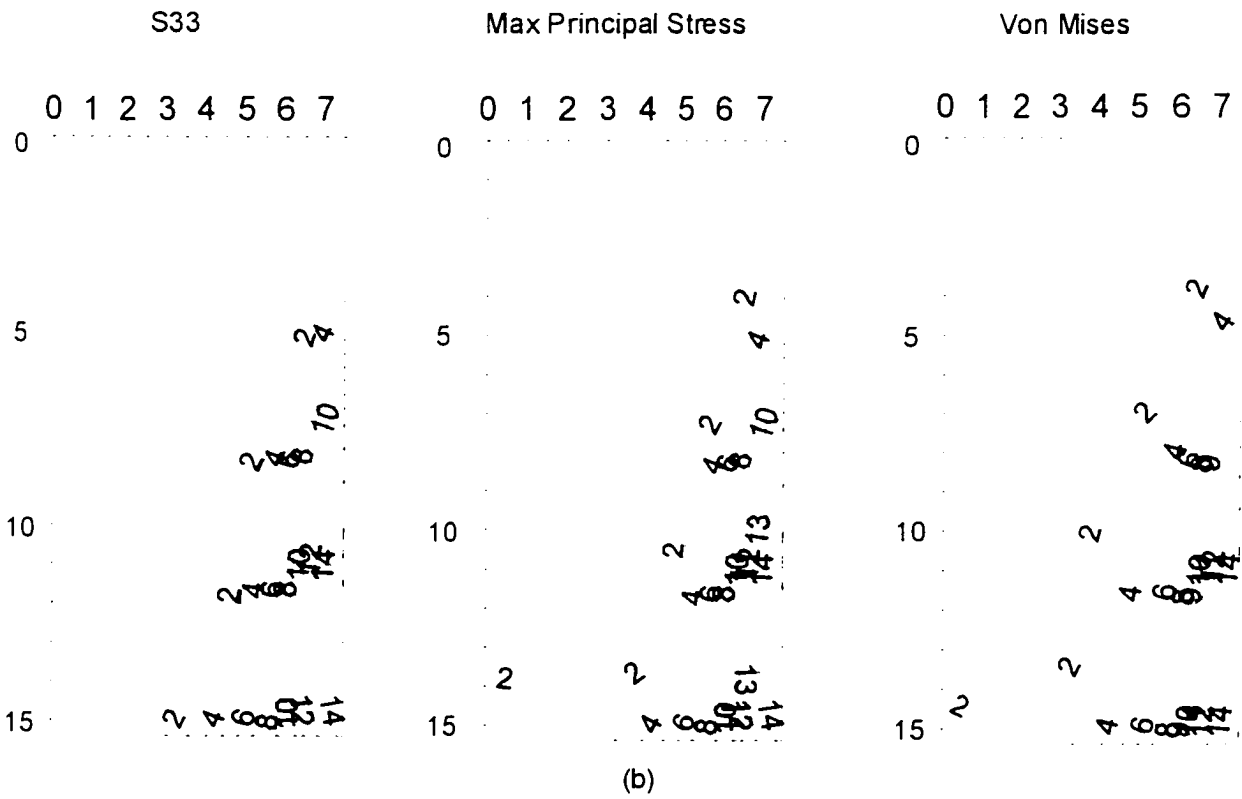
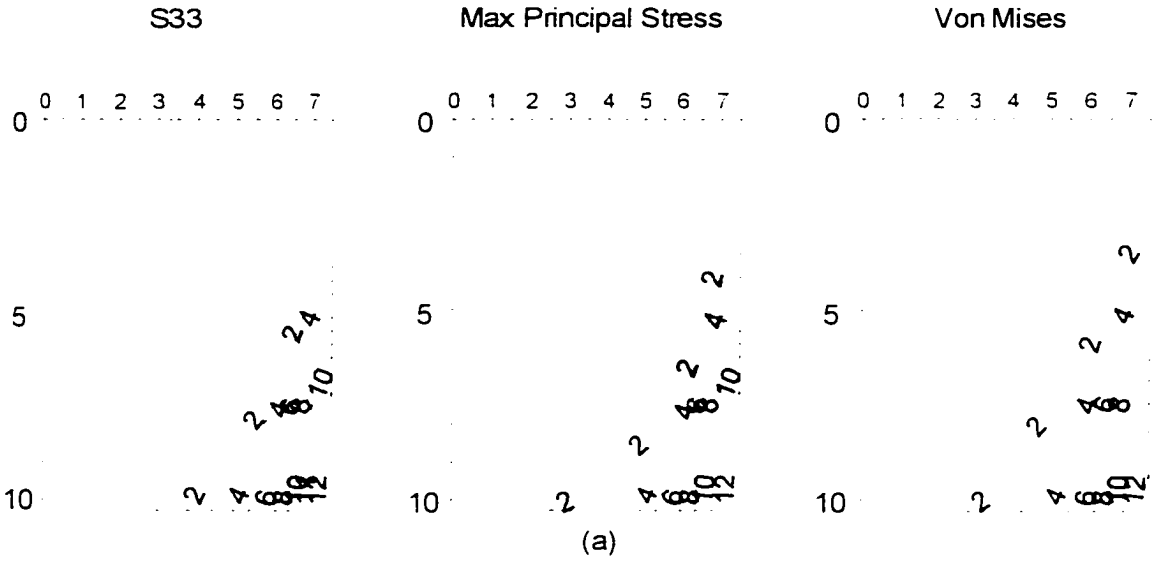


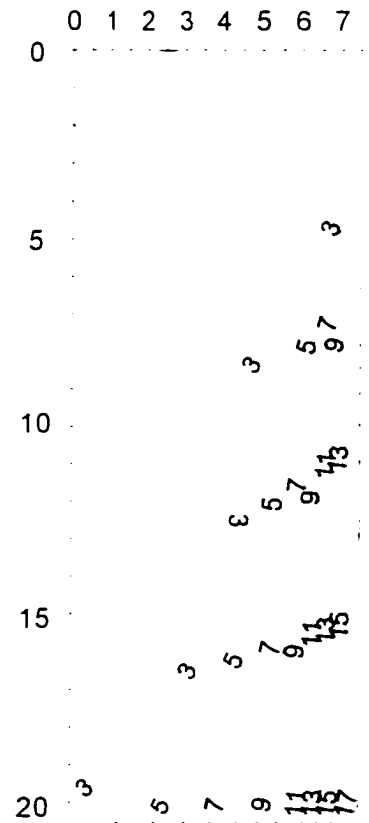
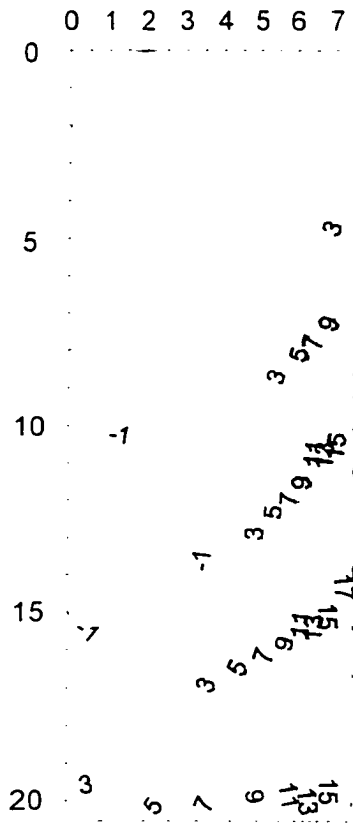
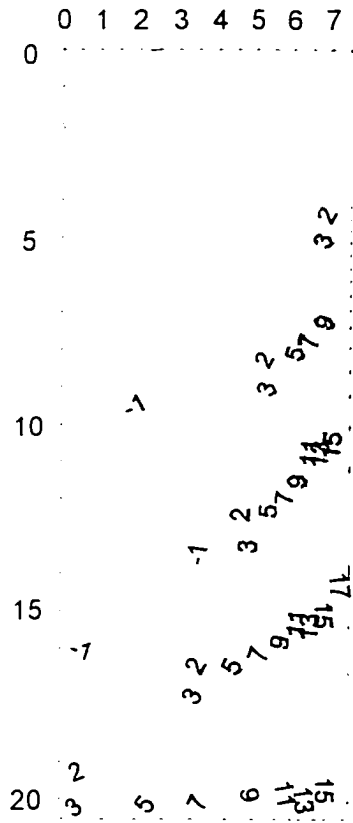
Figure 8.10: Thermal stress distribution for temperature dependent properties of as-cast ingot surface model: (a) increment=10; (b) increment=15; (c) increment=20; (d) increment=25; (e) increment=30



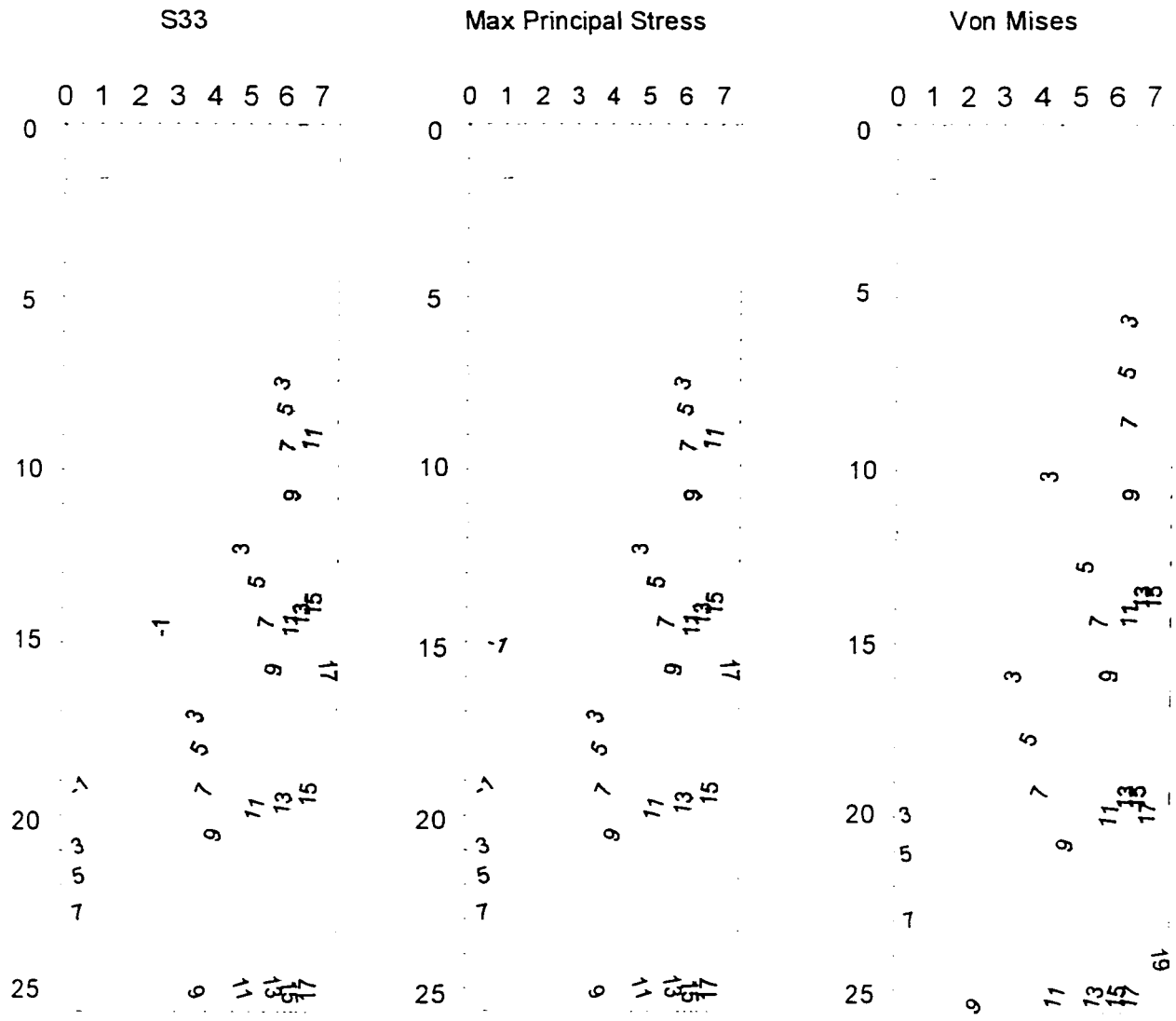
S33

Max Principal Stress

Von Mises



(c)



(d)

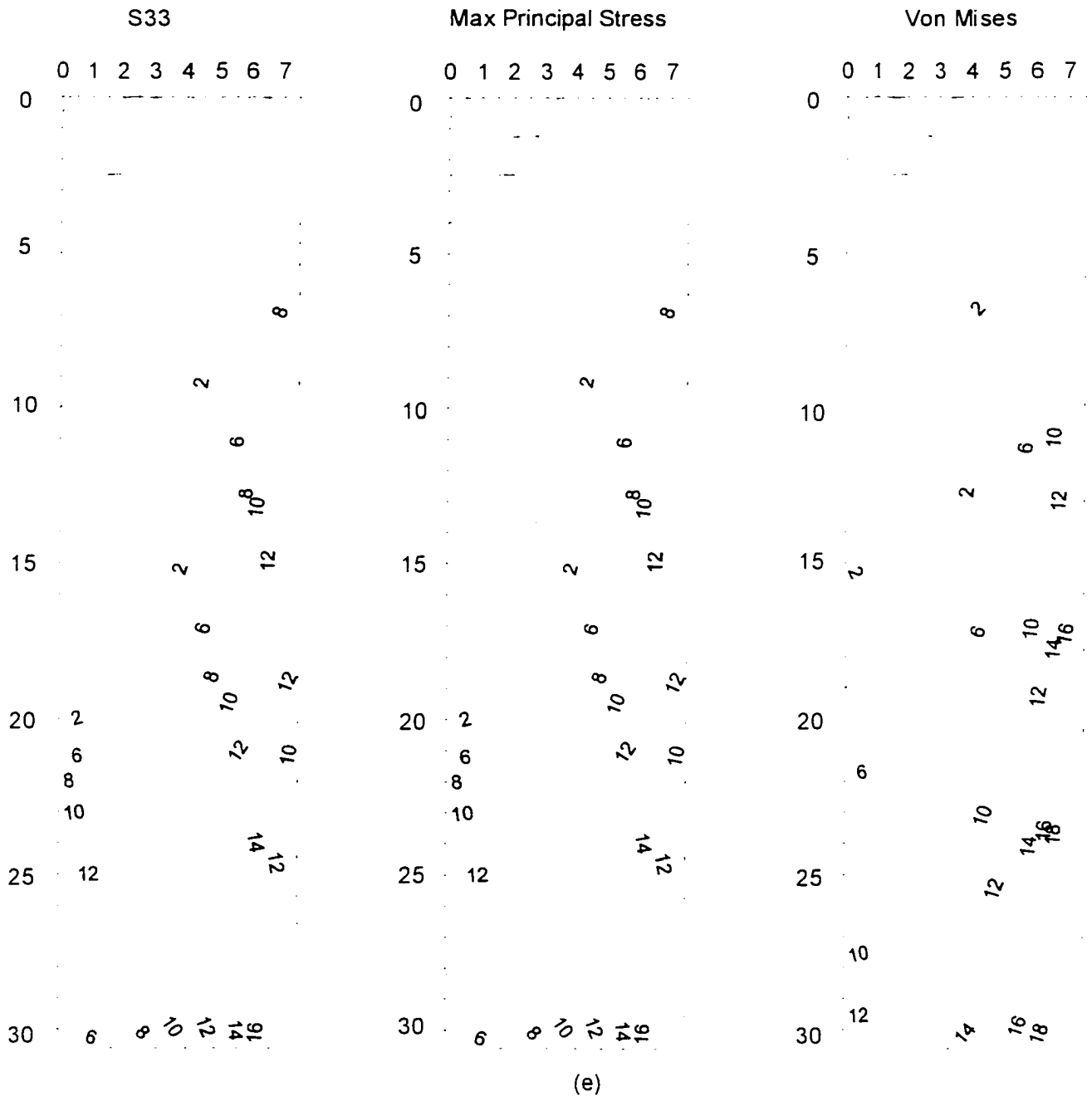
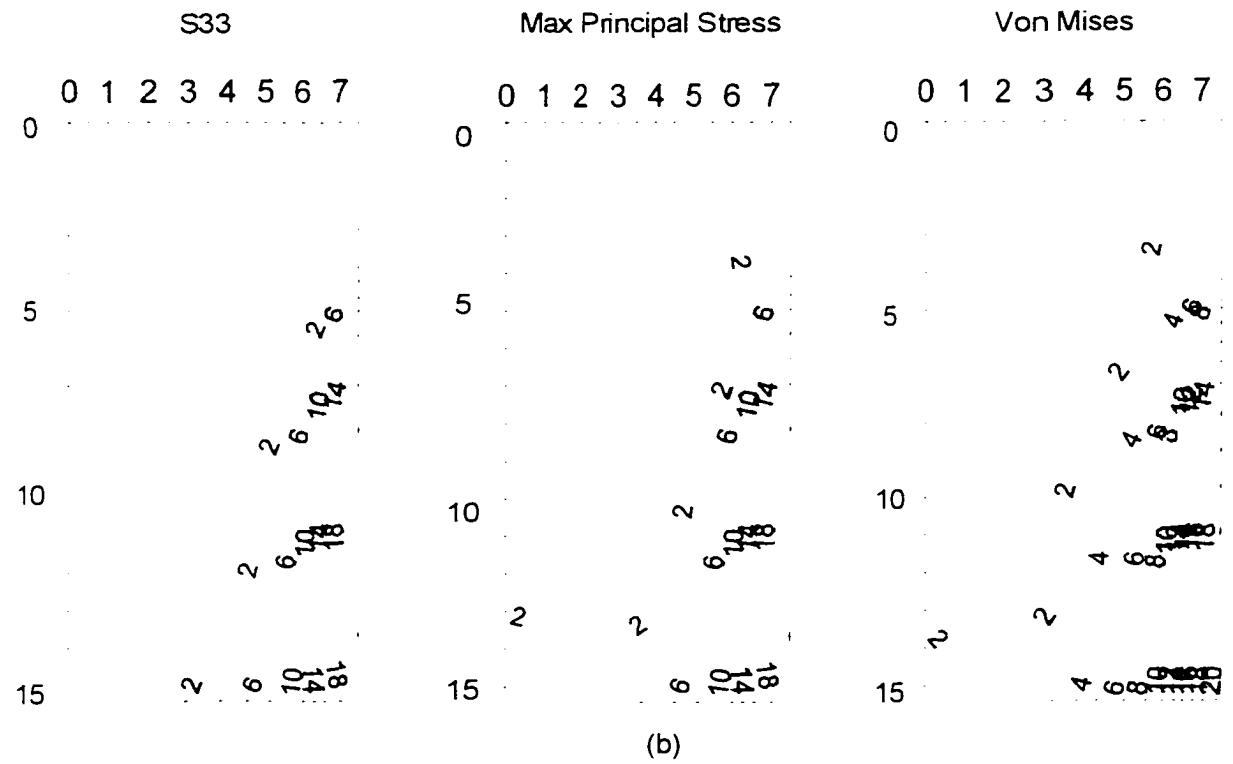
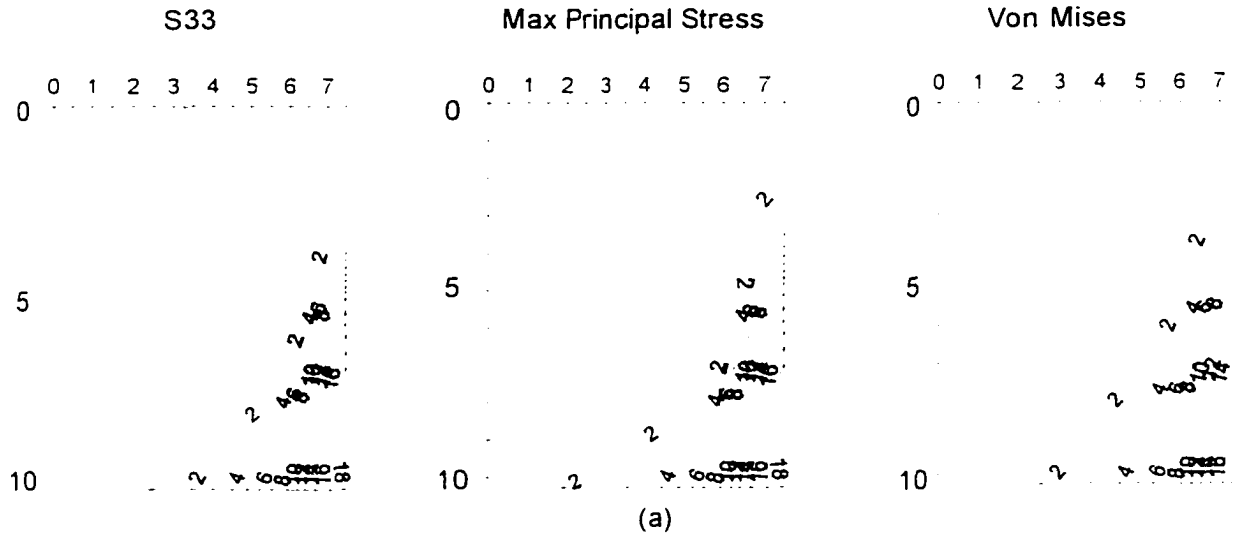
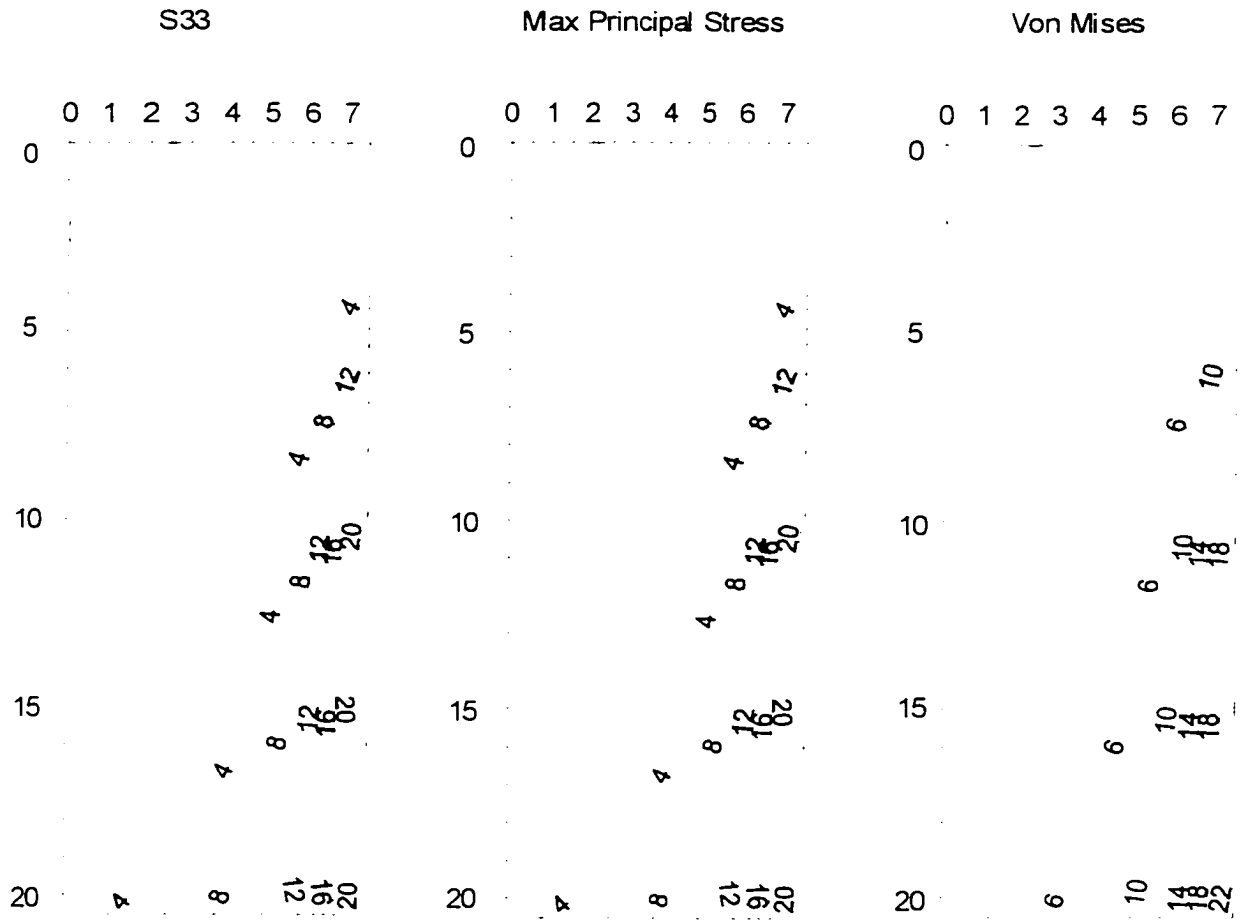
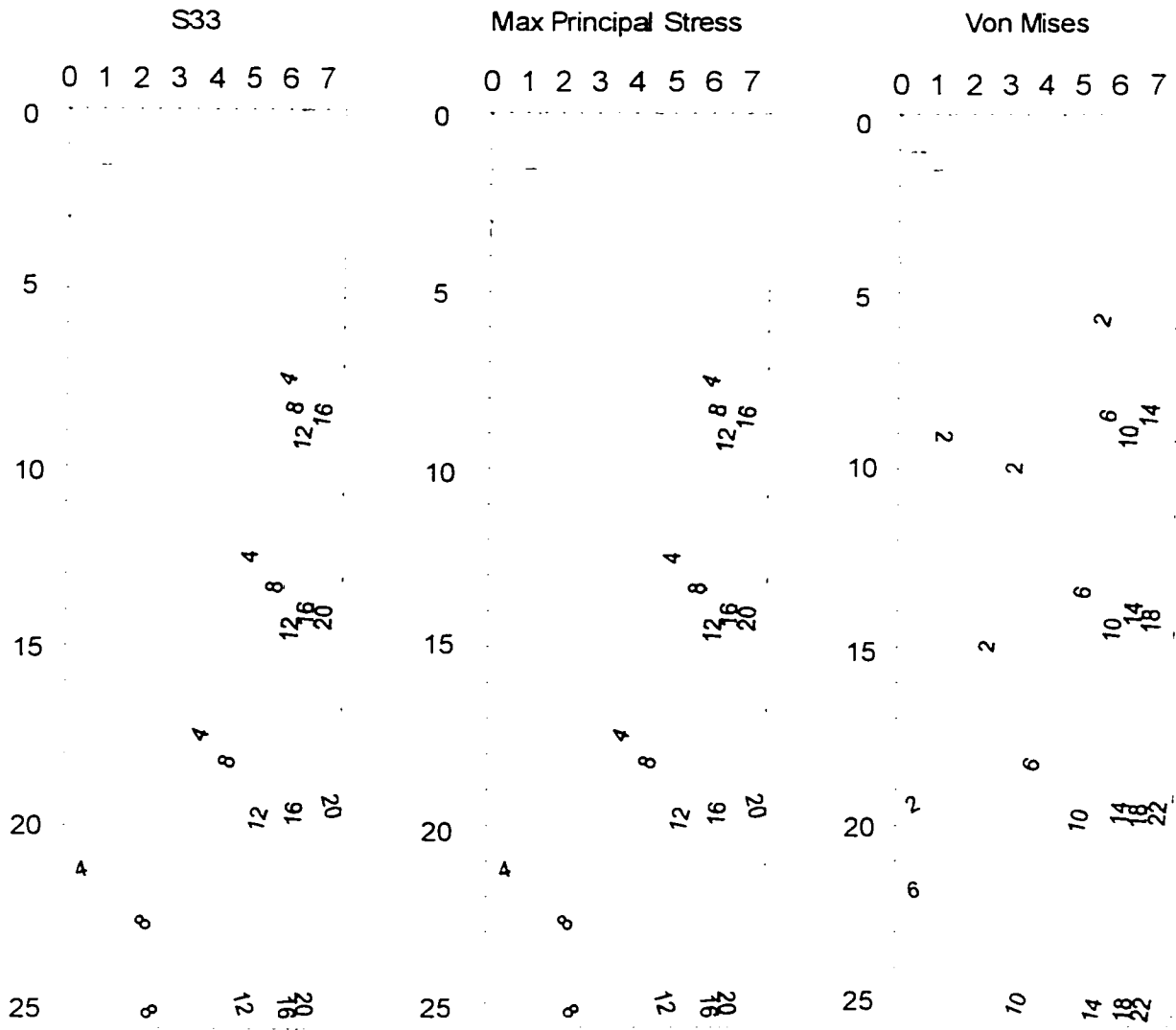


Figure 8.11: Thermal stress distribution for temperature-dependent properties of as-cast ingot center model: (a) increment=10, (b) increment=15, (c) increment=20, (d) increment=25, (e) increment=30

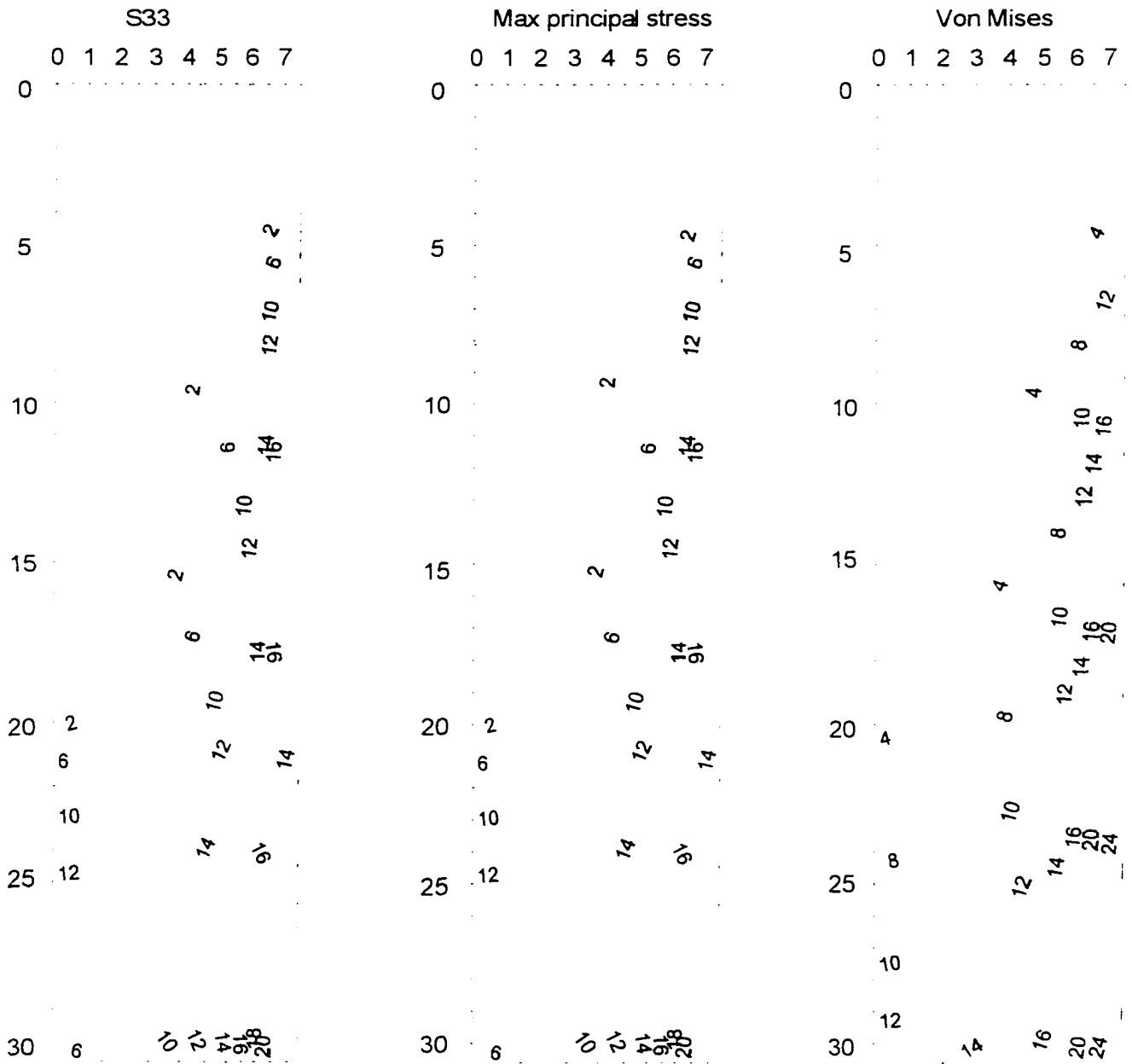




(c)



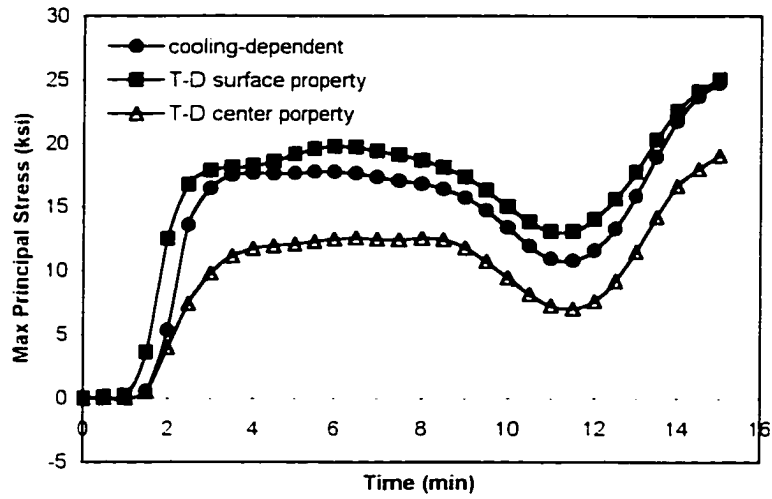
(d)



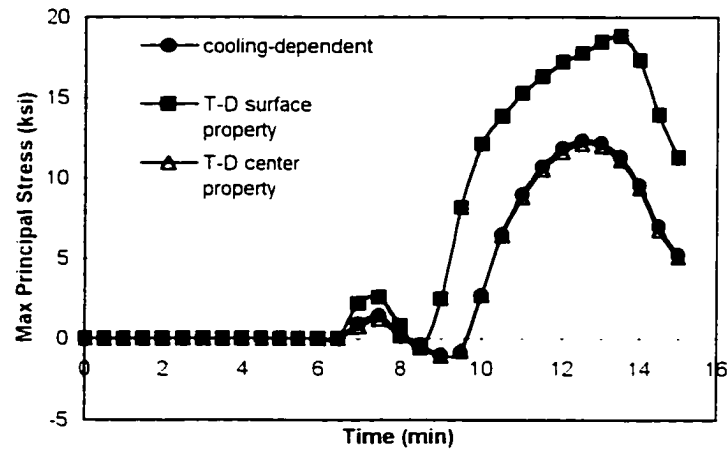
(e)

Figure 8.12: Thermal stress distribution for cooling-dependent properties of as-cast ingot model.

(a) increment=10, (b) increment = 15, (c) increment = 20, (d) increment =25, (e) increment =30

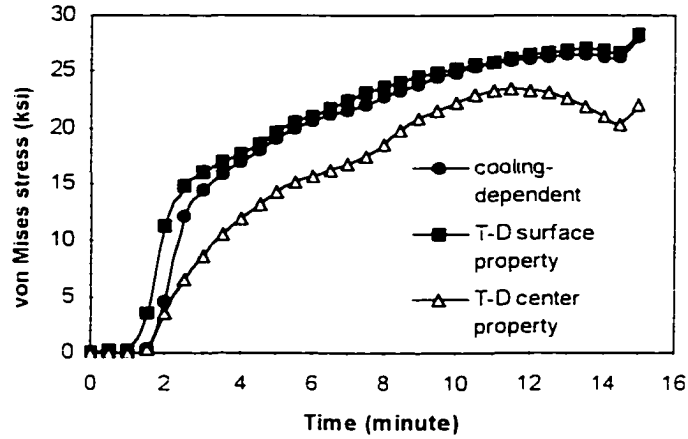


(a) along ingot surface

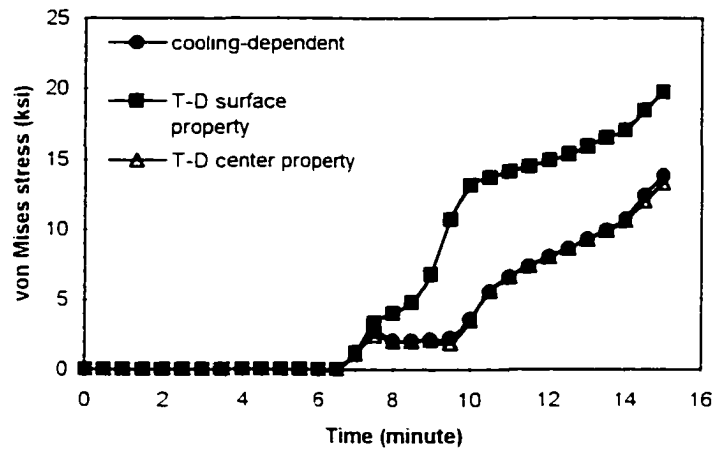


(b) along ingot center

Figure 8.13: Comparison of maximum principal stress of model 3, 4 and 5



(a) along ingot surface



(b) along ingot center

Figure 8.14: Comparison of von Mises stress of model 3, 4 and 5

The final results of von Mises stress distribution were normalized by dividing the stress value at every point by the yield strength with the corresponding conditions for temperature-dependent surface property model, temperature-dependent center property model and cooling-dependent property model. The normalized results are shown in Figure 8.15. The most deformed area is located at the low-right half of the model for all three kinds of material properties. The yielded

area are almost the same for three results. Result of temperature-dependent ingot center property model shows higher deformation at the ingot surface than the results from ingot surface property model and from cooling-dependent model.

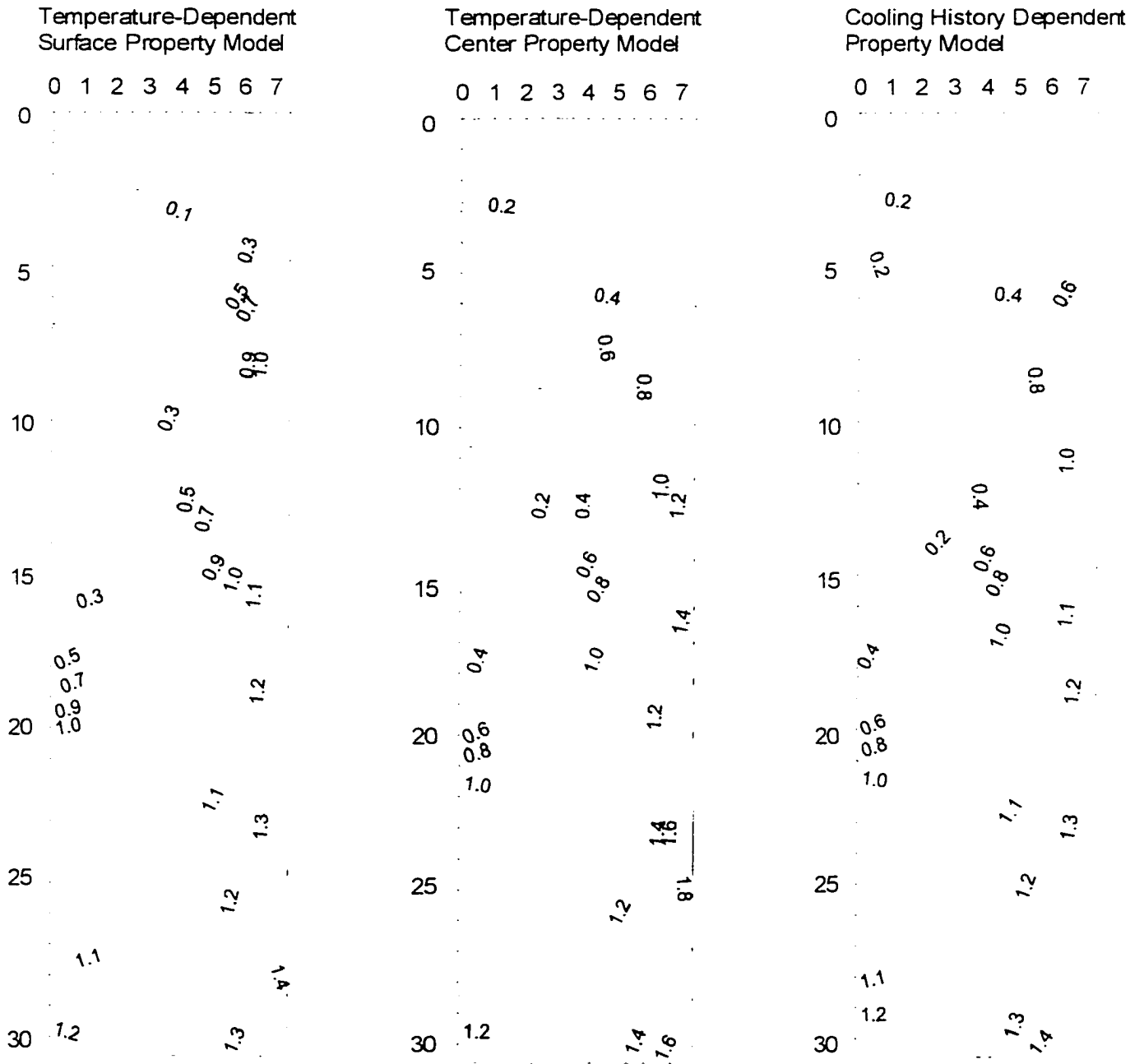


Figure 8 15: Normalized von Mises stress distribution for temperature-dependent and cooling-dependent properties models

All these results indicate that only by using the constitutive model, which reflects cooling history-dependent as-cast material properties, can the simulation predict the thermal stress accurately at every location of ingot. From the location and level of maximum stress in the ingot, critical places where casting cracks mostly tend to occur can be predicted. However, this study was limited by the steady state assumption in the simulation which can not investigate the stress distribution near the ingot bottom where most casting cracks initiate. Further research needs to be carried out through transient three-dimensional modeling, in which the consideration of cooling history dependency will be more critical in the simulation, especially for the location close to ingot bottom where experiences fast cooling through bottom block.

8.7 SUMMARY

In this chapter, thermal stress distribution was calculated for steady state of ingot casting using commercial FEM code ABAQUS. Two-dimensional model was used to describe the longitudinal cross-section at the center of rolling face. In-situ measured temperature profile in steady state was used as input in the stress modeling. Five different constitutive models, including the cooling-dependent as-cast material property model in which effects of both temperature and solidification rate were considered, were compared. Very high error will be brought by using wrought material properties instead of as-cast material properties. Calculated stress levels in wrought material property models, especially the constant property model, showed several times higher than those from as-cast material property models. By comparing temperature-dependent and cooling-dependent as-cast material property models, it can be indicated that only cooling-dependent model can obtain more accurate stress distribution by considering the inhomogeneous material properties of casting ingot. Therefore, the critical places, where maximum stresses are calculated, in the

ingot can be more accurately located through the simulation, and the corresponding measures in the casting can be applied to control them.

CHAPTER 9

CONCLUSION AND FUTURE WORK

9.1 CONCLUSION

A new methodology of thermal stress modeling of D.C. casting of high strength aluminum alloy ingot has been proposed and verified through both experimental work and finite element analysis. The research emphasizes the cooling history dependence of thermo-mechanical properties of as-cast aluminum ingot material, and focuses its effort on establishing a thermal-elastic-plastic constitutive model with the consideration of cooling rate during D.C. casting of high strength aluminum alloy, such as Al-7050. The study correlated the properties of ingot material with its cooling history through a series of experimental work including temperature profile measurement, metallurgical analysis and thermo-mechanical property measurement. The constitutive model established was implemented in a thermal stress numerical simulation. Principal findings through this research are following:

- 1) Cooling history of ingot material continuously changes from ingot rolling surface to ingot center during D.C. casting. Solidification rate changes from more than 524°F/min (4.9°C/sec) near ingot surface to about 40 °F/min (0.37°C/sec) at ingot center.
- 2) Notable inhomogeneity of ingot structure results from this uneven cooling of ingot casting. Grain size changes from 140 μm near ingot surface to 370 μm at ingot center, volume fraction of eutectic phases changes from 4.6% at the surface to 11.2% at the center.
- 3) Thermo-mechanical properties of as-cast Al 7050 ingot material depend on both temperature and cooling history the material experienced during casting.

- A. Yield strength of as-cast ingot material decreases with increasing temperature. For ingot surface with solidification rate of $524^{\circ}\text{F}/\text{min}$ ($4.9^{\circ}\text{C}/\text{sec}$), yield strength decreased from 19 ksi at 200°F (93°C) to 12 ksi at 800°F (427°C). For ingot center with solidification rate of $50^{\circ}\text{F}/\text{min}$ ($0.46^{\circ}\text{C}/\text{sec}$), yield strength decreased from 12 ksi at 200°F (93°C) to 5 ksi at 800°F (427°C).
- B. For a given testing temperature, yield strength of as-cast Al 7050 ingot about increases linearly as solidification rate increases.
- C. Continuous cooling rate does not have significant effect on mechanical properties of as-cast Al-7050 ingot at high temperature (above $400^{\circ}\text{F}/204^{\circ}\text{C}$). Slower cooling and aging at lower temperature range (below $400^{\circ}\text{F}/204^{\circ}\text{C}$) have some effects on mechanical properties of ingot material. Yield strength increases with decreasing cooling rate from $400^{\circ}\text{F}/204^{\circ}\text{C}$ to $200^{\circ}\text{F}/93^{\circ}\text{C}$ and with increasing aging time at $200^{\circ}\text{F}/93^{\circ}\text{C}$
- 4) Casting crack tendency of Al-7050 ingot is highly related to the grain boundary eutectic phases of ingot material. At room temperature, ingot surface shows higher fracture toughness than ingot center.
- 5) Cooling history dependence of material properties needs to be considered in thermal stress modeling for D.C casting. The results of thermal stress calculation, which applied the constitutive model considering both temperature and solidification rate, showed significant difference in stress level and distribution with those applying temperature-only-dependent constitutive models. The introduction of cooling history dependency of constitutive model into thermal stress simulation for D.C. casting will greatly improve the accuracy of thermal stress prediction of a casting ingot.

9.2 LIMITATION OF THIS RESEARCH

This research is limited in following aspects:

- 1) Errors may appear in the in-situ temperature profile measurement because of unprotected T/C leads. It was difficult to implement the protection in the measurement during production ingot casting.
- 2) Location of the ingot specimens may not locate exactly at the center between two end surfaces of ingot. This may bring errors on the cooling rates represented by the specimens from different ingot locations.
- 3) Creep effect is neglected in this study, which needs to be considered, especially for the material near the liquid pool of ingot.
- 4) The stress distribution close to the bottom of numerical model is artificial caused by the "end effect" of the calculation. For steady state, the length of the model is supposed to be infinite. However, only 30 inches data were available in the calculation. The bottom of the model became a free end which may bring artificial stress profile near this area.

9.3 SUGGESTION FOR FUTURE WORK

Future research includes following aspects.

- 1) 3D FEM model needs to replace the current 2D model which, although simplifying the problem, can not completely represent the stress condition of the whole ingot.
- 2) Sensitivity of casting parameters needs to be studied through the simulation, such as, casting speed, water rate, with and without wipe, etc.

- 3) Microstructure modeling, which establishes the correlation between ingot microstructure with the cooling history, needs to be further studied.
- 4) Alloy properties modeling, which establishes the correlation between microstructure and alloy properties, needs to be developed.
- 5) Quenching crack method needs to be employed in addition to the traditional room temperature K_{IC} test, because the driving force for casting crack propagation was thermal stress instead of uniaxial tensile stress.

REFERENCES

- [1] P. C. Valley, The Technology of Aluminum and It's Alloy. (Cleveland, OH. CRC Press, 1970). pp9-23
- [2] M.B.Cortie, "The Occurrence, Recognition, and Revention of Hot Cracking". Forensic Engineering, vol 3, no.1, 1991, pp23-35
- [3] E. D. Tarapore, "Thermal Modeling of DC Continuous Billet Casting". Light Metals 1989. Edited by P. G. Campbell, The Minerals, Metals & Materials Society, 1989, pp 875-880
- [4] T. S. El-Raghy, "Modeling of the Transient and Steady State Periods during Aluminum DC Casting". Light Metals 1995. Edited by J. Evans, The Minerals, Metals & Materials Society, 1995
- [5] E. K. Jensen, "Development of a New Starting Block Shape for D C. Casting of Aluminum Sheet Ingots. Part II: Modeling Results". Light Metals 1995. Edited by J. Evans, The Minerals, Metals & Materials Society, 1995, pp969-978
- [6] G. -U. Grun and W. Schneider, "3-D Modeling of the Start-up Phase of DC Casting of Sheet Ingots". Light Metals 1996.
- [7] S. C. Flood, *et al.*, "Modeling of Fluid Flow and Stress Phenomena During DC Casting of Aluminum Alloys". Light Metals 1989, Edited by P. G. Campbell, The Minerals, Metals & Materials Society, 1988, pp943-947
- [8] T. Inoue and D Y. Ju, "Simulation of Solidification and Viscoplastic Stresses During Vertical Semicontinuous Direct Chill Casting of Aluminum Alloy". *International Journal of Plasticity*, Vol.8, pp. 161-183,1992
- [9] Hallvard G. Fjaer and Asbjorn Mo, "ALSPEN- A Mathematical Model for Thermal Stresses in Direct Chill Casting of Aluminum Billets". *Metallurgical Transaction B*, vol 21B, 1990, pp 1049-1061
- [10] Hallvard G. Fjaer and E. K. Jensen, "Mathematical Modeling of Butt Curl Deformation of Sheet Ingots. Comparison with Experimenta Results for Different Starter Block Shape". Light Metals 1995. Edited by J. Evans, The Minerals, Metals & Materials Society, 1995, pp 951-959
- [11] Hallvard G. Fjaer and Arid Hakonsen, "The Mechanism of Pull-in during DC-casting of Aluminum Sheet Ingots". Light Metals 1997. Edited by R. Huglen, The Minerals, Metals & Materials Society, 1997, pp 683-690
- [12] J.-M Drezet and M. Plata, "Thermomechanical Effects During Direct Chill and Electromagnetic Casting of Aluminum Alloys, Part I: Experimental Investigation". Light Metals 1995. Edited by J. Evans, The Minerals, Metals & Materials Society, 1995, pp 931-940
- [13] J. -M Drezet and M. Rappaz, "Thermomechanical Effects During Direct Chill and Electromagnetic Casting of Aluminum Alloys, Part II: Numerical Simulation". Light Metals 1995. Edited by J. Evans, The Minerals, Metals & Materials Society, 1995, pp 941-950
- [14] J.-M Drezet and M. Rappaz, "Modeling of Ingot Distortions During Direct Chill Casting of Aluminum Alloys". *Metallurgical and Material Transactions A*, Vol 27A, Oct. 1996, pp 3214-3225
- [15] J.-M Drezet and M. Rappaz, "Direct Chill Casting of Aluminum Alloys: Ingot Distortions and Mold Design Optimization". Light Metals 1997. Edited by R. Huglen, The Minerals, Metals & Materials Society, 1997, pp 1071-1080

- [16] B. Magnin, *et al.*, "Ductility and Rheology of an Al-4.5%Cu Alloy from Room Temperature to Coherency Temperature", Material Science Forum, Vols 217-222 (1996) pp 1209-1214
- [17] Yuri Estrin, "Constitutive Modelling of Alloys Implementing Metallurgical Variables", Material Science Forum, Vols 217-222 (1996), pp1001-1006
- [18] H. Gehanno, *et al.*, "Use of Internal Variable Models to Predict the High Temperature Behavior of a 6xxx Industrial Alloy", Material Science Forum, Vols 217-222 (1996) pp1413-1418
- [19] J. -L. Duval, *et al.*, "Microstructure-based Models of the Plastic Behaviour of 3104 Aluminum Alloy", Material Science Forum, Vols 217-222 (1996) pp1007-1012
- [20] M. G. Chu and D. A. Granger, "The Tensile strength and Fracture Behavior of Partially Solidified Aluminum Alloys", Material Science Forum, Vols 217-222 (1996) pp1505-1510
- [21] Tae Kwon Ha, *et al.*, "High Temperature Deformation Behavior of a 7475 Al Alloy", Material Science Forum, Vols 217-222 (1996), pp1203-1208
- [22] Savamiphakdi and Kropp, "Determination by a Finite Element Method of Stress Distributions During Quenching of Cylindrical Parts", ABAQUS Users Conference Proceedings, 1988 May, Newport, RI, pp 421-438
- [23] J.M. Franchet, *et al.*, "Residual Stress Modelling During the Oil Quenching of an Astrology Turbine Disk", Superalloys 1992, pp 73-82
- [24] R. Becker, "Experimental Validation of Predicted Distortion and Residual Stress in Quenched Bars", Computational Material Modeling, ASME-Publications-PVP, 1994, vol 294, pp 287-311
- [25] S. Denis, *et al.*, "Stress-phase-transformation Interactions—Basic Principles, Modeling, and Calculation of Internal Stresses", Material Science and Technology, Oct. 1985, vol. 1, pp 805-814
- [26] K. F. Wang, *et al.*, "An Efficient 2D Finite Element Procedure for the Quenching Analysis with Phase Change", Transaction of the ASME, Vol. 115, Feb. 1993, pp 124-138
- [27] Hwei-Minn Lu, Keh-Minn Chang, Jerry Harris, "Constitutive Modeling of High-Strength Aluminum Casting", Light Metals 1997, Edited by R. Huglen, The Minerals, Metals & Materials Society, 1997, pp1091-1095
- [28] "ABAQUS user manual", Hibbitt, Karlsson & Sorensen, Inc.
- [29] J. A. Bakken and T. Bergström, "Heat Transfer Measurements During DC Casting of Aluminum, Part I: Measurement Technique", Light Metals 1986, Volume 2, USA Metallurgical Soc. of AIME, Warrendale, PA, pp 883-889
- [30] E. K. Jensen, *et al.*, "Heat Transfer Measurements During DC Casting of Aluminum, Part II: Results and Verification for Extrusion Ingots", Light Metals 1986, The Minerals, Metals & Materials Society, 1986, pp 891-896
- [31] J. Langlais, *et al.*, "Measuring The heat Extraction Capacity of DC Casting Cooling Water",
- [18] H. Gehanno, *et al.*, "Use of Internal Variable Models to Predict the High Temperature Behavior of a 6xxx Industrial Alloy", Material Science Forum, Vols 217-222 (1996) pp1413-1418 "Constitutive Modelling of Alloys Implementing Metallurgical Variables" Light Metals 1995, Edited by J. Evans, The Minerals, Metals & Materials Society, 1995, pp979-986
- [32] Hitoshi Matsuzaki, *et al.*, "Investigation in the Effects of Casting Speed on Inverse Segregation Behavior in D.C. Casting of Aluminum Slabs", Light Metals 1995, Edited by J. Evans, The Minerals, Metals & Materials Society, 1995, pp1033-1037

- [33] H. Kraushaar, *et al*, "Correlation of Surface Temperatures and Heat Transfer by D.C. Casting of Aluminum Ingots". Light Metals 1995, Edited by J. Evans, The Minerals, Metals & Materials Society, 1995, pp1055-1059
- [34] 1990 Annual Book of ASTM Standards, Edited by P.C. Frazio, American Society for Testing and Materials, 1990
- [35] Aluminum, Vol. I. Properties, Physical Metallurgy and Phase Diagrams, 1967, Edit by K. R. Van Horn, American Society for Metals, Metal Park, Ohio, pp55-67
- [36] Jin Yan, "A Microstructural Analysis of 7050 Al Alloy", ACTA METALLURGICA SINICA, Vol 5, No.2,1992
- [37] User Manual of Labview, National Instruments Corporation, Austin, TX
- [38] W. F. Chen, D. J. Han, Plasticity for Structure Engineers, Springer-Verlag New York Inc., 1988
- [39] Keh-Minn Chang and Bruce Kang, Control of Solidification Cracking in High-strength Aluminum alloys – 1996 Annual Report for Research Project sponsored by Century Aluminum Corporation, January 31, 1997
- [40] D. R. J. Owen and E. Hinton, Finite Element in Plasticity: Theory and Practice, Pineridge Press Limited, Swansea, U.K., 1980
- [41] ASM Metal Handbook, J.R.Davis et al, Ed., Vol 2, 10th Ed., Materials Park, OH: ASM International, 1995, pp111-114

APPENDIX

ABAQUS INPUT FILES

APPENDIX A: Input file for constant properties of wrought Al 7050 material model

```
*HEADING
Property for 7050-T7451 at Room Temperature
Perfect Plastic,no work hardening
*NODE, SYSTEM=R,nset=all
15, 7.0000000E+00,-3.6560000E+01, 0.0000000E+00
16, 7.5000005E+00,-3.6360000E+01, 0.0000000E+00
22, 6.4999995E+00,-3.7189999E+01, 0.0000000E+00
23, 7.0000000E+00,-3.7189999E+01, 0.0000000E+00
24, 7.5000005E+00,-3.7189999E+01, 0.0000000E+00
29, 6.2000000E+00,-3.8220001E+01, 0.0000000E+00
30, 6.4999995E+00,-3.8220001E+01, 0.0000000E+00
31, 7.0000000E+00,-3.8220001E+01, 0.0000000E+00
32, 7.5000005E+00,-3.8220001E+01, 0.0000000E+00
37, 5.7000000E+00,-3.9240002E+01, 0.0000000E+00
38, 6.4999995E+00,-3.9240002E+01, 0.0000000E+00
39, 7.0000000E+00,-3.9240002E+01, 0.0000000E+00
40, 7.5000005E+00,-3.9240002E+01, 0.0000000E+00
44, 5.2000000E+00,-4.0270000E+01, 0.0000000E+00
45, 6.0000000E+00,-4.0270000E+01, 0.0000000E+00
46, 6.4999995E+00,-4.0270000E+01, 0.0000000E+00
47, 7.0000000E+00,-4.0270000E+01, 0.0000000E+00
48, 7.5000005E+00,-4.0270000E+01, 0.0000000E+00
52, 4.9000000E+00,-4.1300003E+01, 0.0000000E+00
53, 6.0000000E+00,-4.1300003E+01, 0.0000000E+00
54, 6.4999995E+00,-4.1300003E+01, 0.0000000E+00
55, 7.0000000E+00,-4.1300003E+01, 0.0000000E+00
56, 7.5000005E+00,-4.1300003E+01, 0.0000000E+00
60, 4.7000000E+00,-4.2320004E+01, 0.0000000E+00
61, 6.0000000E+00,-4.2320004E+01, 0.0000000E+00
62, 6.4999995E+00,-4.2320004E+01, 0.0000000E+00
63, 7.0000000E+00,-4.2320004E+01, 0.0000000E+00
64, 7.5000005E+00,-4.2320004E+01, 0.0000000E+00
68, 4.5000000E+00,-4.3349998E+01, 0.0000000E+00
69, 6.0000000E+00,-4.3349998E+01, 0.0000000E+00
70, 6.4999995E+00,-4.3349998E+01, 0.0000000E+00
71, 7.0000000E+00,-4.3349998E+01, 0.0000000E+00
72, 7.5000005E+00,-4.3349998E+01, 0.0000000E+00
75, 4.0000000E+00,-4.4380001E+01, 0.0000000E+00
76, 4.5000000E+00,-4.4380001E+01, 0.0000000E+00
77, 6.0000000E+00,-4.4380001E+01, 0.0000000E+00
78, 6.4999995E+00,-4.4380001E+01, 0.0000000E+00
79, 7.0000000E+00,-4.4380001E+01, 0.0000000E+00
80, 7.5000005E+00,-4.4380001E+01, 0.0000000E+00
```

93, 3.7000000E+00, -4.5410000E+01, 0.0000000E+00
 94, 4.5000000E+00, -4.5410000E+01, 0.0000000E+00
 95, 6.0000000E+00, -4.5410000E+01, 0.0000000E+00
 96, 6.4999995E+00, -4.5410000E+01, 0.0000000E+00
 97, 7.0000000E+00, -4.5410000E+01, 0.0000000E+00
 98, 7.5000005E+00, -4.5410000E+01, 0.0000000E+00
 99, 3.4000000E+00, -4.6430000E+01, 0.0000000E+00
 92, 4.5000000E+00, -4.6430000E+01, 0.0000000E+00
 93, 6.0000000E+00, -4.6430000E+01, 0.0000000E+00
 94, 6.4999995E+00, -4.6430000E+01, 0.0000000E+00
 95, 7.0000000E+00, -4.6430000E+01, 0.0000000E+00
 96, 7.5000005E+00, -4.6430000E+01, 0.0000000E+00
 99, 3.0000000E+00, -4.7460003E+01, 0.0000000E+00
 100, 4.5000000E+00, -4.7460003E+01, 0.0000000E+00
 101, 6.0000000E+00, -4.7460003E+01, 0.0000000E+00
 102, 6.4999995E+00, -4.7460003E+01, 0.0000000E+00
 103, 7.0000000E+00, -4.7460003E+01, 0.0000000E+00
 104, 7.5000005E+00, -4.7460003E+01, 0.0000000E+00
 106, 2.2000000E+00, -4.8489998E+01, 0.0000000E+00
 107, 3.0000000E+00, -4.8489998E+01, 0.0000000E+00
 108, 4.5000000E+00, -4.8489998E+01, 0.0000000E+00
 109, 6.0000000E+00, -4.8489998E+01, 0.0000000E+00
 110, 6.4999995E+00, -4.8489998E+01, 0.0000000E+00
 111, 7.0000000E+00, -4.8489998E+01, 0.0000000E+00
 112, 7.5000005E+00, -4.8489998E+01, 0.0000000E+00
 114, 1.5000000E+00, -4.9510002E+01, 0.0000000E+00
 115, 3.0000000E+00, -4.9510002E+01, 0.0000000E+00
 116, 4.5000000E+00, -4.9510002E+01, 0.0000000E+00
 117, 6.0000000E+00, -4.9510002E+01, 0.0000000E+00
 118, 6.4999995E+00, -4.9510002E+01, 0.0000000E+00
 119, 7.0000000E+00, -4.9510002E+01, 0.0000000E+00
 120, 7.5000005E+00, -4.9510002E+01, 0.0000000E+00
 121, 0.0000000E+00, -5.0539997E+01, 0.0000000E+00
 122, 1.5000000E+00, -5.0539997E+01, 0.0000000E+00
 123, 3.0000000E+00, -5.0539997E+01, 0.0000000E+00
 124, 4.5000000E+00, -5.0539997E+01, 0.0000000E+00
 125, 6.0000000E+00, -5.0539997E+01, 0.0000000E+00
 126, 6.4999995E+00, -5.0539997E+01, 0.0000000E+00
 127, 7.0000000E+00, -5.0539997E+01, 0.0000000E+00
 128, 7.5000005E+00, -5.0539997E+01, 0.0000000E+00
 129, 0.0000000E+00, -5.1570000E+01, 0.0000000E+00
 130, 1.5000000E+00, -5.1570000E+01, 0.0000000E+00
 131, 3.0000000E+00, -5.1570000E+01, 0.0000000E+00
 132, 4.5000000E+00, -5.1570000E+01, 0.0000000E+00
 133, 6.0000000E+00, -5.1570000E+01, 0.0000000E+00
 134, 6.4999995E+00, -5.1570000E+01, 0.0000000E+00
 135, 7.0000000E+00, -5.1570000E+01, 0.0000000E+00
 136, 7.5000005E+00, -5.1570000E+01, 0.0000000E+00
 137, 0.0000000E+00, -5.2590000E+01, 0.0000000E+00
 138, 1.5000000E+00, -5.2590000E+01, 0.0000000E+00
 139, 3.0000000E+00, -5.2590000E+01, 0.0000000E+00
 140, 4.5000000E+00, -5.2590000E+01, 0.0000000E+00

141, 6.0000000E+00,-5.2590000E+01, 0.0000000E+00
142, 6.4999995E+00,-5.2590000E+01, 0.0000000E+00
143, 7.0000000E+00,-5.2590000E+01, 0.0000000E+00
144, 7.5000005E+00,-5.2590000E+01, 0.0000000E+00
145, 0.0000000E+00,-5.3619999E+01, 0.0000000E+00
146, 1.5000000E+00,-5.3619999E+01, 0.0000000E+00
147, 3.0000000E+00,-5.3619999E+01, 0.0000000E+00
148, 4.5000000E+00,-5.3619999E+01, 0.0000000E+00
149, 6.0000000E+00,-5.3619999E+01, 0.0000000E+00
150, 6.4999995E+00,-5.3619999E+01, 0.0000000E+00
151, 7.0000000E+00,-5.3619999E+01, 0.0000000E+00
152, 7.5000005E+00,-5.3619999E+01, 0.0000000E+00
153, 0.0000000E+00,-5.4650002E+01, 0.0000000E+00
154, 1.5000000E+00,-5.4650002E+01, 0.0000000E+00
155, 3.0000000E+00,-5.4650002E+01, 0.0000000E+00
156, 4.5000000E+00,-5.4650002E+01, 0.0000000E+00
157, 6.0000000E+00,-5.4650002E+01, 0.0000000E+00
158, 6.4999995E+00,-5.4650002E+01, 0.0000000E+00
159, 7.0000000E+00,-5.4650002E+01, 0.0000000E+00
160, 7.5000005E+00,-5.4650002E+01, 0.0000000E+00
161, 0.0000000E+00,-5.5679996E+01, 0.0000000E+00
162, 1.5000000E+00,-5.5679996E+01, 0.0000000E+00
163, 3.0000000E+00,-5.5679996E+01, 0.0000000E+00
164, 4.5000000E+00,-5.5679996E+01, 0.0000000E+00
165, 6.0000000E+00,-5.5679996E+01, 0.0000000E+00
166, 6.4999995E+00,-5.5679996E+01, 0.0000000E+00
167, 7.0000000E+00,-5.5679996E+01, 0.0000000E+00
168, 7.5000005E+00,-5.5679996E+01, 0.0000000E+00
169, 0.0000000E+00,-5.6699997E+01, 0.0000000E+00
170, 1.5000000E+00,-5.6699997E+01, 0.0000000E+00
171, 3.0000000E+00,-5.6699997E+01, 0.0000000E+00
172, 4.5000000E+00,-5.6699997E+01, 0.0000000E+00
173, 6.0000000E+00,-5.6699997E+01, 0.0000000E+00
174, 6.4999995E+00,-5.6699997E+01, 0.0000000E+00
175, 7.0000000E+00,-5.6699997E+01, 0.0000000E+00
176, 7.5000005E+00,-5.6699997E+01, 0.0000000E+00
177, 0.0000000E+00,-5.7730000E+01, 0.0000000E+00
178, 1.5000000E+00,-5.7730000E+01, 0.0000000E+00
179, 3.0000000E+00,-5.7730000E+01, 0.0000000E+00
180, 4.5000000E+00,-5.7730000E+01, 0.0000000E+00
181, 6.0000000E+00,-5.7730000E+01, 0.0000000E+00
182, 6.4999995E+00,-5.7730000E+01, 0.0000000E+00
183, 7.0000000E+00,-5.7730000E+01, 0.0000000E+00
184, 7.5000005E+00,-5.7730000E+01, 0.0000000E+00
185, 0.0000000E+00,-5.8759998E+01, 0.0000000E+00
186, 1.5000000E+00,-5.8759998E+01, 0.0000000E+00
187, 3.0000000E+00,-5.8759998E+01, 0.0000000E+00
188, 4.5000000E+00,-5.8759998E+01, 0.0000000E+00
189, 6.0000000E+00,-5.8759998E+01, 0.0000000E+00
190, 6.4999995E+00,-5.8759998E+01, 0.0000000E+00
191, 7.0000000E+00,-5.8759998E+01, 0.0000000E+00
192, 7.5000005E+00,-5.8759998E+01, 0.0000000E+00

193, 0.0000000E+00, -5.9779999E+01, 0.0000000E+00
 194, 1.5000000E+00, -5.9779999E+01, 0.0000000E+00
 195, 3.0000000E+00, -5.9779999E+01, 0.0000000E+00
 196, 4.5000000E+00, -5.9779999E+01, 0.0000000E+00
 197, 6.0000000E+00, -5.9779999E+01, 0.0000000E+00
 198, 6.4999995E+00, -5.9779999E+01, 0.0000000E+00
 199, 7.0000000E+00, -5.9779999E+01, 0.0000000E+00
 200, 7.5000005E+00, -5.9779999E+01, 0.0000000E+00
 201, 0.0000000E+00, -6.0810001E+01, 0.0000000E+00
 202, 1.5000000E+00, -6.0810001E+01, 0.0000000E+00
 203, 3.0000000E+00, -6.0810001E+01, 0.0000000E+00
 204, 4.5000000E+00, -6.0810001E+01, 0.0000000E+00
 205, 6.0000000E+00, -6.0810001E+01, 0.0000000E+00
 206, 6.4999995E+00, -6.0810001E+01, 0.0000000E+00
 207, 7.0000000E+00, -6.0810001E+01, 0.0000000E+00
 208, 7.5000005E+00, -6.0810001E+01, 0.0000000E+00
 209, 0.0000000E+00, -6.1840000E+01, 0.0000000E+00
 210, 1.5000000E+00, -6.1840000E+01, 0.0000000E+00
 211, 3.0000000E+00, -6.1840000E+01, 0.0000000E+00
 212, 4.5000000E+00, -6.1840000E+01, 0.0000000E+00
 213, 6.0000000E+00, -6.1840000E+01, 0.0000000E+00
 214, 6.4999995E+00, -6.1840000E+01, 0.0000000E+00
 215, 7.0000000E+00, -6.1840000E+01, 0.0000000E+00
 216, 7.5000005E+00, -6.1840000E+01, 0.0000000E+00
 217, 0.0000000E+00, -6.2860001E+01, 0.0000000E+00
 218, 1.5000000E+00, -6.2860001E+01, 0.0000000E+00
 219, 3.0000000E+00, -6.2860001E+01, 0.0000000E+00
 220, 4.5000000E+00, -6.2860001E+01, 0.0000000E+00
 221, 6.0000000E+00, -6.2860001E+01, 0.0000000E+00
 222, 6.4999995E+00, -6.2860001E+01, 0.0000000E+00
 223, 7.0000000E+00, -6.2860001E+01, 0.0000000E+00
 224, 7.5000005E+00, -6.2860001E+01, 0.0000000E+00
 225, 0.0000000E+00, -6.3889999E+01, 0.0000000E+00
 226, 1.5000000E+00, -6.3889999E+01, 0.0000000E+00
 227, 3.0000000E+00, -6.3889999E+01, 0.0000000E+00
 228, 4.5000000E+00, -6.3889999E+01, 0.0000000E+00
 229, 6.0000000E+00, -6.3889999E+01, 0.0000000E+00
 230, 6.4999995E+00, -6.3889999E+01, 0.0000000E+00
 231, 7.0000000E+00, -6.3889999E+01, 0.0000000E+00
 232, 7.5000005E+00, -6.3889999E+01, 0.0000000E+00
 233, 0.0000000E+00, -6.4919998E+01, 0.0000000E+00
 234, 1.5000000E+00, -6.4919998E+01, 0.0000000E+00
 235, 3.0000000E+00, -6.4919998E+01, 0.0000000E+00
 236, 4.5000000E+00, -6.4919998E+01, 0.0000000E+00
 237, 6.0000000E+00, -6.4919998E+01, 0.0000000E+00
 238, 6.4999995E+00, -6.4919998E+01, 0.0000000E+00
 239, 7.0000000E+00, -6.4919998E+01, 0.0000000E+00
 240, 7.5000005E+00, -6.4919998E+01, 0.0000000E+00
 241, 0.0000000E+00, -6.5949997E+01, 0.0000000E+00
 242, 1.5000000E+00, -6.5949997E+01, 0.0000000E+00
 243, 3.0000000E+00, -6.5949997E+01, 0.0000000E+00
 244, 4.5000000E+00, -6.5949997E+01, 0.0000000E+00

```

245, 6.0000000E+00, -6.5949997E+01, 0.0000000E+00
246, 6.4999995E+00, -6.5949997E+01, 0.0000000E+00
247, 7.0000000E+00, -6.5949997E+01, 0.0000000E+00
248, 7.5000005E+00, -6.5949997E+01, 0.0000000E+00
249, 8.0000000E+00, -6.6970001E+01, 0.0000000E+00
250, 1.5000000E+00, -6.6970001E+01, 0.0000000E+00
251, 3.0000000E+00, -6.6970001E+01, 0.0000000E+00
252, 4.5000000E+00, -6.6970001E+01, 0.0000000E+00
253, 6.0000000E+00, -6.6970001E+01, 0.0000000E+00
254, 6.4999995E+00, -6.6970001E+01, 0.0000000E+00
255, 7.0000000E+00, -6.6970001E+01, 0.0000000E+00
256, 7.5000005E+00, -6.6970001E+01, 0.0000000E+00

```

```
*ELEMENT, TYPE=CPE4, ELSET=E0000001
```

```

14, 15, 22, 24, 16
10, 20, 29, 31, 23
21, 23, 31, 32, 24
26, 29, 37, 38, 30
27, 30, 38, 39, 31
28, 31, 39, 40, 32
33, 37, 44, 45, 38
34, 38, 45, 47, 39
35, 39, 47, 48, 40
39, 44, 52, 53, 45
40, 45, 53, 54, 46
41, 46, 54, 55, 47
42, 47, 55, 56, 48
45, 52, 60, 61, 53
47, 53, 61, 62, 54
48, 54, 62, 63, 55
49, 55, 63, 64, 56
53, 60, 68, 69, 61
54, 61, 69, 70, 62
55, 62, 70, 71, 63
56, 63, 71, 72, 64
60, 68, 75, 77, 69
61, 69, 77, 78, 70
62, 70, 78, 79, 71
63, 71, 79, 80, 72
66, 75, 83, 84, 75
67, 76, 84, 85, 77
68, 77, 85, 86, 78
69, 78, 86, 87, 79
70, 79, 87, 88, 80
73, 83, 91, 92, 84
74, 84, 92, 93, 85
75, 85, 93, 94, 86
76, 86, 94, 95, 87
77, 87, 95, 96, 88
80, 91, 99, 100, 92
81, 92, 100, 101, 93
82, 93, 101, 102, 94
83, 94, 102, 103, 95

```


94,	95,	103,	104,	95,
99,	99,	103,	106,	100
99,	100,	106,	109,	101
99,	101,	109,	110,	102
99,	102,	110,	111,	103
91,	103,	111,	112,	104
93,	105,	114,	115,	107
94,	107,	115,	116,	108
95,	108,	115,	117,	109
95,	109,	117,	118,	110
97,	110,	118,	119,	111
98,	111,	119,	120,	112
100,	114,	121,	122,	113
101,	115,	123,	124,	115
102,	115,	124,	125,	117
103,	117,	125,	126,	118
104,	118,	125,	127,	119
105,	119,	127,	128,	120
105,	121,	129,	130,	122
107,	122,	130,	131,	123
108,	123,	131,	132,	124
109,	124,	132,	133,	125
110,	125,	133,	134,	125
111,	125,	134,	135,	127
112,	125,	135,	136,	128
113,	129,	137,	138,	130
114,	130,	138,	139,	131
115,	131,	139,	140,	132
115,	132,	140,	141,	133
116,	133,	141,	142,	134
117,	134,	142,	143,	135
118,	135,	143,	144,	135
120,	137,	145,	145,	138
121,	138,	145,	146,	139
123,	140,	148,	149,	141
124,	141,	149,	150,	142
125,	142,	150,	151,	143
125,	143,	151,	152,	144
127,	145,	153,	154,	145
128,	145,	154,	155,	147
129,	147,	155,	156,	148
130,	148,	155,	157,	149
131,	149,	157,	158,	150
132,	150,	158,	159,	151
133,	151,	159,	160,	152
134,	153,	161,	162,	154
135,	154,	162,	163,	155
135,	155,	163,	164,	155
137,	155,	164,	165,	157
138,	157,	165,	166,	158
139,	158,	166,	167,	159

140,	159,	167,	168,	160
141,	161,	169,	170,	162
142,	162,	170,	171,	163
143,	163,	171,	172,	164
144,	164,	172,	173,	165
145,	165,	173,	174,	166
146,	166,	174,	175,	167
147,	167,	175,	176,	168
148,	169,	177,	178,	170
149,	170,	178,	179,	171
150,	171,	179,	180,	172
151,	172,	180,	181,	173
152,	173,	181,	182,	174
153,	174,	182,	183,	175
154,	175,	183,	184,	176
155,	177,	185,	186,	178
156,	178,	186,	187,	179
157,	179,	187,	188,	180
158,	180,	188,	189,	181
159,	181,	189,	190,	182
160,	182,	190,	191,	183
161,	183,	191,	192,	184
162,	185,	193,	194,	185
163,	186,	194,	195,	187
164,	187,	195,	196,	188
165,	188,	196,	197,	189
166,	189,	197,	198,	190
167,	190,	198,	199,	191
168,	191,	199,	200,	192
169,	193,	201,	202,	194
170,	194,	202,	203,	195
171,	195,	203,	204,	196
172,	196,	204,	205,	197
173,	197,	205,	206,	198
174,	198,	206,	207,	199
175,	199,	207,	208,	200
176,	201,	209,	210,	202
177,	202,	210,	211,	203
178,	203,	211,	212,	204
179,	204,	212,	213,	205
180,	205,	213,	214,	206
181,	206,	214,	215,	207
182,	207,	215,	216,	208
183,	209,	217,	218,	210
184,	210,	218,	219,	211
185,	211,	219,	220,	212
186,	212,	220,	221,	213
187,	213,	221,	222,	214
188,	214,	222,	223,	215
189,	215,	223,	224,	216
190,	217,	225,	226,	218
191,	218,	226,	227,	219

192,	219,	227,	228,	220
193,	220,	228,	229,	221
194,	221,	229,	230,	222
195,	222,	230,	231,	223
196,	223,	231,	232,	224
197,	225,	233,	234,	225
198,	226,	234,	235,	227
199,	227,	235,	236,	228
200,	228,	236,	237,	229
201,	229,	237,	238,	230
202,	230,	238,	239,	231
203,	231,	239,	240,	232
204,	233,	241,	242,	234
205,	234,	242,	243,	235
206,	235,	243,	244,	236
207,	236,	244,	245,	237
208,	237,	245,	246,	238
209,	238,	246,	247,	239
210,	239,	247,	248,	240
211,	241,	249,	250,	242
212,	242,	250,	251,	243
213,	243,	251,	252,	244
214,	244,	252,	253,	245
215,	245,	253,	254,	246
216,	246,	254,	255,	247
217,	247,	255,	256,	248

*SOLID SECTION,ELSET=E0000001,MATERIAL=7050T

*MATERIAL,NAME=7050T

*elastic

11e6,.33

*plastic

73e3,.0

*expansion,perc=70.

13.5e-6

*DENSITY

3.102

*CONDUCTIVITY,TYPE=ISO

5.620E+00

*INITIAL CONDITIONS,TYPE=TEMPERATURE

ALL,910

*RESTART,WRITE,FREQUENCY=40

*STEP,AMPLITUDE=STEP,INC=40

*STATIC,direct

1,30

**dload

**E0000001,grav,386,0,1,0

*temperature,user

all

*BOUNDARY,OP=NEW

ES000001, 1,, 0.00000E+00

**249,1,2, 0.00000E+00

*EL FILE,FREQUENCY= 30, position=averaged at nodes

```

S,E,sp
*el print,FREQUENCY=5, position=averaged at nodes
$
*el print,FREQUENCY=5, position=averaged at nodes
sp,mises
*END STEP
*NSET,NSET=BS000001
121,129,137,145,153,161,169,177,185,
193,201,209,217,225,233,241,249
*ELSET,ELSET=SURF67
106,113,120,127,134,141,148,155,162,169,176,183,190,
197,204,211,
93,100,107,114,121,128,135,142,149,156,163,170,177,
184,191,
198,205,212
*ELSET,ELSET=SURF45
66,73,80,87,94,101,108,115,122,129,136,143,150,157,
164,171,178,185,192,199,206,213,
39,46,53,60,67,74,81,88,95,102,109,116,123,130,137,
144,151,158,165,172,179,186,193,200,207,214
*ELSET,ELSET=SURF123
14,20,21,26,27,28,33,34,35,40,41,42,47,48,49,54,
55,56,61,62,63,68,69,70,
75,76,77,82,83,84,89,90,91,96,97,98,103,104,105,110,
111,112,117,118,119,
124,125,126,131,132,133,138,139,140,
145,152,159,166,173,180,187,194,201,208,215,
146,153,160,167,174,181,188,195,202,209,216,
147,154,161,168,175,182,189,196,203,210,217
*user subroutine
      subroutine utemp(temp,nsectp,kstep,kind,time,node,coords)
      include 'aba_param.inc'
      dimension temp(nsectp),time(2),coords(3),rtemp(260)
cccccccccccccccccccccccccccccccc
      DATA rtemp/
$ 910.0, 910.0, 910.0, 910.0,
$ 910.0, 910.0, 910.0, 910.0,
$ 910.0, 910.0, 910.0, 910.0,
$ 910.0, 910.0, 910.0, 910.0,
$ 910.0, 910.0, 910.0, 910.0,
$ 910.0, 910.0, 843.9, 580.7,
$ 910.0, 910.0, 910.0, 910.0,
$ 910.0, 772.1, 645.9, 407.6,
$ 910.0, 910.0, 910.0, 910.0,
$ 910.0, 710.5, 587.4, 377.3,
$ 910.0, 910.0, 910.0, 910.0,
$ 772.9, 652.6, 536.4, 348.9,
$ 910.0, 910.0, 910.0, 910.0,
$ 699.8, 590.4, 484.7, 320.6,
$ 910.0, 910.0, 910.0, 910.0,
$ 655.1, 552.7, 453.7, 307.1,
$ 910.0, 910.0, 910.0, 910.0,

```

```

$ 518.3, 522.3, 428.8, 295.2,
$ 910.0, 910.0, 910.0, 910.0,
$ 580.4, 492.0, 405.7, 295.0,
$ 910.0, 910.0, 910.0, 867.6,
$ 561.4, 475.7, 394.1, 292.6,
$ 910.0, 910.0, 910.0, 829.1,
$ 528.4, 451.1, 374.9, 276.6,
$ 910.0, 910.0, 910.0, 780.8,
$ 515.3, 441.0, 367.6, 274.2,
$ 910.0, 910.0, 877.4, 752.6,
$ 483.7, 416.3, 348.9, 265.2,
$ 910.0, 910.0, 812.2, 699.7,
$ 474.5, 409.3, 343.1, 262.5,
$ 910.0, 881.1, 785.1, 677.8,
$ 441.3, 384.8, 325.7, 257.0,
$ 836.6, 799.0, 718.8, 624.9,
$ 436.6, 381.2, 323.6, 255.9,
$ 809.1, 775.5, 699.6, 609.6,
$ 403.0, 355.1, 306.6, 250.1,
$ 719.0, 696.8, 633.2, 556.4,
$ 401.8, 355.2, 305.8, 249.8,
$ 706.8, 685.6, 623.9, 548.7,
$ 370.3, 330.9, 288.9, 242.3,
$ 628.1, 612.6, 560.9, 497.1,
$ 365.3, 326.2, 285.3, 240.7,
$ 625.6, 610.3, 558.9, 495.4,
$ 346.1, 309.0, 272.9, 236.1,
$ 558.3, 546.2, 503.1, 449.1,
$ 322.4, 290.0, 258.9, 228.5,
$ 546.1, 534.7, 493.0, 440.8,
$ 320.2, 288.4, 257.7, 227.9,
$ 501.8, 491.9, 455.6, 409.6,
$ 301.6, 274.0, 247.6, 222.6,
$ 453.8, 445.6, 414.9, 375.6,
$ 293.9, 257.4, 241.6, 216.0,
$ 449.4, 441.0, 411.3, 372.6,
$ 293.7, 260.4, 238.3, 216.6,
$ 410.9, 406.3, 380.1, 346.6,
$ 276.7, 255.5, 235.5, 216.2,
$ 399.6, 393.3, 368.7, 336.8,
$ 268.9, 249.2, 231.0, 213.7,
$ 378.0, 372.6, 350.2, 321.4,
$ 260.2, 241.8, 224.7, 208.2,
$ 363.5, 358.5, 337.6, 311.2,
$ 255.2, 238.4, 222.0, 206.2,
$ 347.9, 343.6, 324.6, 300.4,
$ 246.9, 232.1, 217.1, 202.9/
nrow=(node-1)/8-1
ncol=node-8*nrow
irow=33-nrow
if(time/2).gt.irow then
  nhis=(time/2)-irow+8+ncol

```

```
        temp(1)=rtemp.nhhs)
else
    temp(1)=910
end if
write(6,*, ' node, time = 2', temp 1
return
end
```

APPENDIX B: Input file for temperature dependent properties of wrought Al 7050 material model

```
*HEADING
Property for 7050-T7451 with temperature dependent
Perfect Plastic, no work hardening
*NODE, SYSTEM=R, nset=all
  Same as Appendix A)
*ELEMENT, TYPE=CPE4      , ELSET=E0000001
  Same as Appendix A,
*SOLID SECTION, ELSET=E0000001, MATERIAL=7050T
*MATERIAL, NAME=7050T
*elastic
10.3e6, .33, 70
9.4e6, .33, 250
8.7e6, .33, 350
8.4e6, .33, 500
1e-5, .4999, 975
*plastic
73e3, .0, 70
62e3, .0, 212
56e3, .0, 300
42e3, .0, 400
21e3, .0, 500
1e-4, .0, 975
*expansion, zero=70.
13.5e-6
*DENSITY
0.102
*CONDUCTIVITY, TYPE=ISO
5.620E+00
*INITIAL CONDITIONS, TYPE=TEMPERATURE
ALL, 910
*RESTART, WRITE, FREQUENCY=40
*STEP, AMPLITUDE=STEP, INC=40
*STATIC, direct
1, 30
**dload
**E0000001, grav, 386, 0, 1, 0
*temperature, user
all
*BOUNDARY, OP=NEW
BS000001, 1,, 0.00000E+00
**249, 1, 2, 0.00000E+00
*EL FILE, FREQUENCY= 30, position=averaged at nodes
S, E, sp
*el print, FREQUENCY=5, position=averaged at nodes
s
*el print, FREQUENCY=5, position=averaged at nodes
sp, mises
*END STEP
```

```

*NSSET, NSET=BS000001
121, 129, 137, 145, 153, 161, 169, 177, 185,
193, 201, 209, 217, 225, 233, 241, 249
*ELSET, ELSET=SURF67
106, 113, 120, 127, 134, 141, 148, 155, 162, 169, 176, 183, 190,
197, 204, 211,
93, 100, 107, 114, 121, 128, 135, 142, 149, 156, 163, 170, 177,
184, 191,
198, 205, 212
*ELSET, ELSET=SURF45
66, 73, 80, 87, 94, 101, 108, 115, 122, 129, 136, 143, 150, 157,
164, 171, 178, 185, 192, 199, 206, 213,
39, 46, 53, 60, 67, 74, 81, 88, 95, 102, 109, 116, 123, 130, 137,
144, 151, 158, 165, 172, 179, 186, 193, 200, 207, 214
*ELSET, ELSET=SURF123
14, 20, 21, 26, 27, 28, 33, 34, 35, 40, 41, 42, 47, 48, 49, 54,
55, 56, 61, 62, 63, 68, 69, 70,
75, 76, 77, 82, 83, 84, 89, 90, 91, 96, 97, 98, 103, 104, 105, 110,
111, 112, 117, 118, 119,
124, 125, 126, 131, 132, 133, 138, 139, 140,
145, 152, 159, 166, 173, 180, 187, 194, 201, 208, 215,
146, 153, 160, 167, 174, 181, 188, 195, 202, 209, 216,
147, 154, 161, 168, 175, 182, 189, 196, 203, 210, 217
*user subroutine
  subroutine utemp temp, nsect, kstep, kind, time, node, coords
  include 'aba_param.inc'
  dimension temp nsect, time 2, coords 3, rtemp 260
  DATA rtemp/
    $ 910.0, 910.0, 910.0, 910.0,
    $ 910.0, 910.0, 910.0, 910.0,
    $ 910.0, 910.0, 910.0, 910.0,
    $ 910.0, 910.0, 910.0, 910.0,
    $ 910.0, 910.0, 910.0, 910.0,
    $ 910.0, 910.0, 843.9, 580.7,
    $ 910.0, 910.0, 910.0, 910.0,
    $ 910.0, 772.1, 645.9, 407.6,
    $ 910.0, 910.0, 910.0, 910.0,
    $ 910.0, 710.5, 587.4, 377.3,
    $ 910.0, 910.0, 910.0, 910.0,
    $ 772.9, 652.6, 536.4, 348.9,
    $ 910.0, 910.0, 910.0, 910.0,
    $ 699.8, 590.4, 484.7, 320.6,
    $ 910.0, 910.0, 910.0, 910.0,
    $ 655.1, 552.7, 453.7, 307.1,
    $ 910.0, 910.0, 910.0, 910.0,
    $ 618.3, 522.3, 428.8, 295.2,
    $ 910.0, 910.0, 910.0, 910.0,
    $ 580.4, 492.0, 405.7, 286.0,
    $ 910.0, 910.0, 910.0, 867.6,
    $ 561.4, 476.7, 394.1, 282.5,
    $ 910.0, 910.0, 910.0, 829.1,
    $ 528.4, 451.1, 374.9, 276.6,

```



```

$ 910.0, 910.0, 910.0, 780.8,
$ 515.3, 441.0, 367.6, 274.2,
$ 910.0, 910.0, 877.4, 752.6,
$ 483.7, 415.3, 348.9, 265.2,
$ 910.0, 910.0, 812.2, 699.7,
$ 474.5, 409.3, 343.1, 262.5,
$ 910.0, 881.1, 785.2, 677.8,
$ 441.3, 384.8, 325.7, 257.0,
$ 936.6, 799.0, 718.8, 624.9,
$ 426.6, 381.2, 322.6, 256.9,
$ 809.1, 775.6, 699.5, 609.6,
$ 403.0, 356.1, 306.5, 250.1,
$ 719.0, 696.8, 633.2, 556.4,
$ 401.8, 355.2, 305.8, 249.8,
$ 706.8, 685.6, 623.8, 548.7,
$ 370.3, 330.9, 288.9, 242.3,
$ 628.1, 612.6, 560.9, 497.1,
$ 365.3, 326.2, 285.3, 240.7,
$ 625.6, 610.3, 558.9, 495.4,
$ 346.1, 309.0, 272.9, 236.1,
$ 558.3, 546.2, 503.2, 449.1,
$ 322.4, 290.0, 258.9, 228.5,
$ 546.1, 534.7, 493.0, 440.8,
$ 320.2, 288.4, 257.7, 227.9,
$ 501.8, 491.9, 455.5, 409.5,
$ 301.6, 274.0, 247.6, 222.5,
$ 453.8, 445.6, 414.9, 375.6,
$ 293.9, 267.4, 241.5, 216.0,
$ 449.4, 441.3, 411.3, 371.5,
$ 283.7, 260.4, 238.3, 216.6,
$ 412.9, 406.3, 380.1, 346.6,
$ 276.7, 255.6, 235.5, 216.2,
$ 399.6, 393.3, 368.7, 336.9,
$ 268.9, 249.2, 231.0, 213.7,
$ 378.0, 372.6, 350.2, 321.4,
$ 260.2, 241.8, 224.7, 208.2,
$ 363.5, 358.6, 337.6, 311.2,
$ 255.2, 238.4, 222.0, 206.2,
$ 347.9, 343.6, 324.6, 300.4,
$ 246.9, 232.1, 217.1, 202.9/
nrow=(node-1)/9-1
ncol=node-9*nrow
irow=33-nrow
if(time(2).gt.irow) then
  nhis=(time(2)-irow)*9+ncol
  temp(1)=rtemp(nhis)
else
  temp(1)=910
end if
write(6,*) node,time(2),temp(1)
return
end

```

APPENDIX C: Input file for temperature dependent properties of as-cast Al 7050 ingot surface model

```

*HEADING
temperature dependent, as-cast Al-7050 ingot surface
Perfect Plastic at temp>600
linear work hardening at temp<600
*NODE, SYSTEM=R,nset=all
  same as Appendix A
*ELEMENT,TYPE=CPE4      ,ELSET=E0000001
  same as Appendix A
*SOLID SECTION,ELSET=E0000001,MATERIAL=7050S
*MATERIAL,NAME=7050S
*elastic
11.4e6,.33,70
10.84e6,.33,200
9.75e6,.33,400
9.19e6,.33,600
5.41e6,.33,800
1e-5,.4999,975
*plastic
20e3,.0,70
30.08e3,.005139,70
19.5e3,.0,200
19.75e3,.007233,200
16e3,.0,400
14.49e3,.02755,400
14.5e3,.0,600
12.5e3,.0,800
1e-4,.0,975
*expansion,zero=70.
13.5e-6
*DENSITY
0.102
*CONDUCTIVITY,TYPE=ISO
5.620E+00
*INITIAL CONDITIONS,TYPE=TEMPERATURE
ALL,910
*RESTART,WRITE,FREQUENCY=999
*STEP,AMPLITUDE=STEP,INC=40
*STATIC,direct
1,30
*temperature,user
all
*BOUNDARY,OP=NEW
BS000001, 1,, 0.00000E+00
**249,1,2, 0.00000E+00
*EL FILE,FREQUENCY= 30, position=averaged at nodes
S,E,sp
*node print, frequency=30

```

```

ccoord
*el print,FREQUENCY=30, position=averaged at nodes
S
*END STEP
*NSET,NSET=BS000001
121,129,137,145,153,161,169,177,185,
193,201,209,217,225,233,241,249
*ELSET,ELSET=SURF67
106,113,120,127,134,141,148,155,162,169,176,183,190,
197,204,211,
93,100,107,114,121,128,135,142,149,156,163,170,177,
184,191,
198,205,212
*ELSET,ELSET=SURF45
66,73,80,87,94,101,108,115,122,129,136,143,150,157,
164,171,178,185,192,199,206,213,
39,46,53,60,67,74,81,88,95,102,109,116,123,130,137,
144,151,158,165,172,179,186,193,200,207,214
*ELSET,ELSET=SURF123
14,20,21,26,27,29,33,34,35,40,41,42,47,48,49,54,
55,56,61,62,63,68,69,70,
75,76,77,82,83,84,89,90,91,96,97,98,103,104,105,110,
111,112,117,118,119,
124,125,126,131,132,133,138,139,140,
145,152,159,166,173,180,187,194,201,208,215,
146,153,160,167,174,181,188,195,202,209,216,
147,154,161,168,175,182,189,196,203,210,217
*user subroutine
      subroutine utemp(temp,nsectp,kstep,kind,time,node,coords
      include 'aba_param.inc'
      dimension temp(nsectp),time(2),coords(3),rtemp(260)
cccccccccccccccccccccccccccccccc
      DATA rtemp/
      $ 910.0, 910.0, 910.0, 910.0,
      $ 910.0, 910.0, 910.0, 910.0,
      $ 910.0, 910.0, 910.0, 910.0,
      $ 910.0, 910.0, 910.0, 910.0,
      $ 910.0, 910.0, 910.0, 910.0,
      $ 910.0, 910.0, 843.9, 580.7,
      $ 910.0, 910.0, 910.0, 910.0,
      $ 910.0, 772.1, 645.9, 407.6,
      $ 910.0, 910.0, 910.0, 910.0,
      $ 910.0, 710.5, 587.4, 377.3,
      $ 910.0, 910.0, 910.0, 910.0,
      $ 772.9, 652.6, 536.4, 348.9,
      $ 910.0, 910.0, 910.0, 910.0,
      $ 699.8, 590.4, 484.7, 320.6,
      $ 910.0, 910.0, 910.0, 910.0,
      $ 655.1, 552.7, 453.7, 307.1,
      $ 910.0, 910.0, 910.0, 910.0,
      $ 618.3, 522.3, 428.8, 295.2,
      $ 910.0, 910.0, 910.0, 910.0,

```

```

$ 580.4, 492.0, 405.7, 285.0,
$ 910.0, 910.0, 910.0, 967.6,
$ 561.4, 475.7, 394.1, 282.6,
$ 910.0, 910.0, 910.0, 929.1,
$ 528.4, 451.1, 374.9, 275.6,
$ 910.0, 910.0, 910.0, 790.8,
$ 515.3, 441.0, 367.6, 274.2,
$ 910.0, 910.0, 977.4, 751.6,
$ 483.7, 416.3, 348.9, 265.2,
$ 910.0, 910.0, 912.0, 699.7,
$ 474.5, 409.3, 343.1, 262.6,
$ 910.0, 881.1, 785.2, 677.8,
$ 441.3, 384.9, 325.7, 257.0,
$ 836.6, 799.0, 718.9, 624.9,
$ 436.6, 381.2, 323.6, 256.9,
$ 809.1, 775.5, 699.5, 609.6,
$ 403.0, 356.1, 306.5, 250.1,
$ 719.0, 696.8, 633.2, 556.4,
$ 401.8, 355.2, 305.8, 249.8,
$ 706.8, 685.6, 623.8, 548.7,
$ 670.3, 630.9, 288.9, 242.3,
$ 628.1, 612.6, 550.9, 497.1,
$ 655.3, 625.2, 285.3, 240.7,
$ 625.6, 610.3, 558.9, 495.4,
$ 646.1, 609.0, 272.9, 236.1,
$ 558.3, 646.2, 503.2, 449.1,
$ 622.4, 290.0, 258.9, 228.5,
$ 646.1, 634.7, 493.0, 440.8,
$ 623.2, 288.4, 257.7, 227.9,
$ 581.8, 491.9, 455.5, 439.5,
$ 601.6, 274.0, 247.6, 222.5,
$ 453.8, 446.6, 414.9, 375.6,
$ 293.9, 267.4, 241.5, 216.0,
$ 449.4, 441.3, 411.3, 372.5,
$ 283.7, 260.4, 238.3, 216.6,
$ 412.9, 406.3, 380.1, 346.6,
$ 276.7, 255.5, 235.6, 216.2,
$ 399.6, 393.3, 368.7, 336.8,
$ 268.9, 249.2, 231.0, 213.7,
$ 378.0, 372.6, 350.2, 321.4,
$ 260.2, 241.8, 224.7, 208.2,
$ 363.5, 358.5, 337.6, 311.2,
$ 255.2, 238.4, 222.0, 206.2,
$ 347.9, 343.6, 324.6, 300.4,
$ 246.9, 232.1, 217.1, 202.9/
nrow=(node-1)/8-1
ncol=node-8*nrow
irow=33-nrow
if(time(2).gt.irow) then
  nhis=(time(2)-irow)*8+ncol
  temp(1)=rtemp(nhis)
else

```

```
        temp(1)=910
    end if
    write(6,*) node,time(2),temp(1)
    return
end
```

APPENDIX D: Input file for temperature dependent properties of as-cast Al 7050 ingot center model

```

*HEADING
temperature-dependent as-cast Al-7050 ingot center
Perfect Plastic at temp>600F,
Linear work hardening at Temp<600
*NODE, SYSTEM=R, nset=all
  same as Appendix A)
*ELEMENT, TYPE=CPE4      , ELSET=E0000001
  same as Appendix A)
*SOLID SECTION, ELSET=E0000001, MATERIAL=7050ac
*MATERIAL, NAME=7050ac
*elastic
11.4e6, .33, 70
10.84e6, .33, 200
9.75e6, .33, 400
9.19e6, .33, 600
8.41e6, .33, 900
1e-5, .499, 975
*plastic
18e3, .0, 70
30.11e3, .006181, 70
11.5e3, .0, 200
28.92e3, .012845, 200
11e3, .0, 400
24.9e3, .044881, 400
9.5e3, .0, 600
5.5e3, .0, 900
1e-4, .0, 975
*expansion, zero=70.
13.5e-6
*DENSITY
0.102
*CONDUCTIVITY, TYPE=ISO
5.620E+00
*INITIAL CONDITIONS, TYPE=TEMPERATURE
ALL, 910
*RESTART, WRITE, FREQUENCY=999
*STEP, AMPLITUDE=STEP, INC=200
*STATIC, direct
0.25, 30
*temperature, user
all
*BOUNDARY, OP=NEW
BS000001, 1,, 0.00000E+00
249, 1, 2, 0.00000E+00
*node print, FREQUENCY=120
coord
*EL FILE, FREQUENCY= 999, position=averaged at nodes
S, E, sp

```

```

*el print,FREQUENCY=999, position=averaged at nodes
$
*END STEP
*NSET,NSET=BS000001
101,129,137,145,153,161,169,177,185,
193,201,209,217,225,233,241,249
*ELSET,ELSET=SURF67
106,113,120,127,134,141,148,155,162,169,176,183,190,
197,204,211,
93,100,107,114,121,128,135,142,149,156,163,170,177,
184,191,
198,205,212
*ELSET,ELSET=SURF45
66,73,80,87,94,101,108,115,122,129,136,143,150,157,
164,171,178,185,192,199,206,213,
39,46,53,60,67,74,81,88,95,102,109,116,123,130,137,
144,151,158,165,172,179,186,193,200,207,214
*ELSET,ELSET=SURF123
14,20,21,26,27,28,33,34,35,40,41,42,47,48,49,54,
55,56,61,62,63,68,69,70,
75,76,77,82,83,84,89,90,91,96,97,98,103,104,105,110,
111,112,117,118,119,
124,125,126,131,132,133,138,139,140,
145,152,159,166,173,180,187,194,201,208,215,
146,153,160,167,174,181,188,195,202,209,216,
147,154,161,168,175,182,189,196,203,210,217
*user subroutine
  subroutine utemp(temp,nsect, kstep, kind, time, node, coords
  include 'aba_param.inc'
  dimension temp(nsect), time(2), coords(3)
  dimension A0(8), A1(8), A2(8), A3(8), A4(8), A5(8),
  $           A6(8), A7(8)
  data A0, A1, A2, A3, A4, A5, A6, A7/
  $           1611.015, 1420.476, 1348.839, 1225.811, 1146.034, 1224.547,
  $           1181.986, 1164.212,
  $           -554.941, -255.201, -135.776, 15.83704, 46.14808, -33.0131,
  $           47.17004, 113.2156,
  $           95.88926, 18.93484, -8.40428, -42.2662, -9.6088, 15.08077,
  $           -23.4835, -47.8849,
  $           -8.78703, 0.37213, 3.37667605, 7.032513443, 0.085934879, -
2.35909938,
  $           4.654794, 8.316509,
  $           0.459647, -0.13145, -0.31434, -0.53395, 0.045811, 0.153657,
  $           -0.44423, -0.71232,
  $           -0.013800891, 0.00743804, 0.01370974, 0.021177,
  $           -0.003036432, -0.005049754,
  $           0.020882286, 0.031098113,
  $           0.000221425, -0.000177967, -0.00029137, -0.000425728,
  $           7.76749e-5, 8.29424e-5,
  $           -0.000474339, -0.000669585,
  $           -1.47127e-6, 1.59287e-6, 2.43408e-6, 3.42794e-6,
  $           -7.2304e-7, -5.38853e-7,

```

```

$          4.18003e-6,5.66095e-6/
nrow=(node-1)/8
ncol0=node-8*nrow
ncol=9-ncol0
irow=33-nrow
if(time/2).gt.irow then
  t=time/2-irow
  ctemp=A0(ncol)+A1(ncol)*t+A2(ncol)*t*t+
$      A3(ncol)*t*t*t+A4(ncol)*t*t*t*t+A5(ncol)*t*t*t*t*t+
$      A6(ncol)*t*t*t*t*t*t+A7(ncol)*t*t*t*t*t*t*t
  temp(1)=ctemp
  if(ctemp.gt.910) temp(1)=910
else
  temp(1)=910
end if
return
end

```


APPENDIX E: Input file for cooling rate dependent properties of as-cast Al 7050 ingot model

```
*HEADING
Cooling rate dependent, as-cast Al-7050 ingot
Perfect Plastic at temperature above 600F,
Linear work hardening below 600F
Elastic modulus using fitted numbers
*NODE, SYSTEM=R, nset=all
  same as Appendix A)
*ELEMENT, TYPE=CPE4      , ELSET=EALL
  Same as Appendix A)
*SOLID SECTION, ELSET=EALL, MATERIAL=7050ac
*MATERIAL, NAME=7050ac
*elastic
11.4e6, .33, 70
10.84e6, .33, 200
9.75e6, .33, 400
8.19e6, .33, 600
5.41e6, .33, 800
1e-5, .4999, 975
*plastic, dependencies=1
19e3, .0, 70, 1
30.11e3, .006181, 70, 1
12.5e3, .0, 200, 1
28.92e3, .012845, 200, 1
11e3, .0, 400, 1
24.9e3, .044881, 400, 1
9.5e3, .0, 600, 1
5.5e3, .0, 800, 1
1e-4, .0, 975, 1
19.5e3, .0, 70, 2
30.11e3, .00592, 70, 2
12.8e3, .0, 200, 2
28.91e3, .012485, 200, 2
11.8e3, .0, 400, 2
24.93e3, .042192, 400, 2
9.5e3, .0, 600, 2
5.5e3, .0, 800, 2
1e-4, .0, 975, 2
19e3, .0, 70, 3
30.1e3, .00566, 70, 3
13.4e3, .0, 200, 3
28.9e3, .01212, 200, 3
12.6e3, .0, 400, 3
24.77e3, .03937, 400, 3
10.2e3, .0, 600, 3
7.3e3, .0, 800, 3
1e-4, .0, 975, 3
19.5e3, .0, 70, 4
```

```

30.09e3, .005399, 70, 4
16.5e3, .0, 200, 4
28.82e3, .009682, 200, 4
14e3, .0, 400, 4
24.63e3, .073478, 400, 4
12.5e3, .0, 600, 4
9.9e3, .0, 800, 4
1e-4, .0, 975, 4
20e3, .0, 70, 5
30.09e3, .005139, 70, 5
19.5e3, .0, 200, 5
18.75e3, .007233, 200, 5
16e3, .0, 400, 5
24.49e3, .02755, 400, 5
14.5e3, .0, 600, 5
12.5e3, .0, 800, 5
1e-4, .0, 975, 5
*expansion, zero=70.
13.5e-6
*DENSITY
  0.102
*CONDUCTIVITY, TYPE=ISO
  5.620E-00
*INITIAL CONDITIONS, TYPE=TEMPERATURE
ALL, 910
*RESTART, WRITE, FREQUENCY=9999
*STEP, AMPLITUDE=STEP, INC=1000
*STATIC, direct
1.05, 30
*temperature, user
all
*field, user
all
*BOUNDARY, CP=NEW
BS000001, 1,, 0.000000E-00
*node print, FREQUENCY=9999
coord, nt
*EL FILE, FREQUENCY= 9999, position=averaged at nodes
3, E, sp
*el print, FREQUENCY=100, position=averaged at nodes
s
*el print, FREQUENCY=100, position=averaged at nodes
sp3, mises
*END STEP
*NSET, NSET=BS000001
121, 129, 137, 145, 153, 161, 169, 177, 185,
193, 201, 209, 217, 225, 233, 241, 249
*user subroutine
  subroutine utemp(temp, nsectp, kstep, kinc, time, node, coords
  include 'aba_param.inc'
  dimension temp(nsectp), time(2), coords(3)
  dimension A0(8), A1(8), A2(8), A3(8), A4(8), A5(8),

```

```

$          A6:A7,A7:A7
data A0,A1,A2,A3,A4,A5,A6,A7/
$          1611.015,1420.476,1348.839,1225.911,1146.034,1024.547,
$          1181.986,1164.212,
$          -554.941,-255.201,-135.776,15.83704,46.14808,-39.0131,
$          47.17004,113.2156,
$          95.88926,18.93484,-8.40428,-42.2662,-9.6088,15.09077,
$          -23.4835,-47.9849,
$          -8.78703,0.37213,3.37667605,7.032513443,0.085934879,-
2.35909938,
$          4.654794,8.316509,
$          0.459647,-0.13145,-0.31434,-0.53395,0.045811,0.153657,
$          -0.44423,-0.71232,
$          -0.013800891,0.00743804,0.01370974,0.021177,
$          -0.003036432,-0.005049754,
$          0.020882286,0.031098113,
$          0.000221425,-0.000177967,-0.00029137,-0.000425728,
$          7.76749e-5,8.29424e-5,
$          -0.000474339,-0.000669585,
$          -1.47127e-6,1.59287e-6,2.43408e-6,3.42794e-6,
$          -7.2304e-7,-5.38853e-7,
$          4.18003e-6,5.66095e-6/
nrow= node-1 /8
ncol0=node-8*nrow
ncol=9-ncol0
irow=33-nrow
if time(2).gt.irow then
  t=time(2)-irow
  ctemp=A0(ncol)+A1(ncol)*t+A2(ncol)*t*t+
$          A3(ncol)*t*t*t+A4(ncol)*t*t*t*t+A5(ncol)*t*t*t*t*t+
$          A6(ncol)*t*t*t*t*t*t+A7(ncol)*t*t*t*t*t*t*t
  temp(1)=ctemp
  if ctemp.gt.910 temp(1)=910
else
  temp(1)=910
end if
return
end

```

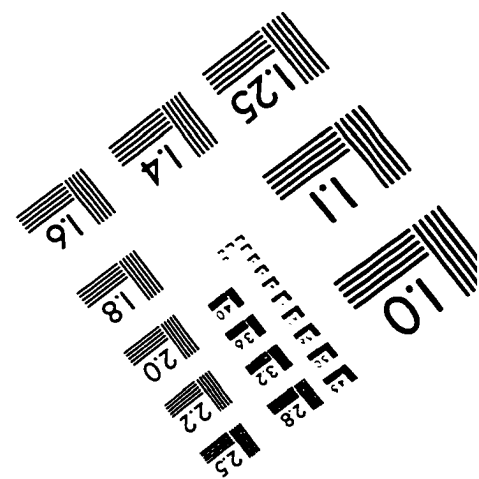
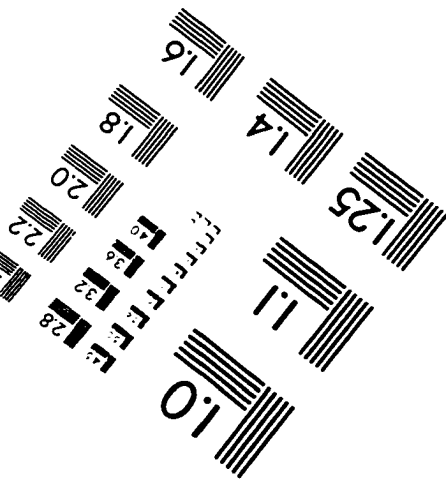
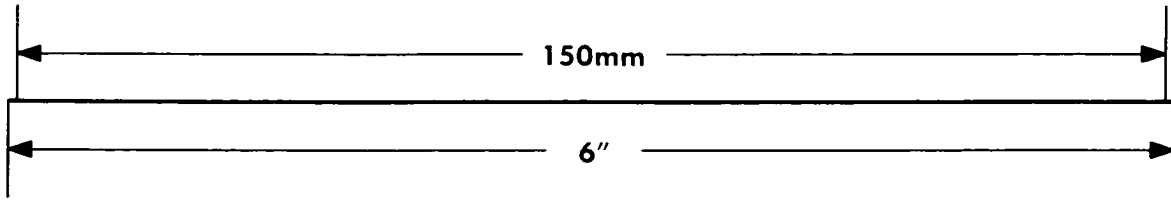
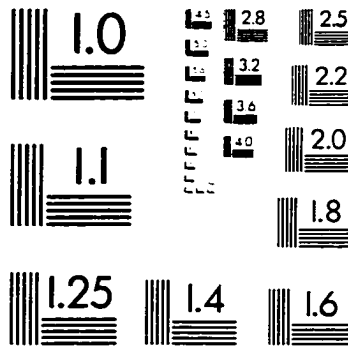
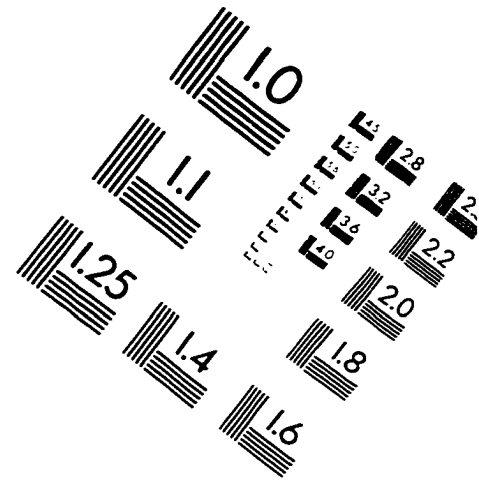
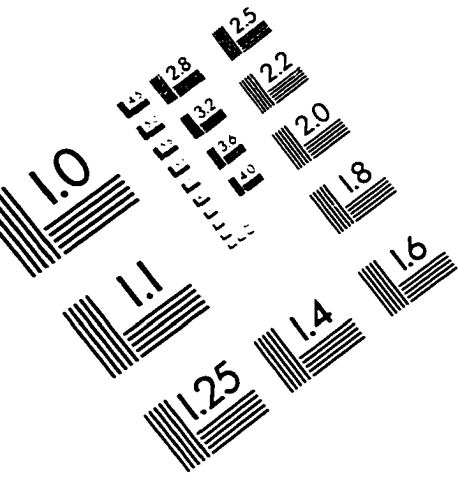
```

subroutine
ufield(field,kfield,nsect, kstep, kinc, time, node, coords, temp, dtemp
include 'aba_param.inc'
dimension
field(nsect), time(2), coords(3), temp(nsect), dtemp(nsect)
nrow=(node-1)/8
ncol=node-8*nrow
if((ncol.ge.1).and.(ncol.le.3)) field(1)=1.
if(ncol.eq.4) field(1)=2.
if(ncol.eq.5) field(1)=3.
if(ncol.eq.6) field(1)=4.
if((ncol.eq.7).or.(ncol.eq.8)) field(1)=5.

```

```
if (time(2).eq.1) write(6,*) node,nrow,ncol,field(1)
return
end
```

IMAGE EVALUATION TEST TARGET (QA-3)



APPLIED IMAGE, Inc
1653 East Main Street
Rochester, NY 14609 USA
Phone: 716/482-0300
Fax: 716/288-5989

© 1993, Applied Image, Inc., All Rights Reserved